THE ROLE OF HYDROGEN IN FIRING AND LIGHT-SOAKING EFFECTS ON DOPED POLYSILICON PASSIVATING CONTACTS FOR SILICON SOLAR CELLS

Di KANG

August 2021

A thesis submitted for the degree of Doctor of Philosophy of The Australian National University

Australian National University

Declaration

I certify that this thesis does not incorporate without acknowledgement any material previously submitted for a degree or diploma in any university, and that, to the best of my knowledge, it does not contain any material previously published or written by another person except where due reference is made in the text. The work in this thesis is my own, except for the contributions made by others as described in the acknowledgements. The thesis is a compilation of 5 manuscripts, all of which I am the corresponding author. The manuscript details are given as below.

Manuscript 1 is presented as Chapter 3 in this thesis.

- Title: Firing stability of phosphorus-doped polysilicon passivating contacts: factors affecting the degradation behavior
- Authors: Di Kang, Hang Cheong Sio, Di Yan, Josua Stuckelberger, Xinyu Zhang, Daniel Macdonald
- Current status: Accepted by Solar Energy Materials and Solar Cells, September 2021, vol. 234, p. 1114407
- Contributions: DK designed the project, prepared the samples, performed the measurements, and wrote the manuscript. HCS and JS supervised the project and helped with the project design. XZ prepared the samples. DY and DM contributed to the data analysis. All the authors reviewed the manuscript.
- Declaration signed from a senior author:

Manuscript 2 is presented as Chapter 4 in this thesis.

- Title: Optimum hydrogen injection in phosphorus-doped polysilicon passivating contacts
- Authors: Di Kang, Hang Cheong Sio, Josua Stuckelberger, Rong Liu, Di Yan, Xinyu Zhang, Daniel Macdonald
- Current status: Published in ACS applied materials & interface, November 2021, vol. 13, pp. 55164 – 55171
- Contributions: DK designed the project, prepared the samples, performed the measurements, and wrote the manuscript. HCS and JS supervised the project and helped with the project design. RL performed the SIMS measurements.

XZ prepared the samples. DY and DM contributed to the data analysis. All the authors reviewed the manuscript.

- Declaration signed from a senior author:

Manuscript 3 is presented as Chapter 5 in this thesis.

- Title: Comparison of firing stability between p- and n-type polysilicon passivating contacts
- Authors: Di Kang, Hang Cheong Sio, Josua Stuckelberger, Di Yan, Sieu Pheng Phang, Rong Liu, Thien N. Truong, Tien Le, Hieu T. Nguyen, Xinyu Zhang, Daniel Macdonald
- Current status: Submitted to Progress in Photovoltaics, June 2021
- Contributions: DK designed the project, prepared the samples, performed the measurements, and wrote the manuscript. HCS and JS supervised the project and helped with the data analysis. RL performed the SIMS measurements. SPP helped with the project design. XZ prepared the samples. DY, TNT, TL, HTN and DM contributed to the data analysis. All the authors reviewed the manuscript.
- Declaration signed from a senior author:

Manuscript 4 is presented as Chapter 6 in this thesis.

- Title: Long-term stability study of the passivation quality of polysilicon-based passivation layers for silicon solar cells
- Authors: Di Kang, Hang Cheong Sio, Di Yan, Wenhao Chen, Jie Yang, Jingsheng Jin, Xinyu Zhang, Daniel Macdonald
- Current status: Published in Solar Energy Materials and Solar Cells, 2020, vol. 215, p. 110691
- Contributions: DK designed the project, prepared the samples, performed the measurements, and wrote the manuscript. HCS and DM supervised the project and helped with the data analysis. DY contributed to the data analysis. WC performed the GIXRD measurements. JY, JJ and XZ prepared the samples. All the authors reviewed the manuscript.

- Declaration signed from a senior author:

Manuscript 5 is presented as Chapter 7 in this thesis.

- Title: Light and Elevated Temperature Induced Degradation in Mono-Like and Float-Zone Silicon: Correlations to Material Types, Silicon Nitride Films and Dopant Diffusion
- Authors: Di Kang, Hang Cheong Sio, Xinyu Zhang, Jie Yang, Jinsheng Jin and Daniel Macdonald
- Current status: Published in IEEE Journal of Photovoltaics, 2021, vol. 11, pp. 1167 – 1175
- Contributions: DK designed the project, prepared the samples, performed the measurements, and wrote the manuscript. HCS and DM supervised the project and helped with the data analysis. JY, JJ and XZ prepared the samples. All the authors reviewed the manuscript.
- Declaration signed from a senior author:

Acknowledgement

I am greatly grateful to the Chair of my supervisory panel, Prof. Daniel Macdonald, for the continuous support. I would like to express my deep gratitude to Dr. Kelvin Sio, for his advice and encouragement, and especially for always being available for discussion. I really appreciate Dr. Josua Stuckelberger. I have been inspired by his profound knowledge and wisdom. I'm truly grateful to my co-supervisor Dr. Chang Sun, with the assistance regarding FTIR characterization and modelling the charge state of hydrogen in doped poly-Si. I would like to thank Dr. Di Yan for sharing his knowledge and insight on silicon solar cells.

Some other members of the group also provided assistance. I am deeply grateful to Dr. Sieu Pheng Phang who has trained me to use the PECVD system, and to do thermal diffusions. Thank Dr. Winney Yang for the help with ion-implantation. I would also like to express my undying appreciation to Dr. Anyao Liu, Dr. Hieu T. Nguyen, Dr. Lachlan Black, Dr. Teng Kho, Thien N. Truong and Tien Le for many fruitful discussions. I am especially thankful to Chris Samundsett, who has helped to process my samples. I'm greatly thankful to Maureen Brauers, James Cotsell and Bruce Condon for their support to keep the laboratory running so well.

I would like to thank Prof. Hoe Tan for training for X-ray diffraction in Chapter 6, and Prof. Fu Lan for generously providing access to FTIR in Chapter 3 and 7. I am also grateful to Dr. Fouad Karouta and Dr. Kaushal Vora for kindly allowing and assisting me in using PECVD and ellipsometry at the ANFF ACT Nodes. I would also like to thank Dr. Rong Liu for the SIMS measurements in Chapter 4 and 5. I am thankful to Dr. Xinyu Zhang, Dr. Jie Yang and Dr. Peiting Zheng from Jinko Solar, for preparing samples of Chapter 3, 4, 5 and 6.

Finally, I would like to express my deepest appreciation to my parents, my husband Weihao Jin, and my fur kid Ham, for their unconditional love and support over the last three years.

Abstract

High-temperature firing treatment is performed on commercial screen-printed solar cells to form metal contacts. However, the high-temperature firing step can directly deteriorate the surface passivation, and indirectly impact the long-term stability of the cell performance by triggering degradation in both the surface and the silicon bulk under illumination, or upon light soaking. This thesis studies the firing and long-term performance of polycrystalline silicon on silicon oxide (poly-Si/SiO_x) passivating contacts, and light and elevated temperature induced degradation (LeTID) in various types of silicon wafers.

First, this thesis examines the firing stability of n-type phosphorus doped poly-Si/SiO_x structures. Samples exhibit a substantial increase in the recombination current density parameter J_0 when the peak firing temperature reaches 800°C. The extent of degradation is sensitive to numerous factors, such as the firing temperature, the phosphorus diffusion conditions, and the dielectric coating layers. Various characterization tools, such as grazing incidence X-ray diffraction (GIXRD), Fourier transform infrared (FTIR) and secondary ion mass spectrometry (SIMS), are employed to investigate the root causes of the firing effect on n-type poly-Si passivation, revealing that the diffusion of hydrogen during firing determines the final passivation quality. The results indicate that an optimum amount of hydrogen surrounding the interfacial SiO_x is beneficial to achieve high-level surface passivation after firing, while an excess or insufficient amount of hydrogen is detrimental.

This thesis then extends to p-type boron-doped poly-Si. P-type poly-Si shows higher firing stability than n-type poly-Si, particularly at a firing temperature of 800°C or above. The combined results from SIMS and FTIR measurements indicate that hydrogen could play a role in the different firing stability of p- and n-type poly-Si. The experimental results suggest that the improved firing stability in p-type poly-Si could be owing to the lower effective hydrogen diffusivity, preventing the accumulation of excess hydrogen, which contributes to the degradation observed in n-type poly-Si.

The second part of this thesis studies the long-term stability of the poly-Si/SiO_x passivating contact structures. The high-temperature firing treatment is found to also activate a degradation and a subsequent recovery in n-type poly-Si/SiO_x passivating

contacts upon light soaking at temperatures between 75℃ and 200℃, which can lead to a pronounced increase in the J_0 and a reduction in the implied open circuit voltage (iV_{oc}). The degradation and regeneration kinetics depend strongly on the temperature and the light intensity. Increasing the light soaking temperature dramatically increases the rate of the degradation and the regeneration process, while at the same time reduces the magnitude of the degradation. Additionally, the regeneration process appears to be affected by the presence of silicon nitride (SiN_x) films during the light soaking treatment. Samples with SiN_x films removed after firing suffer a significantly larger degradation under illumination while showing no lifetime regeneration, suggesting the involvement of hydrogen.

In addition to the light soaking effect on the surface passivation of poly-Si, firing leads to a degradation phenomenon in the silicon bulk upon light soaking at elevated temperature, which is known as LeTID. In this thesis LeTID is compared on various types of silicon wafers, including p-type boron-doped and n-type phosphorus-doped mono-like silicon and float zone silicon. While all the studied materials exhibit degradation kinetics, p-type materials are found to generally suffer a higher degradation extent than their n-type counterparts. The silicon materials show a similar dependence on the SiN_x deposition conditions, with the degradation magnitude correlating strongly to the Si−N bond density and the refractive index of the SiN_x films, measured using FTIR and ellipsometry. It is observed that the degree of degradation can be reduced by phosphorus diffusion gettering and decreasing SiN_x deposition temperature, revealing a potential solution to mitigate LeTID.

Table of Contents

Introduction

Motivation

Solar photovoltaic (PV) technology converts sunlight directly into electricity by using semiconductors, with the global installed capacity growing exponentially. The PV market is largely dominated (above 90%) by crystalline silicon (c-Si) solar cells [1]. Conventional solar cells with full-area aluminum back-surface field (Al-BSF) manufactured by alloying the Al rear contact into the Si substrate have accounted for more than 70% of the c-Si PV production over the past decades [2]. However, recombination losses at the rear side are one limiting factor significantly constraining the conversion efficiencies for Al-BSF solar cells up to ~20% [3, 4].

In recent years, high-efficiency solar cell structures have been a key focus for current research and production. In particular, the passivated emitter and rear cell (PERC) structure, firstly reported by Blakers *et al*. [5] in 1989, received particular attention. The main difference between the Al-BSF and PERC structures is at the rear surface where the full-area Al back surface field is replaced by a dielectric passivation layer (usually with an aluminum oxide (AlO_x)/silicon nitride (SiN_x) stack) and local contacts. With such changes, the recombination of charge carriers at the rear surface can be substantially reduced, resulting in higher efficiency potential. The improved performance, in conjunction with a key advantage that the PERC production line requires only a few modifications and upgrades from the conventional Al-BSF solar cell manufacturing processes, allow the PERC technology to become an industrially predominant solar cell structure. The PERC device on p-type Czochralski-grown silicon (Cz-Si) wafers has reached an average conversion efficiency above 22.5% and a champion efficiency of 23.83% in mass production [6], and LONGi Solar announced a record efficiency of 24.06% on their bifacial PERC cell [7].

On the other hand, even with the use of localized rear contacts, the performance of the PERC cells is still limited by the recombination at the metal/semiconductor interface. To further address this problem, polycrystalline silicon on silicon oxide (poly-Si/SiO_x) passivating contacts were pioneered in the 80s under the name semi-insulating poly-crystalline silicon (SIPOS) [8-10], and then were rediscovered by Feldmann *et al*. [11, 12] and Römer *et al*. [13] in 2014. The poly-Si/SiO_x passivating contact structure [14,

15], also known as tunnel oxide passivated contact (TOPCon) [11, 12] and polysilicon on oxide (POLO) [13, 16, 17], generally features an ultrathin SiO_x film (~1 to 2.5 nm) embedded between the c-Si substrate and the poly-Si film. Extremely low recombination current density parameter J_0 values and contact resistivity at the metal/Si interface have been reported on doped poly-Si passivating contact structures processed in laboratories [17-20]. Yan *et al*. [18] demonstrated phosphorus-doped polysilicon with a 1.4 nm thick SiO_x that achieved a J_0 of ~2 fA/cm^2 and contact resistivity of ~3 × 10^{-3} Ω·cm^2. Moreover, the Institute for Solar Energy Research Hamelin (ISFH) reported a record efficiency as high as 26.1% on interdigitated back contacted (IBC) solar cells with POLO passivating contacts [17], and Fraunhofer ISE achieved 26% on both-sides-contacted solar cells based on TOPCon technology [21]. Due to the remarkable electrical performance and good compatibility with existing Al-BSF and PERC production lines, phosphorus-doped poly-Si/SiO_x passivating contacts have been applied on the rear side of c-Si wafer as passivating electron contact in commercial two-side contacted n-type solar cells, and shows great promise towards excellent performance, with increasing implementation for mass production. PV manufacturers, such as Jinko Solar [22], have achieved an impressive efficiency above 25.2% on large-area bifacial n-type TOPCon monocrystalline silicon solar cells in pilot production, and LONGi [23] reported 25.19% efficiency for p-type TOPCon solar cell. The International Technology Roadmap for Photovoltaic (ITRPV) predicts that the doped poly-Si/SiO_x passivating contact will gain significant market share in the near future [24].

However, there are some challenges when transferring doped poly-Si passivating contact technology from lab-scale to mass production. In particular, it has been reported that the high-temperature firing treatment, required for the screen-printed metallization can impact the passivation quality of n-type phosphorus-doped poly-Si structures in both contacted and non-contacted regions [25-31]. Çiftpınar *et al*. [25] observed a severe degradation in the recombination current density at the metal contacts (J_{0_met}), increasing from ~100 to 1400 fA/cm^2 on 75 nm n-type poly-Si after firing at 825°C. Stöhr *et al*. [31] reported that the J_0 of 100 nm poly-Si on thermal SiO_x passivating contact can increase from 1.5 to ~7 fA/cm^2 in the non-contacted region. In addition to the degraded surface passivation observed directly after firing, the firing process can trigger a degradation and a subsequent recovery in the surface passivation of poly-Si during prolonged illumination at elevated temperature. This is shown in the work by Winter *et al*. [32] who detected a pronounced degradation in the surface passivation of n-type poly-Si when subjected to 1

sun illumination at 185℃, leading to an increase in the J_0 from 49 to 132 fA/cm^2. Therefore, understanding and addressing the observed degradation is of great importance to maintain the performance of poly-Si based solar cells after firing and during long-term operation.

Moreover, firing introduces bulk degradation in the c-Si substrate upon light soaking, a phenomenon known as light and elevated temperature induced degradation (LeTID). It was reported that LeTID can cause performance losses of up to 10% relative in p-type boron-doped multi-crystalline silicon (mc-Si) PERC solar modules [33, 34]. While LeTID on p-type Si has been studied extensively [35-42], there are only a few works investigating degradation in n-type Si materials [39, 43, 44]. Chen *et al*. [43] observed that 2 Ω·cm n-type Cz-Si wafers suffered pronounced degradation in bulk lifetime. For solar cells with poly-Si/SiO_x passivating contacts, n-type c-Si wafers are often utilized, which requires high bulk lifetime. Therefore, it is necessary to study LeTID on n-type materials.

During the fabrication of poly-Si/SiO_x passivating contacts, hydrogenation treatment, a process to inject hydrogen into the poly-Si/SiO_x structure, is often applied to further improve the surface passivation. There are multiple processes that can supply hydrogen, such as forming gas anneal (FGA) [15, 45, 46], or by coating with a hydrogen-rich layer like SiN_x [26, 27, 47] or AlO_x [29, 48, 49], followed by a thermal annealing [50]. In particular, Stodolny *et al*. [26] showed an enhanced passivation quality of n-type poly-Si after SiN_x deposition, in which the J_0 value can decrease drastically from above 70 to ~10 fA/cm^2, depending on the SiO_x and poly-Si film properties. Yan *et al*. [15] observed that FGA at 400℃ for 30 min can result in a considerable improvement in the surface passivation of n-type poly-Si, with the J_0 value dropping from 60 to 7 fA/cm^2. Although hydrogen can be beneficial to poly-Si/SiO_x passivating contacts, it has been reported that hydrogen could attribute to LeTID [42, 51, 52] and the surface degradation observed in poly-Si passivation after firing [27, 29]. A better understanding on the role of hydrogen in poly-Si is thus needed for further improvement in the cell performance.

This thesis aims to assess the firing stability and long-term performance of doped poly-Si solar cells, with special attention given to the changes in the surface passivation of poly-Si/SiO_x passivating contacts. The mechanisms underlying the firing and light-soaking effects, particularly for the role of hydrogen, are explored in this thesis, providing new insights into the study on poly-Si passivating contact. This research on the

degradation behavior helps to identify the factors limiting poly-Si based solar cells, and to investigate the solutions to the impact on cell performance.

Thesis Outline

Chapter 1 introduces various bulk and surface recombination mechanisms in Si solar cells, and provides a brief overview on the doped poly-Si passivating contact technology, in the aspects of the surface passivation mechanism, the fabrication methods for SiO_x growth, poly-Si film deposition and doping methods, hydrogenation, and firing.

Chapter 2 introduces the main characterization techniques used in this thesis, including photoconductance measurement, Fourier transform infrared spectroscopy (FTIR), Secondary ion mass spectroscopy (SIMS) and Grazing incidence X-ray diffraction (GIXRD). The general principles, the system set-up and the applications are demonstrated for each characterization tool.

Chapter 3 provides an overview on the impact of firing on ex-situ doped n-type poly-Si passivating contacts prepared via low pressure chemical vapor deposition (LPCVD) on n-type Cz-Si or FZ-Si. It also evaluates various factors affecting the firing response on the surface passivation, including the peak firing temperature, the growth method of the interfacial SiO_x, the poly-Si deposition temperature, the phosphorus diffusion conditions, and the dielectric coating layers. The J_0 values are extracted to demonstrate the degradation behavior and the corresponding changes in the surface passivation quality. Moreover, GIXRD and FTIR are applied to identify correlations between the thermal stability and the properties of the poly-Si/SiO_x layers, such as the crystal structure and the hydrogen bond density in the dielectric coatings.

Chapter 4 is an extension of Chapter 3, further investigating the firing influence on n-type poly-Si. SIMS is applied to measure hydrogen content in the poly-Si/SiO_x stacks. The hydrogen concentration surrounding the SiO_x is correlated to the surface passivation on samples fired at different temperatures and with various dielectric coating layers. A mechanism underlying the firing impact is proposed. Based on the proposed model, the mechanisms for the dependence on the doping profile and the crystal properties observed in Chapter 3 is further explored.

Chapter 5 further extends the study on firing stability to ex-situ p-type boron-doped poly-Si/SiO_x passivating contacts on n-type FZ-Si. The firing response of p- and n-type poly-Si are compared. Furthermore, the effects of removing hydrogen from and adding additional hydrogen into fired p- and n-type poly-Si are assessed and compared, for which the removal of hydrogen from the SiO_x films is achieved by nitrogen anneal at 300°C after removing the fired SiN_x, and adding more hydrogen is realized by performing a subsequent SiN_x deposition and FGA after removing the fired SiN_x films. SIMS and FTIR characterization tools are employed to identify possible root causes for the different firing behavior in samples passivated by p- or n-type poly-Si.

Chapter 6 investigates the long-term stability (up to 100,000 minutes or 70 days) of phosphorus doped poly-Si passivation layers on n-type silicon substrates under illumination at elevated temperature. It also explores several impacting factors, including the light-soaking temperature, the light intensity, the poly-Si fabrication processes (comparing plasma-enhanced chemical vapor deposition (PECVD) and LPCVD), the firing profile, the properties of SiN_x films, and the presence or absence of SiN_x capping layers during the light soaking. A room temperature super-acid passivation technique is applied to monitor any variations in the bulk lifetimes of the samples during the stability experiments.

Chapter 7 studies LeTID in various types of Si materials, including p-type boron-doped and n-type phosphorus-doped mono-like Si and FZ-Si, and explores the impacts of SiN_x and dopant diffusion on the degradation behavior, to investigate the root causes of LeTID. To evaluate the potential role of hydrogen, the degradation extent in samples fired with different SiN_x films that were deposited at various conditions are compared. The atomic bond densities and the refractive index of the SiN_x films are measured by FTIR and ellipsometry, and are correlated to the degradation magnitude at the maximum degraded stage. Moreover, the influence of phosphorus diffusion on degradation rate and extent is evaluated using n-type mono-like Si and FZ-Si wafers.

References

[1] C. Battaglia, A. Cuevas, and S. De Wolf, "High-efficiency crystalline silicon solar cells: status and perspectives," *Energy & Environmental Science*, 10.1039/C5EE03380B vol. 9, no. 5, pp. 1552-1576, 2016.

[2] *International Technology Roadmap for Photovoltaic (ITRPV), 8th edition*, 2017. [Online]. Available: https://itrpv.vdma.org/en/.

[3] T. Fellmeth, S. Mack, J. Bartsch, D. Erath, U. Jäger, R. Preu, F. Clement, and D. Biro, "20.1% Efficient silicon solar cell with aluminum back surface field," *IEEE Electron Device Letters,* vol. 32, no. 8, pp. 1101-1103, 2011.

[4] A. Richter, M. Hermle, and S. W. Glunz, "Reassessment of the limiting efficiency for crystalline silicon solar cells," *IEEE Journal of Photovoltaics,* vol. 3, no. 4, pp. 1184-1191, 2013.

[5] A. W. Blakers, A. Wang, A. M. Milne, J. Zhao, and M. A. Green, "22.8% efficient silicon solar cell," *Applied Physics Letters,* vol. 55, no. 13, pp. 1363-1365, 1989.

[6] R. Chen, H. Tong, H. Zhu, C. Ding, H. Li, D. Chen, B. Hallam, C. M. Chong, S. Wenham, and A. Ciesla, "23.83% efficient mono-PERC incorporating advanced hydrogenation," *Progress in Photovoltaics: Research and Applications,* vol. 28, no. 12, pp. 1239-1247, 2020.

[7] LONGi, "LONGi Solar sets new bifacial mono-PERC solar cell world record at 24.06 percent," "Press release" [Online] Available: https://en.longi-solar.com/home/events/press_detail/id/89.html, 2019.

[8] E. Yablonovitch, T. Gmitter, R. M. Swanson, and Y. H. Kwark, "A 720 mV open circuit voltage SiOx:c-Si:SiOx double heterostructure solar cell," *Applied Physics Letters,* vol. 47, no. 11, pp. 1211-1213, 1985.

[9] Y. H. Kwark and R. M. Swanson, "N-type SIPOS and poly-silicon emitters," *Solid-State Electronics,* vol. 30, no. 11, pp. 1121-1125, 1987.

[10] Y. H. Kwark, R. Sinton, and R. M. Swanson, "SIPOS Heterojunction contacts to silicon," in *1984 International Electron Devices Meeting*, 1984, pp. 742-745.

[11] F. Feldmann, M. Bivour, C. Reichel, M. Hermle, and S. W. Glunz, "Passivated rear contacts for high-efficiency n-type Si solar cells providing high interface passivation quality and excellent transport characteristics," *Solar Energy Materials and Solar Cells,* vol. 120, pp. 270-274, 2014.

[12] F. Feldmann, M. Bivour, C. Reichel, H. Steinkemper, M. Hermle, and S. W. Glunz, "Tunnel oxide passivated contacts as an alternative to partial rear contacts," *Solar Energy Materials and Solar Cells,* vol. 131, pp. 46-50, 2014.

[13] U. Römer, R. Peibst, T. Ohrdes, B. Lim, J. Krügener, E. Bugiel, T. Wietler, and R. Brendel, "Recombination behavior and contact resistance of n+ and p+ poly-crystalline Si/mono-crystalline Si junctions," *Solar Energy Materials and Solar Cells,* vol. 131, pp. 85-91, 2014.

[14] D. Yan, A. Cuevas, Y. Wan, and J. Bullock, "Passivating contacts for silicon solar cells based on boron-diffused recrystallized amorphous silicon and thin dielectric interlayers," *Solar Energy Materials and Solar Cells,* vol. 152, pp. 73-79, 2016.

[15] D. Yan, A. Cuevas, J. Bullock, Y. Wan, and C. Samundsett, "Phosphorus-diffused polysilicon contacts for solar cells," *Solar Energy Materials and Solar Cells,* vol. 142, pp. 75-82, 2015.

[16] F. Haase, C. Hollemann, S. Schäfer, A. Merkle, M. Rienäcker, J. Krügener, R. Brendel, and R. Peibst, "Laser contact openings for local poly-Si-metal contacts enabling 26.1%-efficient POLO-IBC solar cells," *Solar Energy Materials and Solar Cells,* vol. 186, pp. 184-193, 2018.

[17] C. Hollemann, F. Haase, S. Schäfer, J. Krügener, R. Brendel, and R. Peibst, "26.1%-efficient POLO-IBC cells: Quantification of electrical and optical loss mechanisms," *Progress in Photovoltaics: Research and Applications,* vol. 27, no. 11, pp. 950-958, 2019.

[18] D. Yan, S. P. Phang, Y. Wan, C. Samundsett, D. Macdonald, and A. Cuevas, "High efficiency n-type silicon solar cells with passivating contacts based on PECVD silicon films doped by phosphorus diffusion," *Solar Energy Materials and Solar Cells,* vol. 193, pp. 80-84, 2019.

[19] A. Mewe, M. Stodolny, J. Anker, M. Lenes, X. Pagès, Y. Wu, K. Tool, B. Geerligs, and I. G. Romijn, "Full wafer size IBC cell with polysilicon passivating contacts," in *AIP Conference Proceedings 1999*, 2018, vol. 1999, p. 040014.

[20] K. C. Fong, T. C. Kho, W. Liang, T. K. Chong, M. Ernst, D. Walter, M. Stocks, E. Franklin, K. McIntosh, and A. Blakers, "Phosphorus diffused LPCVD polysilicon passivated contacts with in-situ low pressure oxidation," *Solar Energy Materials and Solar Cells,* vol. 186, pp. 236-242, 2018.

[21] Fraunhofer ISE, "Fraunhofer ISE sets new world record of 26 percent efficiency for both-sides-contacted solar cell," [Online] Available: https://www.ise.fraunhofer.de/en/press-media/press-releases/2021/fraunhofer-ise-sets-new-world-record-of-26-percent-efficiency-for-both-sides-contacted-solar-cell.html, April 2021.

[22] JinkoSolar, "JinkoSolar large-area n-type monocrystalline silicon solar cell reaches record-breaking new high efficiency of 25.25%," "Press release" [Online] Available: http://jinkosolar.com.au/2021/05/jinkosolar-large-area-n-type-monocrystalline-silicon-solar-cell-reaches-record-breaking-new-high-efficiency-of-25-25/, May 2021.

[23] LONGi, " Longi claims 25.19% efficiency for p-type TOPCon solar cell," "Press release" [Online] Available: https://www.pv-magazine.com/2021/07/21/longi-claims-25-19-efficiency-for-p-type-topcon-solar-cell/, July 2021.

[24] *International Technology Roadmap for Photovoltaic (ITRPV),* 10th edition ed., March 2019.

[25] H. E. Çiftpınar, M. K. Stodolny, Y. Wu, G. J. M. Janssen, J. Löffler, J. Schmitz, M. Lenes, J.-M. Luchies, and L. J. Geerligs, "Study of screen printed metallization for polysilicon based passivating contacts," *Energy Procedia,* vol. 124, pp. 851-861, 2017.

[26] M. K. Stodolny, M. Lenes, Y. Wu, G. J. M. Janssen, I. G. Romijn, J. R. M. Luchies, and L. J. Geerligs, "n-Type polysilicon passivating contact for industrial bifacial n-type solar cells," *Solar Energy Materials and Solar Cells,* vol. 158, pp. 24-28, 2016.

[27] B. Steinhauser, F. Feldmann, D. Ourinson, H. Nagel, T. Fellmeth, and M. Hermle, "On the influence of the SiNx composition on the firing stability of poly-Si/SiNx stacks," *physica status solidi (a),* vol. 217, no. 21, p. 2000333, 2020.

[28] F. Feldmann, T. Fellmeth, B. Steinhauser, H. Nagel, D. Ourinson, S. Mack, E. Lohmüller, J.-I. Polzin, J. Benick, J. Rentsch, M. Hermle, and S. Glunz, "Large area TOPCon cells realized by a PECVD tube process," in *36th European Photovoltaic Solar Energy Conference and Exhibition*, 2019, pp. 304-308.

[29] B. W. H. van de Loo, B. Macco, M. Schnabel, M. K. Stodolny, A. A. Mewe, D. L. Young, W. Nemeth, P. Stradins, and W. M. M. Kessels, "On the hydrogenation of Poly-Si passivating contacts by Al2O3 and SiNx thin films," *Solar Energy Materials and Solar Cells,* vol. 215, p. 110592, 2020.

[30] M. R. C. Hollemann, F. Haase, J. Krugener, R. Brendel, R. Peibst, "Influence of firing on the interface state density of n-type poly-Si passivating contacts," in *11th International Confrence on Crystalline Silicon Photovoltaics*, 2021,

[31] M. Stöhr, J. Aprojanz, R. Brendel, and T. Dullweber, "Firing-stable PECVD SiOxNy/n-poly-Si surface passivation for silicon solar cells," *ACS Applied Energy Materials,* vol. 4, no. 5, pp. 4646-4653, 2021.

[32] M. Winter, S. Bordihn, R. Peibst, R. Brendel, and J. Schmidt, "Degradation and Regeneration of n+ Doped Poly-Si Surface Passivation on p-Type and n-Type Cz-Si Under Illumination and Dark Annealing," *IEEE Journal of Photovoltaics,* vol. 10, pp. 1-8, 2020.

[33] F. Kersten, F. Fertig, K. Petter, B. Klöter, E. Herzog, M. B. Strobel, J. Heitmann, and J. W. Müller, "System performance loss due to LeTID," *Energy Procedia,* vol. 124, pp. 540-546, 2017.

[34] F. Kersten, P. Engelhart, H.-C. Ploigt, A. Stekolnikov, T. Lindner, F. Stenzel, M. Bartzsch, A. Szpeth, K. Petter, J. Heitmann, and J. W. Müller, "Degradation of multicrystalline silicon solar cells and modules after illumination at elevated temperature," *Solar Energy Materials and Solar Cells,* vol. 142, pp. 83-86, 2015.

[35] T. Niewelt, F. Schindler, W. Kwapil, R. Eberle, J. Schön, and M. C. Schubert, "Understanding the light-induced degradation at elevated temperatures: Similarities between multicrystalline and floatzone p-type silicon," *Progress in Photovoltaics: Research and Applications,* vol. 26, no. 8, pp. 533-542, 2018.

[36] W. Kwapil, J. Dalke, R. Post, and T. Niewelt, "Influence of dopant elements on degradation phenomena in B- and Ga-doped Czochralski-grown silicon," Solar RRL, vol. 5, no. 5, p. 2100147, 2021.

[37] D. Chen, M. Kim, B. V. Stefani, B. J. Hallam, M. D. Abbott, C. E. Chan, R. Chen, D. N. R. Payne, N. Nampalli, A. Ciesla, T. H. Fung, K. Kim, and S. R. Wenham, "Evidence of an identical firing-activated carrier-induced defect in monocrystalline and multicrystalline silicon," *Solar Energy Materials and Solar Cells,* vol. 172, pp. 293-300, 2017.

[38] K. Ramspeck, S. Zimmermann, H. Nagel, A. Metz, Y. Gassenbauer, and B. Birkmann, "Light induced degradation of rear passivated mc-si solar cells," in *27th European Photovoltaic Solar Energy Conference and Exhibition*, pp. 861-865, 2012.

[39] H. C. Sio, H. Wang, Q. Wang, C. Sun, W. Chen, H. Jin, and D. Macdonald, "Light and elevated temperature induced degradation in p-type and n-type cast-grown multicrystalline and mono-like silicon," *Solar Energy Materials and Solar Cells,* vol. 182, pp. 98-104, 2018.

[40] R. Eberle, W. Kwapil, F. Schindler, S. W. Glunz, and M. C. Schubert, "Firing temperature profile impact on light induced degradation in multicrystalline silicon," *Energy Procedia,* vol. 124, pp. 712-717, 2017.

[41] A. E. Morishige, M. A. Jensen, D. B. Needleman, K. Nakayashiki, J. Hofstetter, T. A. Li, and T. Buonassisi, "Lifetime Spectroscopy Investigation of Light-Induced Degradation in p-type Multicrystalline Silicon PERC," *IEEE Journal of Photovoltaics,* vol. 6, no. 6, pp. 1466-1472, 2016.

[42] J. Schmidt, D. Bredemeier, and D. C. Walter, "On the defect physics behind light and elevated temperature-induced degradation (LeTID) of multicrystalline silicon solar cells," *IEEE Journal of Photovoltaics,* vol. 9, no. 6, pp. 1497-1503, 2019.

[43] D. Chen, P. G. Hamer, M. Kim, T. H. Fung, G. Bourret-Sicotte, S. Liu, C. E. Chan, A. Ciesla, R. Chen, M. D. Abbott, B. J. Hallam, and S. R. Wenham, "Hydrogen induced degradation: A possible mechanism for light- and elevated temperature-induced degradation in n-type silicon," *Solar Energy Materials and Solar Cells,* vol. 185, pp. 174-182, 2018.

[44] C. Vargas, S. Nie, D. Chen, C. Chan, B. Hallam, G. Coletti, and Z. Hameiri, "Degradation and recovery of n-type multi-crystalline silicon under illuminated and dark annealing conditions at moderate temperatures," *IEEE Journal of Photovoltaics,* vol. 9, no. 2, pp. 355-363, 2019.

[45] T. N. Truong, D. Yan, W. Chen, M. Tebyetekerwa, M. Young, M. Al-Jassim, A. Cuevas, D. Macdonald, and H. T. Nguyen, "Hydrogenation mechanisms of poly-Si/SiOx passivating contacts by different capping layers," *Solar RRL,* vol. 4, no. 3, p. 2070033, 2020.

[46] M. Schnabel, B. W. H. v. d. Loo, W. Nemeth, B. Macco, P. Stradins, W. M. M. Kessels, and D. L. Young, "Hydrogen passivation of poly-Si/SiOx contacts for Si solar cells using Al2O3 studied with deuterium," *Applied Physics Letters*, vol. 112, no. 20, p. 203901, 2018.

[47] T. N. Truong, D. Yan, C. Samundsett, R. Basnet, M. Tebyetekerwa, L. Li, F. Kremer, A. Cuevas, D. Macdonald, and H. T. Nguyen, "Hydrogenation of phosphorus-doped polycrystalline silicon films for passivating contact solar cells," *ACS Applied Materials & Interfaces*, vol. 11, no. 5, pp. 5554-5560, 2019.

[48] B. Nemeth, D. L. Young, M. R. Page, V. LaSalvia, S. Johnston, R. Reedy, and P. Stradins, "Polycrystalline silicon passivated tunneling contacts for high efficiency silicon solar cells," *Journal of Materials Research*, vol. 31, no. 6, pp. 671-681, 2016.

[49] M. Schnabel, B. Van de Loo, W. Nemeth, B. Macco, P. Stradins, W. M. M. Kessels, and D. Young, "Hydrogen passivation of poly-Si/SiOx contacts for si solar cells using Al2O3 studied with deuterium," *Applied Physics Letters*, vol. 112, p. 203901, 2018.

[50] S. Mack, J. Schube, T. Fellmeth, F. Feldmann, M. Lenes, and J.-M. Luchies, "Metallisation of Boron-Doped Polysilicon Layers by Screen Printed Silver Pastes," *physica status solidi (RRL) – Rapid Research Letters*, vol. 11, no. 12, p. 1700334, 2017.

[51] C. Vargas, K. Kim, G. Coletti, D. Payne, C. Chan, S. Wenham, and Z. Hameiri, "Carrier-induced degradation in multicrystalline silicon: dependence on the silicon nitride passivation layer and hydrogen released during firing," *IEEE Journal of Photovoltaics*, vol. 8, no. 2, pp. 413-420, 2018.

[52] D. Bredemeier, D. C. Walter, R. Heller, and J. Schmidt, "Impact of hydrogen-rich silicon nitride material properties on light-induced lifetime degradation in multicrystalline silicon," *physica status solidi (RRL) – Rapid Research Letters*, vol. 13, no. 8, p. 1900201, 2019.

Chapter 1 – Carrier recombination and poly-Si passivation

1.1 Carrier recombination

Solar cells convert light energy into electricity. Under illumination, silicon (Si) absorbs the incident photons that have an energy greater than that of the band gap, transferring their energy to electrons and exciting them from the valence band to the conduction band, which creates electron-hole pairs. The opposite process of electron-hole pair generation, where the excess carriers decay back from the conduction band to the valence band by releasing energy, causing annihilation of electron-hole pairs, is known as recombination. Carriers that recombine in Si cannot contribute to the solar cell output. The excess carriers can only exist for only a limited time due to electron-hole recombination, and the term 'minority carrier lifetime' of a semiconductor, denoted by τ, is the average time of excess carriers from generation to recombination. It can be calculated according to:

$$\tau = \frac{\Delta n}{U} \qquad \textit{Eq. 1. 1}$$

where Δn is the excess carrier of electrons (for p-type material) or holes (for n-type material), and U denotes the recombination rate.

The minority carrier lifetime reflects the electrical quality of a material and is a significant parameter for solar cells to achieve a high conversion efficiency. The minority carrier lifetime is affected by numerous independent recombination mechanisms occurring within Si bulk and at surfaces. The effective lifetime τ_{eff} is often used to represent the overall recombination mechanism and is given by:

$$\frac{1}{\tau_{eff}} = \frac{1}{\tau_{bulk}} + \frac{1}{\tau_s} \qquad \textit{Eq. 1. 2}$$

where τ_{bulk} and τ_s represent bulk lifetime and surface lifetime respectively.

There are three fundamental recombination processes affecting the total carrier recombination lifetime: radiative recombination, Auger recombination, and recombination via recombination centers (commonly referred as Shockley-Read-Hall (SRH) recombination). Radiative and Auger recombination are intrinsic recombination in silicon, while recombination through defects is generally classified as extrinsic recombination. For indirect semiconductors such as Si, the radiative recombination is negligible compared to other recombination mechanisms. Therefore, this thesis is particularly concerned with the Auger and SRH recombination in Si bulk.

In addition to the recombination processes occurring within the bulk, the recombination at the surfaces significantly limits the performance of Si solar cells. Changes in surface passivation of polycrystalline silicon on silicon oxide (poly-Si/SiO_x) passivating contacts upon firing and light soaking are the main topic of this thesis. However, it is rather difficult to directly measure the surface recombination rate. The surface recombination mechanisms are commonly evaluated by measuring the effective lifetime and then subtracting the recombination effects from the Si bulk.

An overview of Auger and Shockly-Read-Hall (SRH) recombination in Si bulk, and surface recombination mechanism will be provided below.

1.1.1 Bulk recombination

1.1.1.1 Auger recombination

Auger recombination is the process when an electron recombines with a hole, through releasing the excess energy as heat or a photon to a third charge carrier, either an electron in the conduction band as depicted in Fig. 1. 1, or a hole in the valence band [1]. Auger recombination is the most dominant recombination mechanism in heavily doped regions or at high-level injection.

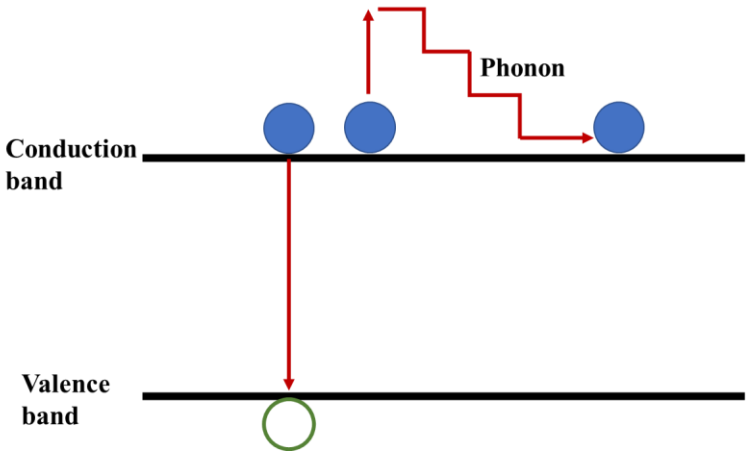

Fig. 1. 1 Auger recombination with the excess energy emitted to an electron in the conduction band.

The Auger recombination rate U_{Auger} is expressed as:

$$U_{Auger} = C_n \times \left(n^2 p - n_i^2\right) + C_p \times \left(np^2 - n_i^2\right) \qquad Eq.\ 1.3$$

where p is the holes concentration, n is the electron concentration, and n_i is the intrinsic carrier concentration. C_n and C_p denote the Auger recombination coefficients for n- and

p-type Si. Dziewior and Schmid [2] reported an Auger recombination coefficient of $C_n = 2.8 \times 10^{-31} cm^6 s^{-1}$ for n-type Si and $C_p = 9.9 \times 10^{-32} cm^6 s^{-1}$ for p-type Si.

The Auger lifetime can be written as:

$$\tau_{Auger} = \frac{1}{C_n(N_D+\Delta n)^2+C_p(N_D+\Delta n)\Delta n} \qquad \textit{for n-type Si} \qquad \textit{Eq. 1. 4}$$

$$\tau_{Auger} = \frac{1}{C_p(N_A+\Delta n)^2+C_n(N_A+\Delta n)\Delta n} \qquad \textit{for p-type Si} \qquad \textit{Eq. 1. 5}$$

where N_A and N_D represent the concentration of acceptor and donor dopants in Si.

The Auger recombination is also affected by other factors, such as Coulomb interactions between charge carriers [3, 4] and phonon participation [5, 6]. Due to the difficulties in theoretically determining the Auger recombination parameters, an empirical parameterization based on experimentally measured lifetimes, such as those reported by Kerr and Cuevas [7], and Richter *et al*. [8], is often applied to describe the Auger recombination.

The empirical determined τ_{Auger} can represent the intrinsic bulk lifetime τ_{bulk} of the sample, to extract the recombination current density parameter J_0 that reflects the overall recombination activities within the heavily doped regions and at the surfaces (the extraction of J_0 will be introduced in detail in Chapter 2). In this thesis, the full empirical formula proposed by Richter *et al*. [8] is used, and the τ_{bulk} of c-Si at 300 K is expressed as [8]:

$$\tau_{bulk} = \frac{\Delta n}{\left(np-n_{i,eff}^2\right)(2.5\times10^{-31}g_{eeh}n_0+8.5\times10^{-32}g_{ehh}p_0+3.0\times10^{-29}\Delta n^{0.92}+B_{rel}B_{low})} \qquad \textit{Eq. 1. 6}$$

With the enhancement factors

$$g_{eeh}(n_0) = 1 + 13\left\{1 - tanh\left[\left(\frac{n_0}{3.3\times10^{17}}\right)^{0.66}\right]\right\} \qquad \textit{Eq. 1. 7}$$

$$g_{ehh}(p_0) = 1 + 7.5\left\{1 - tanh\left[\left(\frac{p_0}{7.0\times10^{17}}\right)^{0.63}\right]\right\} \qquad \textit{Eq. 1. 8}$$

where $n_{i,eff} = 9.7 \times 10^9 cm^{-3}$ is effective intrinsic carrier concentration [9], B_{rel} is relative radiative recombination coefficient, and $B_{low} = 4.73 \times 10^{-15}\, cm^{-3} s^{-1}$ is radiative recombination [10].

1.1.1.2 Shockley-Read-Hall (SRH) recombination

The process of Shockley-Read-Hall (SRH) recombination is shown in Fig. 1. 2. Energy states or defect levels within the bandgap can exist due to crystal defects and impurities, allowing a free electron in the conduction band to transit into the defect level and then moving to the valence band via recombining with a hole. The recombination rate depends on various parameters, such as the electron and hole concentrations, the energy level of the defect, and capture and escape rate for electrons and holes.

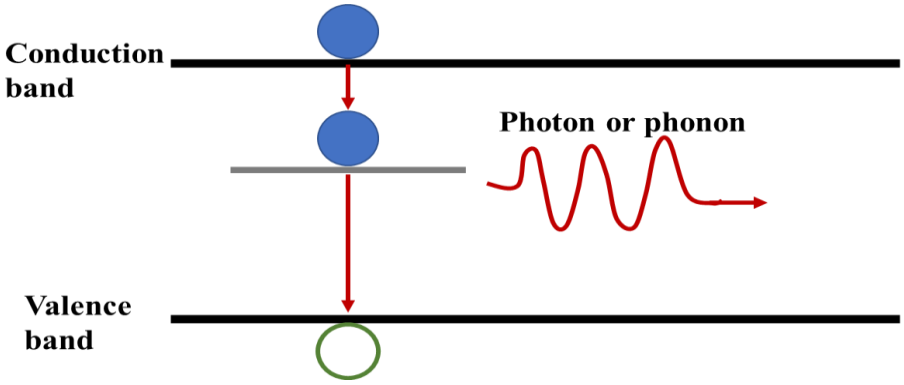

Fig. 1. 2 Representation of recombination via a defect in a semiconductor.

The recombination can be modelled using SRH statistics [11, 12], as shown in the equations below (for a single defect level):

$$U_{SRH} = \frac{v_{th}N_T(np-n_i^2)}{\frac{n+n_1}{\sigma_p}+\frac{p+p_1}{\sigma_n}} = \frac{np-n_i^2}{\tau_{p0}(n+n_1)+\tau_{n0}(p+p_1)} \qquad Eq.\ 1.\ 9$$

where σ_p and σ_n are the capture cross sections of holes and electrons respectively. N_T is the defect density. v_{th} represents the thermal velocity of charge carriers. n_1 and p_1 represent electron and hole density when Fermi level coincides with defect energy level E_T respectively.

The capture time constants τ_{p0} and τ_{n0} in Eq. 1. 9 are:

$$\tau_{p0} = \frac{1}{N_T\sigma_p v_{th}} \qquad Eq.\ 1.\ 10$$

$$\tau_{n0} = \frac{1}{N_T\sigma_n v_{th}} \qquad Eq.\ 1.\ 11$$

The electron density n_1 and hole density p_1 in Eq. 1. 9 are given by:

$$n_1 = N_c exp(\frac{E_T-E_c}{kT}) \qquad Eq.\ 1.\ 12$$

$$p_1 = N_v exp(\frac{E_v-E_T}{kT}) \qquad Eq.\ 1.\ 13$$

where N_c and N_v are the effective densities of states in the conduction and valence band respectively. E_c and E_v denote the conduction and valence band energies respectively.

These SRH parameters are signatures of a defect, hence are commonly used for defect characterization and identification. SRH analysis is performed in Chapter 7 to identify the defects in degraded Si substrates, according to the defect capture cross-section ratio σ_n/σ_p.

1.1.2 Surface recombination

Surface recombination is one of the most important factors constraining the performance of Si solar cells. Recombination is caused by the discontinuity of crystal lattice at the surface of crystalline silicon (c-Si) [13]. The surface is filled with unsaturated dangling bonds that act as defect levels within the Si bandgap, facilitating carrier recombination. Surface recombination is a special case of SRH recombination, with the defect levels commonly occupying multiple energy states, as depicted in Fig. 1. 3.

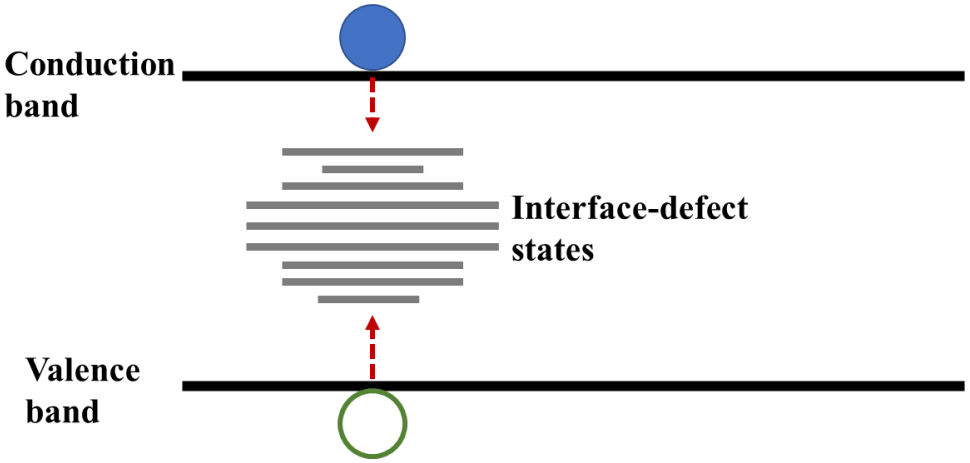

Fig. 1. 3 Representation of surface recombination in a semiconductor.

The surface recombination can be modelled using SRH statistics by integrating over the entire bandgap, as given below:

$$U_s = \int_{Ev}^{Ec} \frac{v_{th}(n_s p_s - n_i^2)}{\frac{n_s+n_1}{\sigma_p(E)} + \frac{p_s+p_1}{\sigma_n(E)}} D_{it}(E)dE \qquad \textit{Eq. 1. 14}$$

where n_s and p_s are the electron and hole densities at the surface. $\sigma_n(E)$ and $\sigma_p(E)$ are the electron and hole capture cross sections for each defect level. D_{it} represents the interface defect density.

However, determining the values of n_s, p_s, σ_n, σ_p and D_{it} is rather difficult. Eq. 1.14 can be simplified by using the effective surface recombination velocity SRV to describe the overall surface recombination rate, as shown below:

$$U_s = SRV \cdot \Delta n_s \qquad \textit{Eq. 1. 15}$$

where Δn_s is the excess carrier concentration at the surface. Most solar cells feature heavily doped regions for charge collection. The recombination behavior in the heavily doped regions is often classified also as a type of surface recombination, with the recombination rate written as:

$$U_s = \frac{J_0 np}{q n_i^2 W} \qquad \textit{Eq. 1. 16}$$

where W is the sample thickness.

The effective recombination lifetime due to the diffused region τ_s is expressed as:

$$\frac{1}{\tau_s} = \frac{U_s}{\Delta n} = \frac{J_0 (N_{dop} + \Delta n)}{q n_i^2 W} \qquad \textit{Eq. 1. 17}$$

where N_{dop} denotes the dopant concentration in Si bulk (acceptor for p-type Si and donor for n-type Si).

1.2 Doped polysilicon passivating contacts

The recombination mechanisms introduced in the previous sections are limiting the performance in Si solar cells. In particular, extremely low surface recombination is crucial for high-efficiency c-Si solar cells. Surface recombination is usually reduced by two ways: i) chemical passivation by terminating the dangling bonds, and ii) field-effect passivation by reducing the concentration of electrons or holes at the surface or interface. A widely implemented technique to efficiently passivate the surface is the deposition of dielectric films. However, due to the insulating nature of these films, for solar cells with such structures, such as PERC, the formation of direct contact of the metal to a semiconductor is required, leading to high recombination losses at the metal/c-Si interface. To reduce the losses, solar cell designs that avoid direct contact between metal and the silicon wafer were developed, without generating a barrier for majority carriers, denoted as passivating contacts. Additionally, carrier selective passivating contacts that passivate defects while simultaneously allow selective extraction of only one type of carrier can further improve the performance of contact structures and have become pivotal research objectives.

Among the carrier selective passivating contacts, doped polycrystalline silicon on silicon oxide (poly-Si/SiO_x) passivating contacts that consist of doped poly-Si film and a 1-2.5 nm ultrathin SiO_x layer have attracted significant attention in both PV industries and laboratories. While both phosphorus- and boron-doped poly-Si passivating contacts have been reported to provide low recombination current density parameter J_0 values and contact resistance at the metal/Si interface [14-24], p-type boron-doped polysilicon passivated contact shows an overall slightly higher J_0 and contact resistivity compared with phosphorus-doped (n-type) polysilicon.

The following sections in this chapter will review doped poly-Si/SiO_x passivating contacts in terms of the passivation mechanism and the fabrication methods.

1.2.1 Passivation mechanism of doped poly-Si/SiO_x passivating contacts

For the doped poly-Si/SiO_x passivating contact structure, recombination losses are reduced by providing a high field effect by the heavily doped poly-Si film, combined with the low-level penetration of dopants in the wafer, and good passivation between the thin oxide and the c-Si. The doped polysilicon film provides a field-effect passivation that arises from induced band-bending at the interface between poly-Si and c-Si, which prevents recombination of minority carriers onto the c-Si surface while allowing the majority carriers to move towards the contacts applied on the poly-Si film [25]. The selectivity and field-effect passivation are determined by the doping concentration within the poly-Si film [26]. The slight dopant penetration into the c-Si wafer supports the charge-carrier selectivity of the contact [21, 27, 28] and further reduces the electronic defect density at the c-Si/SiO_x interface [29].

The SiO_x interfacial layer passivates the defects and dangling bonds at the c-Si/SiO_x interface, and hence deactivating the recombination sites. In addition, the ultrathin SiO_x impedes dopant diffusion from the poly-Si film into the c-Si substrate during high temperature process, suppressing strong penetration of dopants into the c-Si substrate. The transport mechanism of the carriers through the thin oxide layer depends on the thickness of the oxide film, the annealing temperature, and the doping profile, as shown by Feldmann *et al*. [30]. There are mainly two transport mechanisms: the tunneling model, and the pinhole model. The tunneling model describes the transport of electrons or holes through the thin oxide by tunneling, assuming that SiO_x remains intact over the full area [30, 31]. The pinhole model depicts the transport by perturbations in the interfacial SiO_x leading to pinholes and direct contact between the c-Si wafer and the

poly-Si film [19, 32, 33]. While a thin SiO_x (low diffusion temperature) acts dominantly as a tunneling layer, with increasing thickness (or higher diffusion temperature), pinholes through the SiO_x become the dominating transport mechanism. A combination of both transport mechanisms is the most common instance for the thin SiO_x layer under poly-Si films [28, 30].

On the other hand, the surface doping concentration in poly-Si films could play a less significant role in the surface passivation of poly-Si passivating contacts. This is provided by Park *et al*. [26] who observed that, by etching the poly-Si film from 300 nm to 50 nm, the performance of phosphorus-doped poly-Si/SiO_x remained largely unchanged, while the passivation quality decreased substantially with further etch-back treatment.

1.2.2 Fabrication of doped poly-Si/SiO_x passivating contacts

With doped poly-Si/SiO_x passivating contacts, the low concentration of minority carriers at the metal contact and the SiO_x/c-Si interface, in conjunction with the low-level penetration of dopants in the c-Si wafer, lead to excellent passivation performance and great efficiency potential for devices. Another key advantage of poly-Si passivating contact technology is the great industrial compatibility. When upgrading the existing PERC production lines for poly-Si/SiO_x solar cells, addition of minimum number of process steps is required, such as growth of interfacial SiO_x and deposition of poly-Si, making a fast industrial adoption of this technology possible. Production of n-type poly-Si/SiO_x is already underway, and photovoltaics (PV) manufacturers have shown promising results. Jinko Solar [34] and LONGi [35] have reached an impressive efficiency above 25.2% on the double-side contacted cell structure in a pilot production line. Fig. 1. 4 demonstrates a typical double-side contacted cell structure consisting of boron-doped p^+ regions and a stack of AlO_x/SiN_x dielectric films on the front side, and a SiN_x layer on n^+ poly-Si/SiO_x contacts at rear. In this thesis, some of the samples (Cz-Si samples) used in Chapter 3, 4 and 6 were prepared in an industrial production line at Jinko Solar, based on the fabrication procedure for the cell structure shown in Fig. 1. 4.

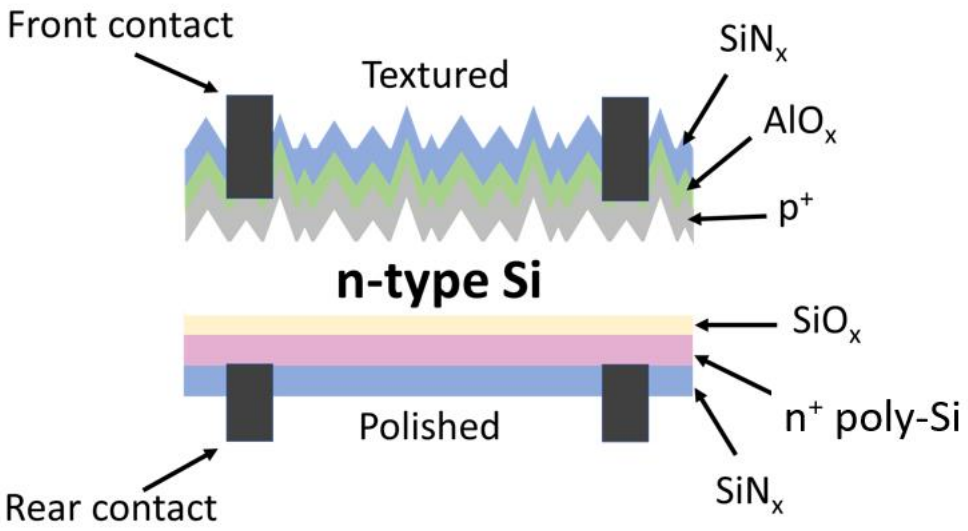

Fig. 1. 4 Schematic diagram for a typical double-side contacted n-type Si solar cell with n-type poly-Si/SiO_x passivating contact structure.

In addition to industrially processed samples, poly-Si passivating contacts prepared at our lab are also studied. Due to the remarkable electrical properties, many research groups have been working on the application of doped poly-Si, using different processing methods. The technology is also denoted by different names, such as Tunnel Oxide Passivated Contact (TOPCon) [17, 36] and polysilicon on oxide (POLO) [18, 37]. Nevertheless, the main processing flow to fabricate poly-Si/SiO_x passivating contacts used in research groups and PV industries is similar, including growth of thin oxide, deposition of amorphous silicon (a-Si), doping, activation of dopants and crystallization, and hydrogenation. The commonly used processing tools and methods are summarized in Fig. 1. 5, and details will be described below.

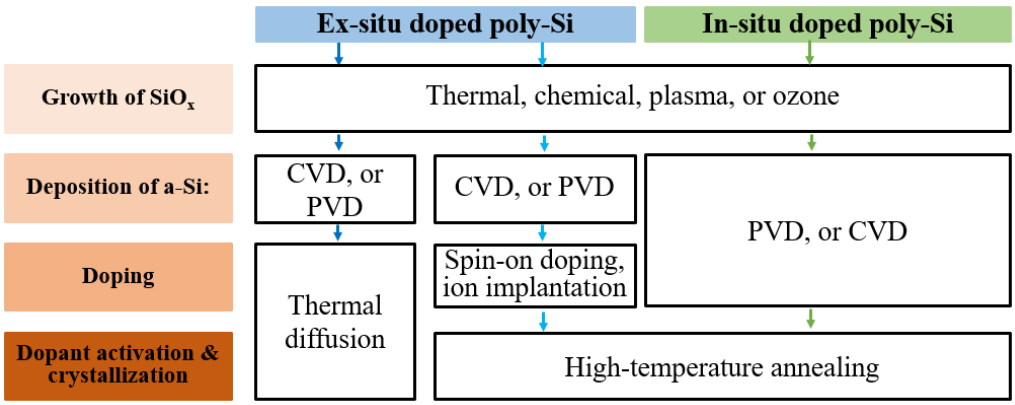

Fig. 1. 5 Key process flow for the fabrication of poly-Si/SiO_x passivating contacts.

1.2.2.1 Growth of SiO_x

The thin SiO_x film can be grown either in wet chemical [38-40], using ozone oxidation [41, 42], plasma-assisted nitrous-oxide (N_2O) gas oxidation [43, 44] or in thermal furnace with oxygen [20, 45, 46]. This thesis studies poly-Si samples with chemical (68 wt% nitric acid bath at a temperature of ~90℃ for 30 min) or thermal oxide (at 600℃ for 5 min in O_2).

The SiO_x growth conditions and properties of the SiO_x film are of great significance for the passivation quality and contact resistivity. The thickness of the SiO_x interlayer is one of the key parameters influencing the passivation quality of poly-Si/SiO_x contacts [22, 47, 48]. While SiO_x with a thickness larger than 2 nm was reported to block the penetration of phosphorus into the c-Si [47] and does not allow tunneling through the SiO_x, a SiO_x film thinner than 0.5 nm was found to be insufficient to provide good chemical passivation [49]. For ex-situ doped n-type PECVD poly-Si processed in our lab, an optimum SiO_x thickness of ~1.4 nm was reported by Yan *et al*. [47]. Therefore, in this thesis, SiO_x films with a thickness of ~1.4 nm are used for the poly-Si samples in Chapter 3, 4, 5 and 6. In addition, the properties of the thin oxide can affect the thermal stability of poly-Si passivating contacts, evident from the literature [42, 48, 50]. In Chapter 3, firing stability of chemical and thermal oxide with a similar thickness will be compared, to further explore the correlation between oxide properties and thermal stability.

1.2.2.2 Poly-Si deposition and doping

The a-Si film is deposited either using chemical vapor deposition (CVD) tools, such as PECVD [17, 47, 51] and low-pressure chemical vapor deposition (LPCVD) [15, 16, 18, 52], or physical vapor deposition (PVD) systems like sputter coater [53] and electron beam [54]. Among the techniques for a-Si deposition, LPCVD is one of the most commonly used tools for mass production. Depending on the deposition method, the doping of poly-Si is performed either in-situ or ex-situ, as shown in Fig. 1. 5. In-situ doping technology simultaneously introduces dopants and deposits a-Si on thin SiO_x, which can be performed using CVD or PVD, followed by a high-temperature anneal (above 750°C) to activate dopants and crystalize poly-Si. A thermal diffusion using $POCl_3$ or BBr_3 source after the deposition of a-Si are widely used to fabricate commercial poly-Si passivated devices [16, 51], due to the simplicity of process flow and their similarity with the fabrication process of PERC cells. One key advantage of the process is that additional anneal for activation and crystallization is not required. Alternatively,

low-temperature ex-situ doping processes, such as spin-on doping [55-57], or ion implantation [58] are also applied to produce poly-Si passivating contacts in laboratories. Similar to the in-situ doping method, the processes also require a post annealing for dopant activation and crystallization. An optimum doping profile is essential for the quality of poly-Si passivation, to ensure a low doping level in the c-Si substrate via the thin SiO_x, since heavy doping in the wafer can lead to increased Auger recombination [16, 47, 56] and the diffusion through the SiO_x interlayer can deteriorate the surface passivation [47, 59, 60].

This thesis investigates ex-situ doped PECVD or LPCVD poly-Si, which are considered as two main technologies for high-performance cells in combination with high volume production. Samples prepared using our laboratory process are studied in Chapter 3, 5, and 6. For LPCVD deposited poly-Si processed at our lab, Fong *et al*. [15] reported that a J_0 of ~3 fA/cm^2 and contact resistivity below 3 × 10^{-3} Ω·cm^2 have been achieved on laboratory n-type poly-Si with 1.5 nm interfacial thermal oxide. Ex-situ doped LPCVD poly-Si has been already implemented for high volume production in PV industries [34, 46, 52, 61] and shown promising results. With an industrial fabrication process, Trina Solar achieved a J_0 of ~3.7 fA/cm^2 (passivated region on textured surface), a median efficiency of 23.91% and a champion efficiency of 24.58% on large-area n-type solar cells [52]. For ex-situ doped PECVD poly-Si processed using our laboratory facilities, a J_0 of ~2 fA/cm^2 and contact resistivity of ~3 × 10^{-3} Ω·cm^2 was demonstrated by Yan *et al*. [14] on n-type poly-Si with a 1.4 nm thick SiO_x. In addition, PECVD technology offers higher deposition rates compared to LPCVD technology [62] and allows single-side deposition, thereby potential improvement in cost-effectiveness and flexibility in fabrication flow.

On the other hand, poly-Si layers deposited using LPCVD and PECVD exhibit different film properties, leading to different passivation quality and thermal stability. It was reported that blistering in thick poly-Si layers caused by a high concentration of hydrogen is a key challenge limiting the performance of PECVD deposited poly-Si [63, 64]. This is a crucial aspect considering that the current industrial manufacturing process features high temperature steps, which can cause further blistering and hence degrade the surface passivation [64-66]. For ex-situ doped LPCVD and PECVD poly-Si technologies, researchers have investigated the influence of the poly-Si deposition parameters [46, 67, 68] and doping conditions [15, 47] on the properties of SiO_x and poly-Si. In this thesis,

these processing parameters are also adjusted, to explore their impacts on the firing stability, with the results shown in Chapter 3.

1.2.2.3 Hydrogenation of poly-Si/SiO_x passivating contacts

After doping and crystallization steps, dangling bonds and electrically active defects at the c-Si/SiO_x interface and within the doped poly-Si film may not be fully passivated, which limits the performance of poly-Si passivation. Therefore, additional level of chemical passivation can be achieved by introducing hydrogen to the SiO_x interlayer through the poly-Si film, to passivate the dangling bonds [69-74] and the defects within the poly-Si layers [71, 75].

There are multiple methods to hydrogenate the poly-Si and the underlying c-Si/SiO_x interface. Exposure to hydrogen plasma [76, 77], or capping with a hydrogen-rich layer, such as SiN_x [16, 71, 78] or AlO_x [79-81], have been proven to effectively hydrogenate poly-Si/SiO_x passivating contacts. Note that a subsequent thermal annealing after SiN_x or AlO_x deposition is generally needed to release hydrogen into the poly-Si/SiO_x for hydrogenation purpose [71, 81, 82]. Forming gas anneal (FGA) is also a commonly used process to hydrogenate poly-Si, but appears to be less effective compared to annealing with hydrogen-rich layers [75, 83]. Other techniques, such as annealing in atmosphere containing water vapor [84], and coating with a transparent conducting oxide (TCO) layer [85], can also passivate the defects in poly-Si devices.

In this thesis, the poly-Si samples were either hydrogenated by depositing SiN_x or AlO_x single layers, AlO_x/SiN_x stacks (with or without annealing), or a combination of FGA and SiN_x deposition. These passivation techniques have been confirmed to effectively supply hydrogen to the poly-Si contact, leading to increased hydrogen content surrounding the SiO_x and improvement in the J_0 [81, 83]. For such hydrogenation techniques, the concentration of hydrogen released into the sample and the improvement of surface passivation strongly depend on the properties of the dielectric coating film [83] and annealing temperature [80]. Therefore, in this thesis, the role of hydrogen in the changes of poly-Si passivation is examined using samples fired with various dielectric capping layers, or at different temperatures, with the details shown in Chapter 3, 6 and 7. The effectiveness of hydrogenation can be also affected by the doping profile in the poly-Si sample [47, 86]. Yan *et al*. [47] observed that FGA is only beneficial to lightly doped poly-Si, whereas poly-Si with an excessive level of doping shows minimal changes after

hydrogenation. The mechanism for influence of doping profile in hydrogenation will be studied in Chapter 4.

1.2.2.4 Firing

The hydrogenation treatment for large-scale mass production of poly-Si solar cells is slightly different compared to the laboratory process. For commercial cells, the cells do not receive any FGA nor any additional thermal anneal after the deposition of dielectric coating films, and the hydrogen is commonly introduced into the device by deposition of dielectric layers and a subsequent metallization firing step. The high-temperature firing step for poly-Si cells enables screen-printed metal paste to penetrate the SiN_x film and form ohmic contact with the doped poly-Si. Screen-printing contacts employs a paste consisting of metal particles, organic binders and metal-oxide glass frit. During contact firing, the frit used in the paste assists contact formation by promoting reactions between the metal paste and the antireflective coating. In PV industries, belt furnace is commonly used for the firing treatment, with a typical peak firing temperature in a range from 750℃ to 800℃ [52, 87, 88], depending on the metallization paste. Fig. 1. 6 (a) presents a typical firing profile used for Si solar cells with screen-printed silver (Ag) paste on the front and aluminum (Al) paste metallization at rear [89]. During heating, the ramp-up rate is 30 ℃/s to 40 ℃/s (cell temperature increasing from 50℃ to 600℃). Al starts to melt at ~660℃, and forms Si-Al composition. The temperature then increases from 660℃ to the peak firing temperature of ~800℃ with a ramp-up rate of ~30 ℃/s. The peak temperature lasts 1 to 2 s to induce Ag sintering, which enables SiN_x burn-through and the formation of Ag-Si contacts. The process is then followed by a cooling process with a ramp-down rate of 20 ℃/s to 30 ℃/s. When the temperature is below the eutectic point at ~577 ℃, the Al particles react with the Si surface, resulting in an eutectic layer [90].

In this thesis, the firing step was performed using a rapid thermal processing (RTP) tool, with samples covered by a 180 μm dummy wafer on each side to avoid potential influence caused by the strong illumination from the lamps. As an example, the temperature profile (temperature measured on the bottom dummy wafer by a thermocouple) for the 800℃ firing treatment in Chapter 3, 4 and 5 is given in Fig. 1. 6 (b). During firing, the ramp-up rate was set to 30 ℃/s until reaching the peak firing temperature. The samples were fired for 1 s at the peak firing temperature, followed by a cooling step with a ramp-down rate of 60 ℃/s in nitrogen environment. The peak firing temperature was varied from 600℃ to 900℃, while remaining the heating and cooling rate unchanged.

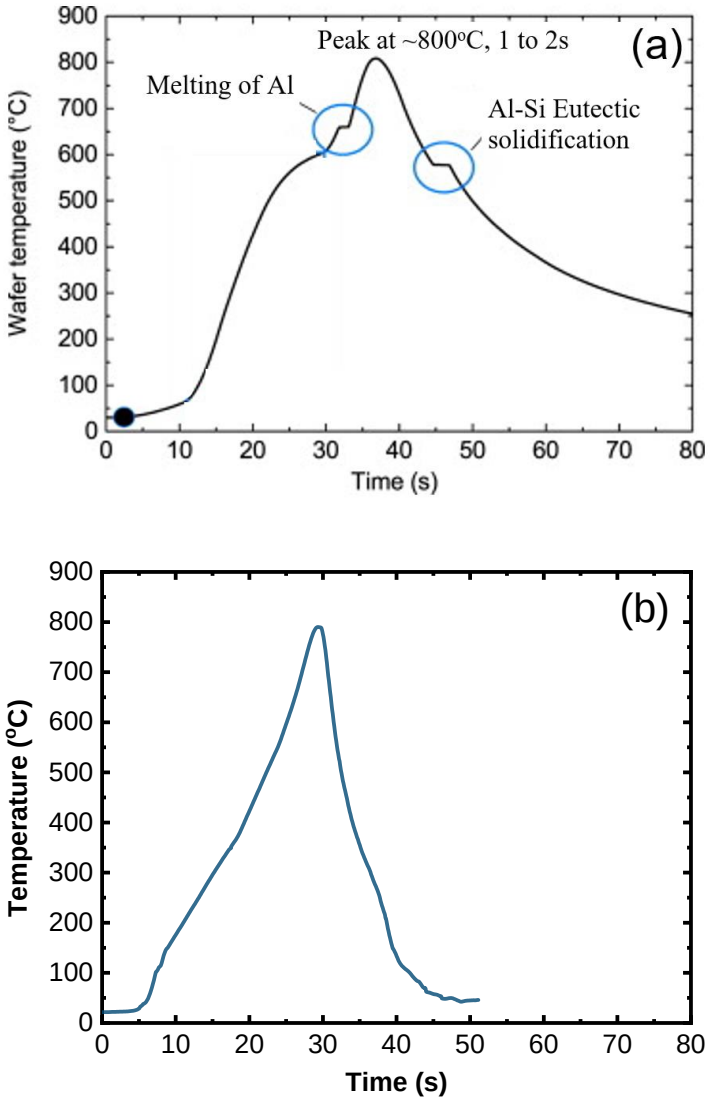

Fig. 1. 6 (a) A typical firing profile used for commercial screen-printed Si solar cells with silver (Ag) front contact and rear aluminum (Al) contact, reprinted from Ref. [89]. (b) The temperature profile employed for the 800℃ firing treatment in Chapter 3, 4 and 5 (the temperature values were measured on the bottom dummy wafer by a thermocouple).

The high-temperature rapid firing could potentially impact the performance of poly-Si, depending on the properties of the poly-Si/SiO_x passivating contact [16, 17, 64, 66, 78, 91, 92]. Feldmann *et al*. [17] observed a lower level of n-type poly-Si passivation after a 760℃ belt-furnace firing, with the surface degradation recovered by a subsequent FGA after firing. Stodolny *et al*. [16] detected degradation only on lightly doped poly-Si, whereas the heavily doped poly-Si showed improved firing stability. Steinhauser, *et al*. [78] reported that firing is detrimental to n-type poly-Si passivation, with the degradation in J_0 upon firing increases with increasing firing temperature. They also showed a direct

correlation between the firing stability of poly-Si capped with SiN_x and the refractive index of the SiN_x coating, reporting that a refractive index > 2 allows samples to be resistant to firing damage, indicating the involvement of hydrogen [78]. Hollemann *et al*. [92] suggested that, in addition to hydrogen, thermally induced stress generated by the large temperature gradient during the rapid firing could be responsible for the surface degradation after firing. The preliminary results given in the literature also indicate that p-type poly-Si exhibits improved firing stability compared to n-type poly-Si [80, 91]. This thesis will further study the firing stability of n- and p-type poly-Si in Chapter 3, 4 and 5.

References

[1] M. A. Green, *Solar cells : operating principles, technology and system applications* (Accessed from https://nla.gov.au/nla.cat-vn1641381). Kensington, N.S.W: University of New South Wales, 1992.

[2] J. Dziewior and W. Schmid, "Auger coefficients for highly doped and highly excited silicon," *Applied Physics Letters,* vol. 31, no. 5, pp. 346-348, 1977.

[3] P. P. Altermatt, J. Schmidt, G. Heiser, and A. G. Aberle, "Assessment and parameterisation of Coulomb-enhanced Auger recombination coefficients in lowly injected crystalline silicon," *Journal of Applied Physics,* vol. 82, no. 10, pp. 4938-4944, 1997.

[4] A. Hangleiter and R. Häcker, "Enhancement of band-to-band Auger recombination by electron-hole correlations," *Physical Review Letters,* vol. 65, no. 2, pp. 215-218, 1990.

[5] D. B. Laks, G. F. Neumark, and S. T. Pantelides, "Accurate interband-Auger-recombination rates in silicon," *Physical Review B,* vol. 42, no. 8, pp. 5176-5185, 1990.

[6] M. Govoni, I. Marri, and S. Ossicini, "Auger recombination in Si and GaAs semiconductors: Ab initio results," *Physical Review B,* vol. 84, no. 7, p. 075215, 2011.

[7] M. J. Kerr and A. Cuevas, "General parameterization of Auger recombination in crystalline silicon," *Journal of Applied Physics,* vol. 91, no. 4, pp. 2473-2480, 2002.

[8] A. Richter, S. W. Glunz, F. Werner, J. Schmidt, and A. Cuevas, "Improved quantitative description of Auger recombination in crystalline silicon," *Physical Review B,* vol. 86, no. 16, p. 165202, 2012.

[9] P. P. Altermatt, A. Schenk, F. Geelhaar, and G. Heiser, "Reassessment of the intrinsic carrier density in crystalline silicon in view of band-gap narrowing," *Journal of Applied Physics,* vol. 93, no. 3, pp. 1598-1604, 2003.

[10] T. Trupke, M. A. Green, P. Würfel, P. P. Altermatt, A. Wang, J. Zhao, and R. Corkish, "Temperature dependence of the radiative recombination coefficient of intrinsic crystalline silicon," *Journal of Applied Physics,* vol. 94, no. 8, pp. 4930-4937, 2003.

[11] W. Shockley and W. T. Read, "Statistics of the recombinations of holes and electrons," *Physical Review,* vol. 87, no. 5, pp. 835-842, 1952.

[12] R. N. Hall, "Electron-hole recombination in germanium," *Physical Review,* vol. 87, no. 2, pp. 387-387, 1952.

[13] J. I. Pankove, "Chapter 3 Hydrogenation of Defects in Crystalline Silicon," in *Semiconductors and Semimetals*, vol. 34, J. I. Pankove and N. M. Johnson Eds.: Elsevier, 1991, pp. 35-47.

[14] D. Yan, S. P. Phang, Y. Wan, C. Samundsett, D. Macdonald, and A. Cuevas, "High efficiency n-type silicon solar cells with passivating contacts based on PECVD silicon films doped by phosphorus diffusion," *Solar Energy Materials and Solar Cells*, vol. 193, pp. 80-84, 2019.

[15] K. C. Fong, T. C. Kho, W. Liang, T. K. Chong, M. Ernst, D. Walter, M. Stocks, E. Franklin, K. McIntosh, and A. Blakers, "Phosphorus diffused LPCVD polysilicon passivated contacts with in-situ low pressure oxidation," *Solar Energy Materials and Solar Cells*, vol. 186, pp. 236-242, 2018.

[16] M. K. Stodolny, M. Lenes, Y. Wu, G. J. M. Janssen, I. G. Romijn, J. R. M. Luchies, and L. J. Geerligs, "n-Type polysilicon passivating contact for industrial bifacial n-type solar cells," *Solar Energy Materials and Solar Cells*, vol. 158, pp. 24-28, 2016.

[17] F. Feldmann, T. Fellmeth, B. Steinhauser, H. Nagel, D. Ourinson, S. Mack, E. Lohmüller, J.-I. Polzin, J. Benick, J. Rentsch, M. Hermle, and S. Glunz, "Large area TOPCon cells realized by a PECVD tube process," in *36th European Photovoltaic Solar Energy Conference and Exhibition*, 2019, pp. 304-308.

[18] C. Hollemann, F. Haase, S. Schäfer, J. Krügener, R. Brendel, and R. Peibst, "26.1%-efficient POLO-IBC cells: Quantification of electrical and optical loss mechanisms," *Progress in Photovoltaics: Research and Applications*, vol. 27, no. 11, pp. 950-958, 2019.

[19] R. Peibst, U. Römer, Y. Larionova, M. Rienäcker, A. Merkle, N. Folchert, S. Reiter, M. Turcu, B. Min, J. Krügener, D. Tetzlaff, E. Bugiel, T. Wietler, and R. Brendel, "Working principle of carrier selective poly-Si/c-Si junctions: Is tunnelling the whole story?," *Solar Energy Materials and Solar Cells*, vol. 158, pp. 60-67, 2016.

[20] D. Yan, A. Cuevas, Y. Wan, and J. Bullock, "Passivating contacts for silicon solar cells based on boron-diffused recrystallized amorphous silicon and thin dielectric interlayers," *Solar Energy Materials and Solar Cells*, vol. 152, pp. 73-79, 2016.

[21] J. Y. Gan and R. M. Swanson, "Polysilicon emitters for silicon concentrator solar cells," in *IEEE Conference on Photovoltaic Specialists*, 1990, pp. 245-250 vol.1.

[22] F. Feldmann, M. Bivour, C. Reichel, H. Steinkemper, M. Hermle, and S. W. Glunz, "Tunnel oxide passivated contacts as an alternative to partial rear contacts," *Solar Energy Materials and Solar Cells*, vol. 131, pp. 46-50, 2014.

[23] M. Stodolny, J. Anker, C. Tool, M. Koppes, A. Mewe, P. Manshanden, M. Lenes, and I. G. Romijn, "Novel schemes of p+ polySi hydrogenation implemented in industrial 6" bifacial front-and-rear passivating contacts solar cells," in *35th European Photovoltaic Solar Energy Conference and Exhibition*, 2018, pp. 414 - 417.

[24] G. Yang, A. Ingenito, O. Isabella, and M. Zeman, "IBC c-Si solar cells based on ion-implanted poly-silicon passivating contacts," *Solar Energy Materials and Solar Cells*, vol. 158, pp. 84-90, 2016.

[25] A. Cuevas, Y. Wan, D. Yan, C. Samundsett, T. Allen, X. Zhang, J. Cui, and J. Bullock, "Carrier population control and surface passivation in solar cells," *Solar Energy Materials and Solar Cells*, vol. 184, pp. 38-47, 2018.

[26] H. Park, S. Bae, S. Park, J. Hyun, C. Lee, D. Choi, D. Kang, H. Han, Y. Kang, H.-S. Lee, and D. Kim, "Role of polysilicon in poly-Si/SiOx passivating contacts for high-efficiency silicon solar cells," *RSC Advances*, vol. 9, pp. 23261-23266, 2019.

[27] S. W. Glunz, M. Bivour, C. Messmer, F. Feldmann, R. Müller, C. Reichel, A. Richter, F. Schindler, J. Benick, and M. Hermle, "Passivating and carrier-selective contacts - Basic requirements and implementation," in *2017 IEEE 44th Photovoltaic Specialist Conference (PVSC)*, 2017, pp. 2064-2069.

[28] R. Brendel and R. Peibst, "Contact selectivity and efficiency in crystalline silicon photovoltaics," *IEEE Journal of Photovoltaics*, vol. 6, no. 6, pp. 1413-1420, 2016.

[29] A. Stesmans, "Dissociation kinetics of hydrogen-passivated Pb defects at the (111)Si/SiO2 interface," *Physical Review B*, vol. 61, no. 12, pp. 8393-8403, 2000.

[30] F. Feldmann, G. Nogay, P. Löper, D. L. Young, B. G. Lee, P. Stradins, M. Hermle, and S. W. Glunz, "Charge carrier transport mechanisms of passivating contacts studied by temperature-dependent J-V measurements," *Solar Energy Materials and Solar Cells*, vol. 178, pp. 15-19, 2018.

[31] H. Steinkemper, F. Feldmann, M. Bivour, and M. Hermle, "Numerical simulation of carrier-selective electron contacts featuring tunnel oxides," *IEEE Journal of Photovoltaics*, vol. 5, no. 5, pp. 1348-1356, 2015.

[32] M. A. Green, "Effects of pinholes, oxide traps, and surface states on MIS solar cells," *Applied Physics Letters*, vol. 33, no. 2, pp. 178-180, 1978.

[33] R. Peibst, U. Römer, K. R. Hofmann, B. Lim, T. F. Wietler, J. Krügener, N. Harder, and R. Brendel, "A simple model describing the symmetric I-V characteristics of p polycrystalline Si/n monocrystalline Si, and n polycrystalline Si/p monocrystalline Si Junctions," *IEEE Journal of Photovoltaics*, vol. 4, no. 3, pp. 841-850, 2014.

[34] JinkoSolar, "JinkoSolar large-area n-type monocrystalline silicon solar cell reaches record-breaking new high efficiency of 25.25%," "Press release" [Online] Available: http://jinkosolar.com.au/2021/05/jinkosolar-large-area-n-type-monocrystalline-silicon-solar-cell-reaches-record-breaking-new-high-efficiency-of-25-25/, May 2021.

[35] LONGi, "LONGi breaks three more world records for solar cell efficiency," "Press release" [Online] Available: https://en.longi-solar.com/home/events/press_detail/id/335.html, June 2021.

[36] F. Feldmann, M. Bivour, C. Reichel, H. Steinkemper, M. Hermle, and S. W. Glunz, "Tunnel oxide passivated contacts as an alternative to partial rear contacts," *Solar Energy Materials and Solar Cells*, vol. 131, pp. 46-50, 2014.

[37] R. Peibst, C. Kruse, S. Schäfer, V. Mertens, S. Bordihn, T. Dullweber, F. Haase, C. Hollemann, B. Lim, B. Min, R. Niepelt, H. Schulte-Huxel, and R. Brendel, "For none, one, or two polarities—How do POLO junctions fit best into industrial Si solar cells?," *Progress in Photovoltaics: Research and Applications*, vol. 28, no. 6, pp. 503-516, 2020.

[38] B. Stegemann, K. M. Gad, P. Balamou, D. Sixtensson, D. Vössing, M. Kasemann, and H. Angermann, "Ultra-thin silicon oxide layers on crystalline silicon wafers: Comparison of advanced oxidation techniques with respect to chemically abrupt SiO2/Si interfaces with low defect densities," *Applied Surface Science*, vol. 395, pp. 78-85, 2017.

[39] F. Feldmann, M. Bivour, C. Reichel, M. Hermle, and S. W. Glunz, "A passivated rear contact for high-efficiency n-type si solar cells enabling high voc's and FF>82 %," in *European PV Solar Energy Conference Exhibition*, Paris, France, 2013,

[40] H. K. Asuha, O. Maida, M. Takahashi, and H. Iwasa, "Nitric acid oxidation of Si to form ultrathin silicon dioxide layers with a low leakage current density," *Journal of Applied Physics*, vol. 94, no. 11, pp. 7328-7335, 2003.

[41] Y. Larionova, M. Turcu, S. Reiter, R. Brendel, D. Tetzlaff, J. Krügener, T. Wietler, U. Höhne, J.-D. Kähler, and R. Peibst, "On the recombination behavior of p+-type polysilicon on oxide junctions deposited by different methods on textured and planar surfaces," *physica status solidi (a)*, vol. 214, no. 8, p. 1700058, 2017.

[42] A. Moldovan, F. Feldmann, K. Kaufmann, S. Richter, M. Werner, C. Hagendorf, M. Zimmer, J. Rentsch, and M. Hermle, "Tunnel oxide passivated carrier-selective contacts based on ultra-thin SiO2 layers grown by photo-oxidation or wet-chemical oxidation in ozonized water," in *2015 IEEE 42nd Photovoltaic Specialist Conference (PVSC)*, 2015, pp. 1-6.

[43] Y. Huang, M. Liao, Z. Wang, X. Guo, C. Jiang, Q. Yang, Z. Yuan, D. Huang, J. Yang, X. Zhang, Q. Wang, H. Jin, M. Al-Jassim, C. Shou, Y. Zeng, B. Yan, and J. Ye, "Ultrathin silicon oxide prepared by in-line plasma-assisted N2O oxidation (PANO) and the application for n-type polysilicon passivated contact," *Solar Energy Materials and Solar Cells*, vol. 208, p. 110389, 2020.

[44] M. Jeon, J. Kang, G. Shim, S. Ahn, N. Balaji, C. Park, Y.-J. Lee, and J. Yi, "Passivation effect of tunnel oxide grown by N2O plasma for c-Si solar cell applications," *Vacuum*, vol. 141, pp. 152-156, 2017.

[45] Y. Lee, W. Oh, A. Dao, S. Hussain, and J. Yi, "Ultrathin Oxide Passivation Layer by Rapid Thermal Oxidation for the Silicon Heterojunction Solar Cell Applications," *International Journal of Photoenergy*, vol. 753456, 2012.

[46] M. K. Stodolny, J. Anker, B. L. J. Geerligs, G. J. M. Janssen, B. W. H. van de Loo, J. Melskens, R. Santbergen, O. Isabella, J. Schmitz, M. Lenes, J.-M. Luchies, W. M. M. Kessels, and I. Romijn, "Material properties of LPCVD processed n-type polysilicon passivating contacts and its application in PERPoly industrial bifacial solar cells," *Energy Procedia*, vol. 124, pp. 635-642, 2017.

[47] D. Yan, A. Cuevas, J. Bullock, Y. Wan, and C. Samundsett, "Phosphorus-diffused polysilicon contacts for solar cells," *Solar Energy Materials and Solar Cells*, vol. 142, pp. 75-82, 2015.

[48] A. S. Kale, W. Nemeth, S. P. Harvey, M. Page, D. L. Young, S. Agarwal, and P. Stradins, "Effect of silicon oxide thickness on polysilicon based passivated contacts for high-efficiency crystalline silicon solar cells," *Solar Energy Materials and Solar Cells*, vol. 185, pp. 270-276, 2018.

[49] A. Stesmans and V. V. Afanas'ev, "Si dangling-bond-type defects at the interface of (100)Si with ultrathin layers of SiOx, Al2O3, and ZrO2," *Applied Physics Letters*, vol. 80, no. 11, pp. 1957-1959, 2002.

[50] J.-I. Polzin, F. Feldmann, B. Steinhauser, M. Hermle, and S. W. Glunz, "Study on the interfacial oxide in passivating contacts," *AIP Conference Proceedings*, vol. 2147, no. 1, p. 040016, 2019.

[51] T. Gao, Q. Yang, X. Guo, Y. Huang, Z. Zhang, Z. Wang, M. Liao, C. Shou, Y. Zeng, B. Yan, G. Hou, X. Zhang, Y. Zhao, and J. Ye, "An industrially viable TOPCon structure with both ultra-thin SiOx and n+-poly-Si processed by PECVD for p-type c-Si solar cells," *Solar Energy Materials and Solar Cells*, vol. 200, p. 109926, 2019.

[52] D. Chen, Y. Chen, Z. Wang, J. Gong, C. Liu, Y. Zou, Y. He, Y. Wang, L. Yuan, W. Lin, R. Xia, L. Yin, X. Zhang, G. Xu, Y. Yang, H. Shen, Z. Feng, P. P. Altermatt, and P. J. Verlinden, "24.58% total area efficiency of screen-printed, large area industrial silicon solar cells with the tunnel oxide passivated contacts (i-TOPCon) design," *Solar Energy Materials and Solar Cells*, vol. 206, p. 110258, 2020.

[53] D. Yan, A. Cuevas, S. P. Phang, Y. Wan, and D. Macdonald, "23% efficient p-type crystalline silicon solar cells with hole-selective passivating contacts based on physical vapor deposition of doped silicon films," *Applied Physics Letters*, vol. 113, no. 6, p. 061603, 2018.

[54] J. H. J. Lossen, S. Eisert, D. Amkreutz, M. Muske, J. Plentz, G. Andrä, "Electron beam evaporation of silicon for poly-silicon/sio2 passivated contacts," in *35th European PV Solar Energy Conference Exhibition*, Brussels, Belgium, pp. 418-421, 2018.

[55] Z. Ding, T. N. Truong, H. T. Nguyen, D. Yan, X. Zhang, J. Yang, Z. Wang, P. Zheng, Y. Wan, D. Macdonald, and J. Stuckelberger, "Boron spin-on doping for poly-Si/SiOx passivating contacts," *ACS Applied Energy Materials*, vol. 4, no. 5, pp. 4993-4999, 2021.

[56] Z. Ding, D. Yan, J. Stuckelberger, S. P. Phang, W. Chen, C. Samundsett, J. Yang, Z. Wang, P. Zheng, X. Zhang, Y. Wan, and D. Macdonald, "Phosphorus-doped polycrystalline silicon passivating contacts via spin-on doping," *Solar Energy Materials and Solar Cells*, vol. 221, p. 110902, 2021.

[57] D. Fogel, "Encapsulant characterization and doped passivated contacts for use in luminescent solar concentrator," Colorado School of Mines, 2017.

[58] F. Haase, F. Kiefer, S. Schäfer, C. Kruse, J. Krügener, R. Brendel, and R. Peibst, "Interdigitated back contact solar cells with polycrystalline silicon on oxide passivating contacts for both polarities," *Japanese Journal of Applied Physics*, vol. 56, no. 8S2, p. 08MB15, 2017.

[59] G. Wolstenholme, N. Jorgensen, P. Ashburn, and G. R. Booker, "An investigation of the thermal stability of the interfacial oxide in polysilicon emitter bipolar transistors using high resolution TEM," *J. Appl. Phys*, vol. 61, pp. 225-233, 1987.

[60] J. L. Egley and J. L. Gray, "Demonstration of the importance of the oxide breakup in polysilicon-contacted-emitter modeling," *IEEE Transactions on Electron Devices*, vol. 38, no. 9, pp. 2112-2117, 1991.

[61] Y. Chen, D. Chen, C. Liu, Z. Wang, Y. Zou, Y. He, Y. Wang, L. Yuan, J. Gong, W. Lin, X. Zhang, Y. Yang, H. Shen, Z. Feng, P. P. Altermatt, and P. J. Verlinden, "Mass production of industrial tunnel oxide passivated contacts (i-TOPCon) silicon solar cells with average efficiency over 23% and modules over 345 W," *Progress in Photovoltaics: Research and Applications*, vol. 27, no. 10, pp. 827-834, 2019.

[62] T. N. Truong, D. Yan, C.-P. T. Nguyen, T. Kho, H. Guthrey, J. Seidel, M. Al-Jassim, A. Cuevas, D. Macdonald, and H. T. Nguyen, "Morphology, microstructure, and doping behaviour: A comparison between different deposition methods for poly-Si/SiOx passivating contacts," *Progress in Photovoltaics: Research and Applications*, vol. 29, no. 7, pp. 857-868, 2021.

[63] A. Morisset, R. Cabal, B. Grange, C. Marchat, J. Alvarez, M.-E. Gueunier-Farret, S. Dubois, and J.-P. Kleider, "Improvement of the conductivity and surface passivation properties of boron-doped poly-silicon on oxide," *AIP Conference Proceedings*, vol. 1999, no. 1, p. 040017, 2018.

[64] M. Stöhr, J. Aprojanz, R. Brendel, and T. Dullweber, "Firing-stable PECVD SiOxNy/n-poly-Si surface passivation for silicon solar cells," *ACS Applied Energy Materials*, vol. 4, no. 5, pp. 4646-4653, 2021.

[65] B. Nemeth, S. P. Harvey, J. V. Li, D. L. Young, A. Upadhyaya, V. LaSalvia, B. G. Lee, M. R. Page, and P. Stradins, "Effect of the SiO2 interlayer properties with solid-source hydrogenation on passivated contact performance and surface passivation," *Energy Procedia*, vol. 124, pp. 295-301, 2017.

[66] C. Hollemann, N. Folchert, S. P. Harvey, P. Stradins, D. L. Young, C. L. Salles de Souza, M. Rienäcker, F. Haase, R. Brendel, and R. Peibst, "Changes in hydrogen concentration and defect state density at the poly-Si/SiOx/c-Si interface due to firing," *Solar Energy Materials and Solar Cells*, vol. 231, p. 111297, 2021.

[67] W. Chen, T. N. Truong, H. T. Nguyen, C. Samundsett, S. P. Phang, D. MacDonald, A. Cuevas, L. Zhou, Y. Wan, and D. Yan, "Influence of PECVD deposition temperature on phosphorus doped poly-silicon passivating contacts," *Solar Energy Materials and Solar Cells,* vol. 206, p. 110348, 2020.

[68] W. Chen, J. Stuckelberger, W. Wang, S. P. Phang, D. Kang, C. Samundsett, D. MacDonald, A. Cuevas, L. Zhou, Y. Wan, and D. Yan, "Influence of PECVD deposition power and pressure on phosphorus-doped polysilicon passivating contacts," *IEEE Journal of Photovoltaics,* vol. 10, no. 5, pp. 1239-1245, 2020.

[69] G. L. Patton, J. C. Bravman, and J. D. Plummer, "Physics, technology, and modeling of polysilicon emitter contacts for VLSI bipolar transistors," *IEEE Transactions on Electron Devices,* vol. 33, no. 11, pp. 1754-1768, 1986.

[70] P. A. Potyraj, D. Chen, M. K. Hatalis, and D. W. Greve, "Interfacial oxide, grain size, and hydrogen passivation effects on polysilicon emitter transistors," *IEEE Transactions on Electron Devices,* vol. 35, no. 8, pp. 1334-1343, 1988.

[71] T. N. Truong, D. Yan, C. Samundsett, R. Basnet, M. Tebyetekerwa, L. Li, F. Kremer, A. Cuevas, D. Macdonald, and H. T. Nguyen, "Hydrogenation of phosphorus-doped polycrystalline silicon films for passivating contact solar cells," *ACS Applied Materials & Interfaces,* vol. 11, no. 5, pp. 5554-5560, 2019.

[72] M. L. Reed and J. D. Plummer, "Chemistry of Si-SiO2 interface trap annealing," *Journal of Applied Physics,* vol. 63, no. 12, pp. 5776-5793, 1988.

[73] J. Schmidt, M. Kerr, and A. Cuevas, "Surface passivation of silicon solar cells using plasma-enhanced chemical-vapour-deposited SiN films and thin thermal SiO2/plasma SiN stacks," *Semiconductor Science and Technology,* vol. 16, no. 3, pp. 164-170, 2001.

[74] H. Dekkers, G. Beaucarne, M. Hiller, H. Charifi, and A. Slaoui, "Molecular hydrogen formation in hydrogenated silicon nitride," *Applied Physics Letters,* vol. 89, p. 211914, 2006.

[75] M. Schnabel, B. W. H. v. d. Loo, W. Nemeth, B. Macco, P. Stradins, W. M. M. Kessels, and D. L. Young, "Hydrogen passivation of poly-Si/SiOx contacts for Si solar cells using Al2O3 studied with deuterium," *Applied Physics Letters,* vol. 112, no. 20, p. 203901, 2018.

[76] M. Mews, T. F. Schulze, N. Mingirulli, and L. Korte, "Hydrogen plasma treatments for passivation of amorphous-crystalline silicon-heterojunctions on surfaces promoting epitaxy," *Applied Physics Letters,* vol. 102, no. 12, p. 122106, 2013.

[77] K. Nishioka, T. Yagi, Y. Uraoka, and T. Fuyuki, "Effect of hydrogen plasma treatment on grain boundaries in polycrystalline silicon solar cell evaluated by laser-beam-induced current," *Solar Energy Materials and Solar Cells,* vol. 91, no. 1, pp. 1-5, 2007.

[78] B. Steinhauser, F. Feldmann, D. Ourinson, H. Nagel, T. Fellmeth, and M. Hermle, "On the influence of the SiNx composition on the firing stability of poly-Si/SiNx stacks," *physica status solidi (a),* vol. 217, no. 21, p. 2000333, 2020.

[79] B. Nemeth, D. L. Young, M. R. Page, V. LaSalvia, S. Johnston, R. Reedy, and P. Stradins, "Polycrystalline silicon passivated tunneling contacts for high efficiency silicon solar cells," *Journal of Materials Research,* vol. 31, no. 6, pp. 671-681, 2016.

[80] B. W. H. van de Loo, B. Macco, M. Schnabel, M. K. Stodolny, A. A. Mewe, D. L. Young, W. Nemeth, P. Stradins, and W. M. M. Kessels, "On the hydrogenation of Poly-Si passivating contacts by Al2O3 and SiNx thin films," *Solar Energy Materials and Solar Cells,* vol. 215, p. 110592, 2020.

[81] M. Schnabel, B. Van de Loo, W. Nemeth, B. Macco, P. Stradins, W. M. M. Kessels, and D. Young, "Hydrogen passivation of poly-Si/SiOx contacts for si solar cells using Al2O3 studied with deuterium," *Applied Physics Letters*, vol. 112, p. 203901, 2018.

[82] S. Mack, J. Schube, T. Fellmeth, F. Feldmann, M. Lenes, and J.-M. Luchies, "Metallisation of Boron-Doped Polysilicon Layers by Screen Printed Silver Pastes," *physica status solidi (RRL) – Rapid Research Letters*, vol. 11, no. 12, p. 1700334, 2017.

[83] T. N. Truong, D. Yan, W. Chen, M. Tebyetekerwa, M. Young, M. Al-Jassim, A. Cuevas, D. Macdonald, and H. T. Nguyen, "Hydrogenation mechanisms of poly-Si/SiOx passivating contacts by different capping layers," *Solar RRL*, vol. 4, no. 3, p. 2070033, 2020.

[84] Z. Zhang, M. Liao, Y. Huang, X. Guo, Q. Yang, Z. Wang, T. Gao, C. Shou, Y. Zeng, B. Yan, and J. Ye, "Improvement of surface passivation of tunnel oxide passivated contact structure by thermal annealing in mixture of water vapor and nitrogen environment," *Solar RRL*, vol. 3, no. 10, p. 1900105, 2019.

[85] L. Tutsch, F. Feldmann, J. Polzin, C. Luderer, M. Bivour, A. Moldovan, J. Rentsch, and M. Hermle, "Implementing transparent conducting oxides by DC sputtering on ultrathin SiOx / poly-Si passivating contacts," *Solar Energy Materials and Solar Cells*, vol. 200, p. 109960, 2019.

[86] T. Truong, D. Yan, A. Cuevas, D. Macdonald, and H. Nguyen, "Effects of hydrogenation on poly-Si/SiOx passivating contacts for silicon solar cells," in *2019 Asia-Pacific Solar Research Conference*, Canberra, 2019,

[87] J. Benick, A. Richter, M. Hermle, and S. W. Glunz, "Thermal stability of the Al2O3 passivation on p-type silicon surfaces for solar cell applications," *physica status solidi (RRL) – Rapid Research Letters*, vol. 3, no. 7-8, pp. 233-235, 2009.

[88] J. D. Fields, M. I. Ahmad, V. L. Pool, J. Yu, D. G. Van Campen, P. A. Parilla, M. F. Toney, and M. F. A. M. van Hest, "The formation mechanism for printed silver-contacts for silicon solar cells," *Nature Communications*, vol. 7, no. 1, p. 11143, 2016.

[89] G. Hahn and S. Joos, *Semiconductors and Semimetals* (Semiconductors and Semimetals). Elsevier, 2014, pp. 1-72.

[90] D.-H. Neuhaus and A. Münzer, "Industrial silicon wafer solar cells," *Advances in OptoElectronics*, vol. 2007, p. 024521, 2007.

[91] H. E. Çiftpınar, M. K. Stodolny, Y. Wu, G. J. M. Janssen, J. Löffler, J. Schmitz, M. Lenes, J.-M. Luchies, and L. J. Geerligs, "Study of screen printed metallization for polysilicon based passivating contacts," *Energy Procedia*, vol. 124, pp. 851-861, 2017.

[92] C. Hollemann, F. Haase, J. Krügener, R. Brendel, and R. Peibst, "Firing stability of n-type poly-Si on oxide junctions formed by quartz tube annealing," in *2020 47th IEEE Photovoltaic Specialists Conference (PVSC)*, 2020, pp. 1274-1278.

Chapter 2 – Characterization methods

2.1 Photoconductance measurement

2.1.1 Effective lifetime

In this thesis, the effective lifetime τ_{eff} of samples is determined by photoconductance measurements using a Sinton Instruments WCT-120 lifetime tester. During the measurement, a silicon wafer is placed above an inductive coil to form a bridge circuit, with the initial conductance measured by the system. Subsequently, a flash is applied to illuminate the wafer, leading to generation of excess carriers, which contributes to an increase in conductance. As the excess carriers recombine, the changes in the conductance of the wafer are measured by the inductive coil and used to determine the average excess carrier density Δn based on the equation below:

$$\Delta n = \frac{\Delta\sigma}{qW(\mu_n+\mu_p)} \qquad \textit{Eq. 2. 1}$$

where μ_n and μ_p are the mobility of electrons and holes. W denotes the wafer thickness, and $\Delta\sigma$ represents the change in conductance.

The generation rate G for the electron-hole pairs can be determined using a calibrated reference cell and calculated based on the following equation:

$$G = \frac{f_{optical} \cdot J_{sc}}{qW} \qquad \textit{Eq. 2. 2}$$

where J_{sc} is the short circuit current of the reference solar cell, and $f_{optical}$ is the difference in absorption between the sample and the reference cell.

Based on the continuity equation, the rate of change in excess carrier concentration equals to the difference between the generation rate and the recombination rate, which can be expressed as:

$$\frac{d\Delta n}{dt} = G - U \qquad \textit{Eq. 2. 3}$$

Rearranging U and substituting it into Eq.1.1, the effective lifetime can then be obtained by:

$$\tau_{eff} = \frac{\Delta n}{G - \frac{d\Delta n}{dt}} \qquad \textit{Eq. 2. 4}$$

Measurements can be performed using either quasi-steady state (QSS) mode or transient mode. In the QSS mode, the flash provides a long but slow-decaying pulse of light. The illumination time is longer than the lifetime, thus the decay of the excess carrier

concentration ($\frac{d\Delta n}{dt}$) can be neglected. In this case, the lifetime can be calculated using the equation below:

$$\tau_{eff} = \frac{\Delta n}{G} \qquad \textit{Eq. 2. 5}$$

During the transient measurements, the flash provides a very short pulse of illumination and the subsequent decay of excess carrier concentration is monitored assuming $G = 0$. For this instance, the lifetime can be calculated by:

$$\tau_{eff} = \frac{\Delta n}{\frac{d\Delta n}{dt}} \qquad \textit{Eq. 2. 6}$$

The QSS mode is generally applied for samples with a low lifetime, whilst the transient mode is widely used to measure high-lifetime samples, as it requires the lifetime (commonly above 200 µs) to be considerably longer than the decay of the illumination. In this thesis, the measurements were all performed using the transient mode, and the reported lifetime values were an average of 5 photoconductance measurements.

2.1.2 Extraction of J_0

This thesis utilizes the effective lifetime τ_{eff} measured by photoconductance to extract the recombination current density parameter J_0, based on the method of Kane and Swanson [1].

For symmetrical passivation wafers, substituting Eq. 1.17 to Eq. 1.2, τ_{eff} can be rewritten as:

$$\frac{1}{\tau_{eff}} = \frac{1}{\tau_{bulk}} + J_0 \frac{2(N_{dop}+\Delta n)}{q n_i^2 W} \qquad \textit{Eq. 2. 7}$$

J_0 can then be obtained from the slope of line correlating $\frac{1}{\tau_{eff}} - \frac{1}{\tau_{bulk}}$ and $N_{\mathrm{dop}} + \Delta n$. In this thesis, τ_{bulk} is determined by the empirical parameterization proposed by Richter *et al*. [2] (Eq. 1.6). Note that the J_0 values are usually extracted using high-resistivity Si wafers. This is because, at high injection, the SRH effect on the Si bulk can be eliminated and the Auger recombination is dominant, allowing us to utilize τ_{Auger} to represent τ_{bulk}.

2.2 Fourier transform infrared (FTIR) spectroscopy

Fourier transform infrared spectroscopy (FTIR) is a technique used to probe the molecular structure of a substance, by acquiring and analyzing an infrared (IR) spectrum

absorbed from or transmitted through a sample. The schematic diagram in Fig. 2. 1 demonstrates the key components of a typical FTIR spectroscopy system, including an IR source, interferometer, sample compartment, detector, and a computer. The interferometer that consists of a beam splitter, a fixed mirror and a moving mirror, is used to modulate the wavelength from a broadband infrared light source. During operation, the IR photons are absorbed by the sample when the frequency of the IR light matches the vibrational frequency of a chemical bond [3]. The detector collects the transmission spectrum, with the data analyzed and processed by a computer using Fourier transform. In this thesis, FTIR is applied to identify the bonding configuration in SiN_x films (in Chapter 7) and poly-Si/SiO_x passivating contacts (Chapter 3 and 5).

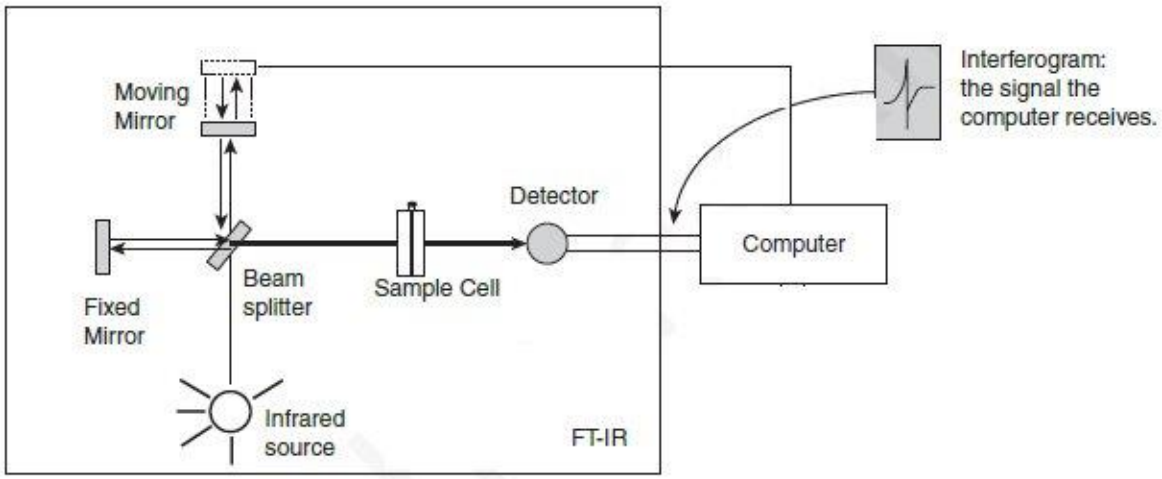

Fig. 2. 1 Schematic diagram of typical FTIR spectrophotometer. The figure is reprinted from Ref. [4].

The IR absorption or transmission spectrum of the sample as a function of wavenumber is given by each measurement. The position of each peak corresponds to a compound, and the peak intensity correlates to the concentration of the chemical bond. The bond density $[X-Y]$, defined as the number of bonds per unit volume, can be calculated from the FTIR spectrum using the following expression [5]:

$$[X-Y] = ln(10) \cdot k_{X-Y} \int \alpha(\omega)\omega^{-1} d\omega \qquad Eq.\ 2.8$$

where $\alpha(\omega)$ represents the absorption coefficient at wavenumber ω, and d denotes the thickness. k_{X-Y} is the proportionality constant of the bond X–Y in cm^{-2}, with the data given in the literature [6-10].

The FTIR measurements in this work were performed using a Bruker Vertex 80V FTIR, over the wavenumber range of 400–4000 cm^{-1} with a resolution of 10 cm^{-1}. There are

minimal uncertainties introduced by moisture, oxygen and carbon dioxide, as the measurements were performed in a vacuum environment and a background scan was taken prior to each measurement. The data shown in this thesis represent the studied SiN_x or poly-Si/SiO_x films instead of the entire sample. This was achieved by using the FTIR spectrum for the as-grown c-Si wafers as the background subtraction, and then proceeding with the spectrum acquisition of wafers coated with a thin film on one side.

2.2.1 Chemical bonds in SiN_x

Fig. 2. 2 presents a typical FTIR spectrum for a SiN_x film. Si–N, Si–H and N–H bonds locate at 850 cm^{-1}, 2140 cm^{-1} and 3340 cm^{-1} [6] are commonly used to analyze the properties of SiN_x films. The spectrum for the Si–H and N–H bonds measured by FTIR are often used for hydrogen analysis. In particular, the sum of $[Si-H]$ and $[N-H]$ can be used to reflect the concentration of hydrogen in SiN_x films, due to the fact that atomic hydrogen in SiN_x is mainly bonded with Si and N atoms [11, 12]. Although Si–H and N–H bonds correspond to the hydrogen concentration in SiN_x, the effectiveness of hydrogenation can depend on the Si–N bond density [13-18]. Hong *et al*. [16] showed that the quality of bulk passivation in mc-Si increases with $[Si-N]$, possibly explained by the enhanced SiN_x film density, as denser films appear to prevent the effusion of hydrogen from the SiN_x film into the ambient [16, 18].

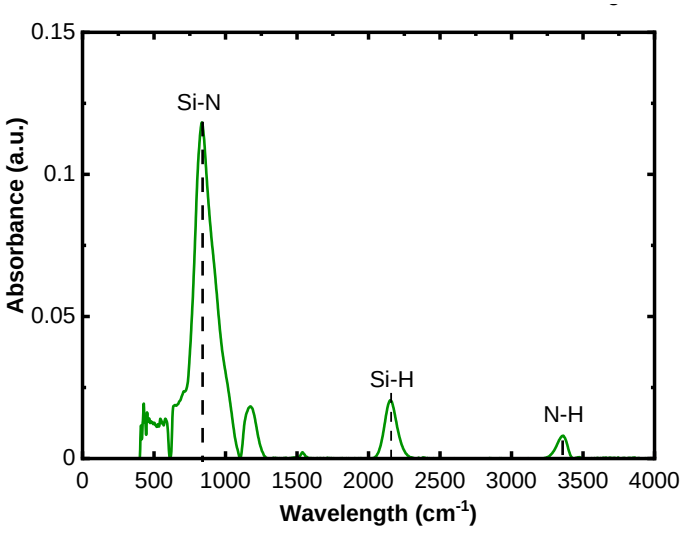

Fig. 2. 2 A typical FTIR spectrum for SiN_x film

2.2.2 Chemical bonds in poly-Si/SiO_x passivating contacts

This thesis also applies FTIR to characterize poly-Si/SiO_x passivating contacts, to compare the changes in hydrogen and oxygen bonds before and after thermal annealing.

The FTIR spectrum for a typical n-type LPCVD poly-Si is given in Fig. 2. 3, showing Si–Si at a wavelength of ~600 cm^{-1}, Si–O at 730 cm^{-1}, Si–O bending at 810 cm^{-1}, Si–H at 870 cm^{-1}, Si–O–H at 970 cm^{-1}, Si–O–Si at 1120 cm^{-1}, and $Si–H_x$ (x = 1, 2, 3) from 2330 to 2360 cm^{-1}. To characterize poly-Si/SiO_x structures, the peaks for Si–O, Si–H, Si–O–H, $Si–H_1$ and $Si–H_2$ are commonly assessed. The Si–H, $Si–H_1$ and $Si–H_2$ bonds have been used for hydrogen analysis in poly-Si, as introduced by the literature [19-24]. Chen *et al.* [21] and Truong *et al.* [24] observed a clear increase in the intensity of the $Si–H_1$ peak at a wavelength of ~2100 nm in ex-situ doped n-type PECVD poly-Si after hydrogenation treatment. The Si–O–Si bond corresponds to properties of the SiO_x film in poly-Si/SiO_x structures [23, 25]. Kaur *et al.* [25] showed that, for poly-Si/SiO_x passivating contacts annealed at different temperature, the area of Si–O–Si FTIR peak at ~1100 cm^{-1} increases with the annealing temperature, which directly corresponds to the thickness of the ultra-thin SiO_x, as confirmed by ellipsometry. Note that the wavelength of the chemical bonds varies with the poly-Si film properties. While ex-situ doped n-type PECVD poly-Si samples showed the $Si–H_1$ and $Si–H_2$ peaks at a wavelength of 2100–2200 cm^{-1} [21, 26], the hydrogen peaks were detected at 2330 to 2360 cm^{-1} on p-type LPCVD poly-Si samples in this work and Ref. [23].

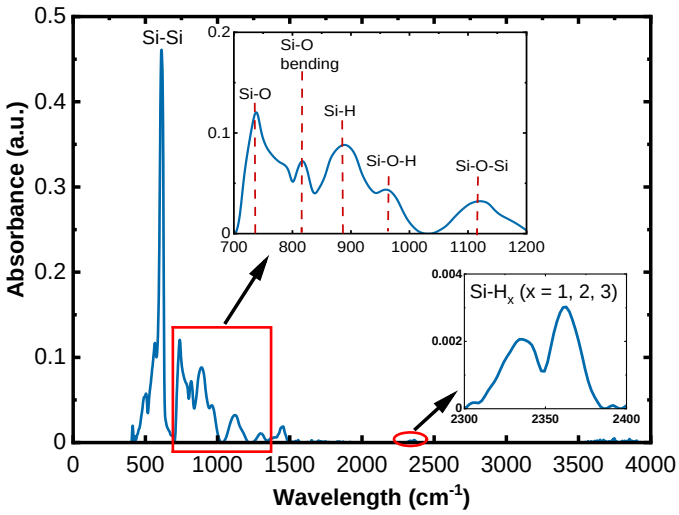

Fig. 2. 3 A typical FTIR spectrum for the boron-doped LPCVD poly-Si/SiO_x passivating contact.

2.3 Secondary ion mass spectrometry (SIMS)

Secondary ion mass spectrometry (SIMS) is a technique capable of characterizing the composition of thin films and surfaces by using a focused primary ion beam to sputter the surface of the specimen and analyze the ejected secondary ions. Typical schematic of

a SIMS instrument is shown in Fig. 2. 4. The main components of the system include ion source, sample stage, mass analyzer and detector. During operation, the surface of the sample is hit with a high-energy ion beam under vacuum, sputtering some atoms off the surface and creating small spots with shallow pit depth. Subsequently, the ejected secondary ions are collected by ion lenses and filtered by an atomic mass analyzer. SIMS is an effective tool for hydrogen analysis, due to the high sensitivity in detecting substances present at trace levels with a great depth resolution, hence the technique has been widely applied to determine hydrogen content in Si and poly-Si [24, 27-29]. In this thesis, SIMS is used to measure the hydrogen concentration as a function of depth in poly-Si/SiO_x passivating contacts, with the results shown in Chapter 4 and 5.

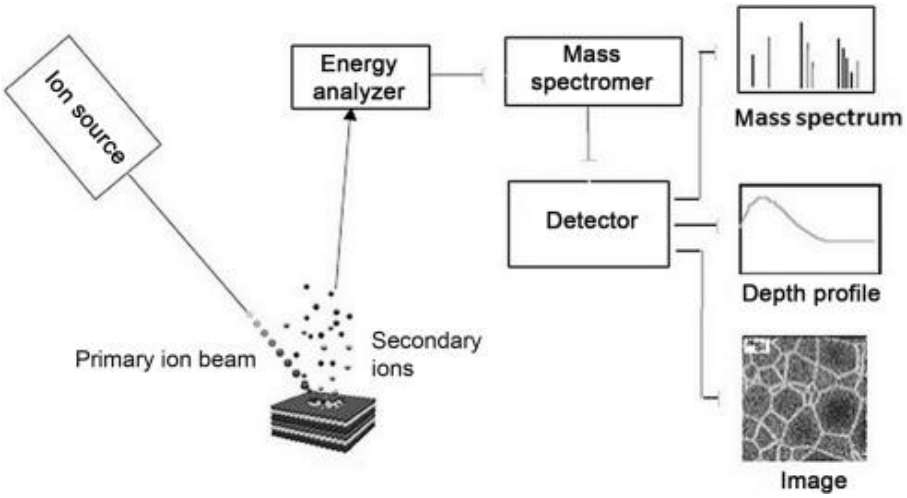

Fig. 2. 4 Schematic diagram for a SIMS setup. Reprinted from Ref. [30].

In this thesis, a Cameca IMS 5fE7 SIMS tool (Cameca, France) was used to acquire the depth profile for hydrogen in doped poly-Si/SiO_x passivating contacts. A primary ion beam of Cs^+ with an impact energy of 5.0 keV and beam current of 16 nA was applied to raster a 125 × 125 μm region of the sample surface, with a sputtering rate of around 0.5 nm/s. Fig. 2. 5 (grey solid line) shows a typical hydrogen profile measured on n-type poly-Si sample using the secondary H^+ ions. The hydrogen concentration surrounding the SiO_x is of particular interest in this work. However, SIMS is more sensitive to hydrogen in oxides than in poly-Si or c-Si, potentially causing measurement artifacts when detecting hydrogen in poly-Si/SiO_x contacts on c-Si wafer [28]. Therefore, in addition to the hydrogen profiles acquired by measuring H^+ species, a separate SIMS profiling (red dash line) for the same poly-Si sample was obtained by detecting complex ions of HCs_2^+, which can improve spatial resolution and eliminate the artifacts in multi-layer depth

profiling [31, 32]. The results confirm that the detected hydrogen peaks around SiO_x are not artifacts of the measurement.

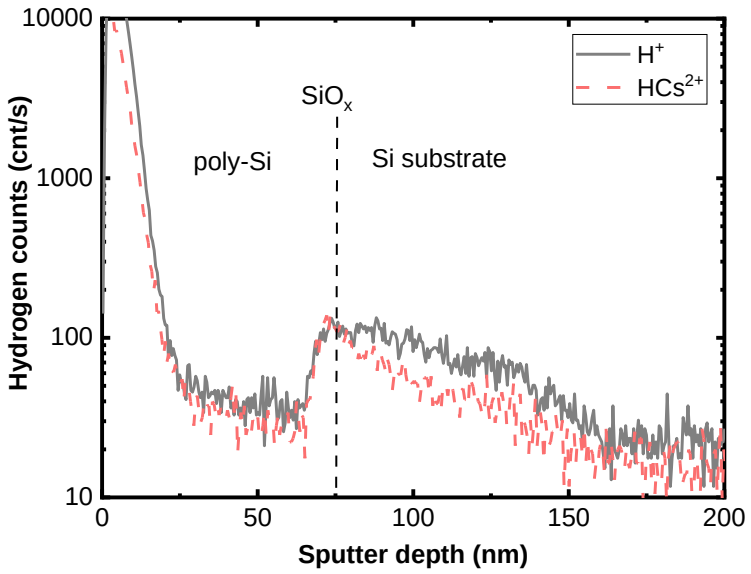

Fig. 2. 5 SIMS profiles acquired using the single ion beam of H^+ and HCs^{2+} ion cluster measured on the same sample.

2.4 Grazing incidence X-ray diffraction (GIXRD)

Grazing incidence X-ray diffraction (GIXRD) is a technique to determine the crystallographic phases and properties present at the sample surface or crystallographic properties in thin films, based on Bragg's law. During an X-ray scan, periodic arrays of atoms in a sample cause a constructive and destructive interference of the scattered X-ray beam, creating diffraction patterns that present Bragg diffraction peaks. The diffraction peaks, combined with the peak intensities that are determined by the atomic positions within the lattice planes, can be used to identify the atomic structure [33]. X-ray is suitable for measuring the crystalline structure, because the X-ray wavelengths are comparable to the interatomic spacing of crystalline solids [33]. Fig. 2. 6 shows the schematic diagram for a typical GIXRD instrument that consists of an X-ray tube, a divergence slit, a receiving slit, a monochromator, and a detector. The X-ray beam is directed towards a sample, and the scattered X-ray is reflected off the sample and collected by the detector. A small grazing incident angle is utilized to limit the penetration depth of X-ray to ~1000 nm [34], making it sensitive to the characteristics of the surface.

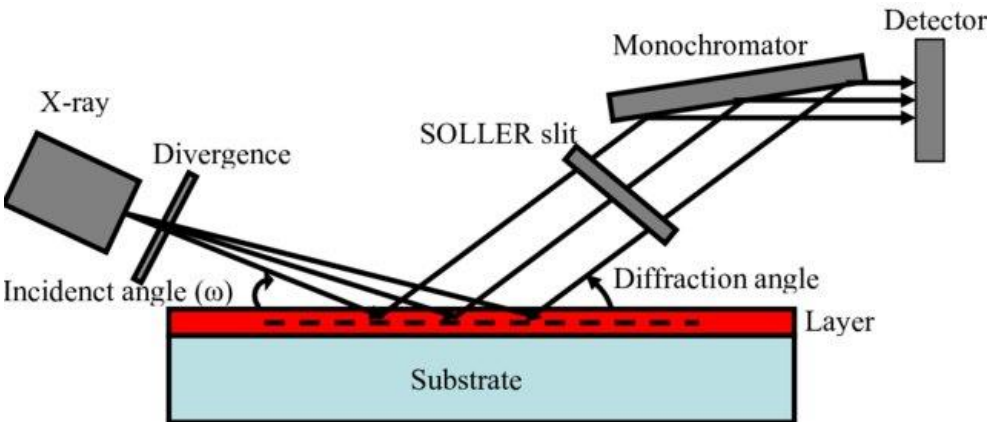

Fig. 2. 6 The schematic diagram for a typical GIXRD characterization tool. This figure is reprinted from Ref. [35].

For the samples studied in this work, the GIXRD scan was collected with a grazing incidence angle of 1º. The measurements were performed using a PANalytical X'Pert PRO MRD high resolution X-ray diffractometer with Cu Kα radiation and a graphite monochromator. The current and acceleration voltages were set to 40 mA, 45 kV respectively. Fig. 2. 7 presents the XRD spectrum measured on a phosphorus-doped LPCVD poly-Si sample after firing, with the diffraction angle (2θ) range tuned from 25º to 60º. From the XRD spectrum, the <111>, <220> and <311> peaks can be observed, with the <111> orientation being dominant. It has been reported that four silicon crystal orientations <111>, <220>, <311> and <400> can be detected from poly-Si films [21, 36], at 2θ of 28.5º, 47.4º, 56º, 69.4º respectively. However, the <311> and <400> peaks often overlap with noise from XRD, leading to confound analysis [21, 37]. Therefore, the <111> and <220> peaks are commonly applied to characterize the properties of poly-Si films. The full width at half maximum (FWHM) of XRD peaks is commonly used to determine the crystallite size, using the Scherrer formula [38-40]:

$$Average\ crystallite\ size = \frac{k\lambda}{FWHM \cdot cos\theta} \qquad Eq.\ 2.\ 9$$

where k denotes a shape factor of 0.9, λ is the wavelength of the X-ray, and θ is the Bragg angle. According to the equation, a sharper peak reflects a larger crystallite size.

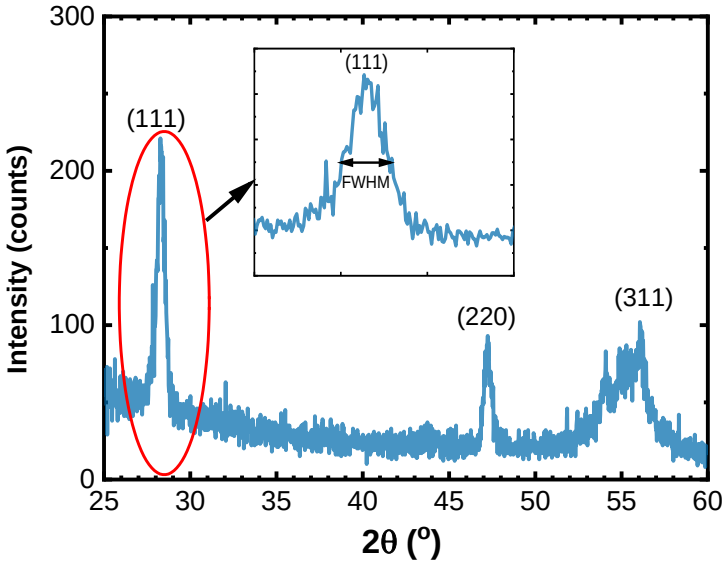

Fig. 2. 7 The XRD spectrum of a phosphorus-doped LPCVD poly-Si sample after firing.

References

[1] D. E. Kane and R. M. Swanson, "Measurement of the emitter saturation current by a contactless photoconductivity decay method," *Proceedings of the IEEE 18th Photovoltaic Specialist Conference*, p. 578, 1985.

[2] A. Richter, S. W. Glunz, F. Werner, J. Schmidt, and A. Cuevas, "Improved quantitative description of Auger recombination in crystalline silicon," *Physical Review B*, vol. 86, no. 16, p. 165202, 2012.

[3] D. K. Schroder, *Semiconductor Material and Device Characterization*. John Wiley & Sons, Inc., 2005, pp. 563-626.

[4] J. Jalvandi, "Novel chemical and physical approaches for sustainable drug release from biodegradable electrospun nanofibres," 2016.

[5] M. Cardona, "Vibrational spectra of hydrogen in silicon and germanium," *physica status solidi (b)*, vol. 118, no. 2, pp. 463-481, 1983.

[6] F. Giuliani, C. F. Pirri, E. Tresso, C. Summonte, R. Rizzoli, R. Galloni, A. Desalvo, and P. Rava, "Optical, structural and electrical properties of device-quality hydrogenated amorphous silicon-nitrogen films deposited by plasma-enhanced chemical vapour deposition AU - Giorgis, F," *Philosophical Magazine B*, vol. 77, no. 4, pp. 925-944, 1998.

[7] E. Bustarret, M. Bensouda, M. C. Habrard, J. C. Bruyère, S. Poulin, and S. C. Gujrathi, "Configurational statistics in a-SixNyHz alloys: A quantitative bonding analysis," (in eng), *Phys Rev B Condens Matter*, vol. 38, no. 12, pp. 8171-8184, 1988.

[8] V. Verlaan, C. H. M. van der Werf, W. M. Arnoldbik, H. D. Goldbach, and R. E. I. Schropp, "Unambiguous determination of Fourier-transform infrared spectroscopy proportionality factors: The case of silicon nitride," *Physical Review B*, vol. 73, no. 19, p. 195333, 2006.

[9] S. Hasegawa, L. He, Y. Amano, and T. Inokuma, "Analysis of SiH and SiN vibrational absorption in amorphous SiNx:H films in terms of a charge-transfer model," (in eng), *Phys Rev B Condens Matter,* vol. 48, no. 8, pp. 5315-5325, 1993.

[10] W. A. Lanford and M. J. Rand, "The hydrogen content of plasma-deposited silicon nitride," *Journal of Applied Physics,* vol. 49, no. 4, pp. 2473-2477, 1978.

[11] G. Scardera, T. Puzzer, G. Conibeer, and M. Green, "Fourier transform infrared spectroscopy of annealed silicon-rich silicon nitride thin films," *Journal of Applied Physics,* vol. 104, pp. 104310-104310, 2008.

[12] I. Jonak-Auer and F. Kuchar, *Accurate determination of the hydrogen concentration of silicon nitride layers by Fourier transform spectroscopy* (Microelectronic Manufacturing). SPIE, 1998.

[13] H. F. W. Dekkers, L. Carnel, and G. Beaucarne, "Carrier trap passivation in multicrystalline Si solar cells by hydrogen from SiNx:H layers," *Applied Physics Letters,* vol. 89, no. 1, p. 013508, 2006.

[14] H. F. W. Dekkers, G. Beaucarne, M. Hiller, H. Charifi, and A. Slaoui, "Molecular hydrogen formation in hydrogenated silicon nitride," *Applied Physics Letters,* vol. 89, no. 21, p. 211914, 2006.

[15] H. F. W. Dekkers, S. De Wolf, G. Agostinelli, F. Duerinckx, and G. Beaucarne, "Requirements of PECVD SiNx:H layers for bulk passivation of mc-Si," *Solar Energy Materials and Solar Cells,* vol. 90, no. 18, pp. 3244-3250, 2006.

[16] J. Hong, W. M. M. Kessels, W. J. Soppe, A. W. Weeber, W. M. Arnoldbik, and M. C. M. v. d. Sanden, "Influence of the high-temperature “firing” step on high-rate plasma deposited silicon nitride films used as bulk passivating antireflection coatings on silicon solar cells," *Journal of Vacuum Science & Technology B: Microelectronics and Nanometer Structures Processing, Measurement, and Phenomena,* vol. 21, no. 5, pp. 2123-2132, 2003.

[17] A. W. Weeber, H. C. Rieffe, M. Goris, J. Hong, W. M. M. Kessels, M. C. M. Banden, and W. J. Soppe, "Improved thermally stable surface and bulk passivation of PECVD SiN X:H using N2 and SiH4," *Proceedings of the 3rd World Conference on Photovoltaic Energy Conversion,* pp. 1131-1134, 2003.

[18] W. S. I. Romijn, H. Rieffe, A. Burgers, and A. Weeber, "Passivating mc-Si solar cells using SiNx:H: from magic to physics," in *20th European Photovoltaic Solar Energy Conference and Exhibition,*, 2005,

[19] A. Ingenito, G. Nogay, Q. Jeangros, E. Rucavado, C. Allebé, S. Eswara, N. Valle, T. Wirtz, J. Horzel, T. Koida, M. Morales-Masis, M. Despeisse, F.-J. Haug, P. Löper, and C. Ballif, "A passivating contact for silicon solar cells formed during a single firing thermal annealing," *Nature Energy,* vol. 3, no. 9, pp. 800-808, 2018.

[20] T. N. Truong, D. Yan, C. Samundsett, R. Basnet, M. Tebyetekerwa, L. Li, F. Kremer, A. Cuevas, D. Macdonald, and H. T. Nguyen, "Hydrogenation of phosphorus-doped polycrystalline silicon films for passivating contact solar cells," *ACS Applied Materials & Interfaces,* vol. 11, no. 5, pp. 5554-5560, 2019.

[21] W. Chen, T. N. Truong, H. T. Nguyen, C. Samundsett, S. P. Phang, D. MacDonald, A. Cuevas, L. Zhou, Y. Wan, and D. Yan, "Influence of PECVD deposition temperature on phosphorus doped poly-silicon passivating contacts," *Solar Energy Materials and Solar Cells,* vol. 206, p. 110348, 2020.

[22] A. Morisset, R. Cabal, V. Giglia, A. Boulineau, E. De Vito, A. Chabli, S. Dubois, J. Alvarez, and J.-P. Kleider, "Evolution of the surface passivation mechanism during the fabrication of ex-situ doped poly-Si(B)/SiOx passivating contacts for high-efficiency c-Si solar cells," vol. 221, p. 110899, 2021.

[23] M. Bouzerdoum and B. Birouk, "Characterization by SEM and FTIR of B-LPCVD polysilicon films after thermal oxidation," in *2012 24th International Conference on Microelectronics (ICM)*, 2012, pp. 1-4.

[24] T. N. Truong, D. Yan, W. Chen, M. Tebyetekerwa, M. Young, M. Al-Jassim, A. Cuevas, D. Macdonald, and H. T. Nguyen, "Hydrogenation mechanisms of poly-Si/SiOx passivating contacts by different capping layers," *Solar RRL*, vol. 4, no. 3, p. 2070033, 2020.

[25] G. Kaur, Z. Xin, T. Dutta, R. Sridharan, R. Stangl, and A. Danner, "Improved silicon oxide/polysilicon passivated contacts for high efficiency solar cells via optimized tunnel layer annealing," *Solar Energy Materials and Solar Cells*, vol. 217, p. 110720, 2020.

[26] T. N. Truong, D. Yan, C. Samundsett, A. Liu, S. P. Harvey, M. Young, Z. Ding, M. Tebyetekerwa, F. Kremer, M. Al-Jassim, A. Cuevas, D. Macdonald, and H. T. Nguyen, "Hydrogen-assisted defect engineering of doped poly-si films for passivating contact solar cells," *ACS Applied Energy Materials*, vol. 2, no. 12, pp. 8783-8791, 2019.

[27] F. Stevie, C. Zhou, M. Hopstaken, M. Saccomanno, Z. Zhang, and A. Turansky, "SIMS measurement of hydrogen and deuterium detection limits in silicon: Comparison of different SIMS instrumentation," *Journal of Vacuum Science & Technology B*, vol. 34, 2016.

[28] M. Schnabel, B. Van de Loo, W. Nemeth, B. Macco, P. Stradins, W. M. M. Kessels, and D. Young, "Hydrogen passivation of poly-Si/SiOx contacts for si solar cells using Al2O3 studied with deuterium," *Applied Physics Letters*, vol. 112, p. 203901, 2018.

[29] B. Nemeth, D. L. Young, M. R. Page, V. LaSalvia, S. Johnston, R. Reedy, and P. Stradins, "Polycrystalline silicon passivated tunneling contacts for high efficiency silicon solar cells," *Journal of Materials Research*, vol. 31, no. 6, pp. 671-681, 2016.

[30] M. C. Tanzi, S. Farè, and G. Candiani, *Foundations of biomaterials engineering* (Foundations of Biomaterials Engineering). Academic Press, 2019, pp. 393-469.

[31] S. Sheraz née Rabbani, I. Berrueta Razo, T. Kohn, N. P. Lockyer, and J. C. Vickerman, "Enhancing ion yields in time-of-flight-secondary ion mass spectrometry: A comparative study of argon and water cluster primary beams," *Analytical Chemistry*, vol. 87, no. 4, pp. 2367-2374, 2015.

[32] H. Gnaser and H. Oechsner, "Hydrogen analysis by secondary ion mass spectrometry using HCs+ ions," *Nuclear Instruments and Methods in Physics Research Section B: Beam Interactions with Materials and Atoms*, vol. 64, no. 1, pp. 646-649, 1992.

[33] M. Kaliva and M. Vamvakaki, *Polymer science and nanotechnology* (Polymer Science and Nanotechnology). Elsevier, 2020, pp. 401-433.

[34] M. Birkholz, "Thin Film Analysis by X-Ray Scattering," 2005, pp. 1-40.

[35] G. Sun, "Surface-enhanced Raman spectroscopy investigation of surfaces and interfaces in thin films on metals," *http://www-brs.ub.ruhr-uni-bochum.de/netahtml/HSS/Diss/SunGuoguang/diss.pdf*, 2021.

[36] T. N. Truong, D. Yan, C.-P. T. Nguyen, T. Kho, H. Guthrey, J. Seidel, M. Al-Jassim, A. Cuevas, D. Macdonald, and H. T. Nguyen, "Morphology, microstructure, and doping behaviour: A comparison between different deposition methods for poly-Si/SiOx passivating contacts," *Progress in Photovoltaics: Research and Applications*, vol. 29, no. 7, pp. 857-868, 2021.

[37] T. N. Truong, D. Yan, W. Chen, W. Wang, H. Guthrey, M. Al-Jassim, A. Cuevas, D. Macdonald, and H. T. Nguyen, "Deposition pressure dependent structural and optoelectronic properties of ex-situ boron-doped poly-Si/SiOx passivating contacts based on sputtered silicon," *Solar Energy Materials and Solar Cells*, vol. 215, p. 110602, 2020.

[38] J. I. Langford and A. J. C. Wilson, "Scherrer after sixty years: A survey and some new results in the determination of crystallite size," *Journal of Applied Crystallography*, vol. 11, no. 2, pp. 102-113, 1978.

[39] P. Scherrer, "Bestimmung der Größe und der inneren Struktur von Kolloidteilchen mittels Röntgenstrahlen,"

[40] J. Dash, L. Chen, M. Topka, P. Dinolfo, L. Zhang, K. Kisslinger, T.-M. Lu, and G. C. Wang, "A simple growth method for Nb2O5 films and their optical properties," *RSC Adv.*, vol. 5, 2015.

Chapter 3 – Firing stability of phosphorus-doped polysilicon passivating contacts: factors affecting the degradation behavior

Solar Energy Materials & Solar Cells 234 (2022) 111407

Contents lists available at ScienceDirect

Solar Energy Materials and Solar Cells

journal homepage: www.elsevier.com/locate/solmat

Firing stability of phosphorus-doped polysilicon passivating contacts: Factors affecting the degradation behavior

Di Kang [a,*], Hang Cheong Sio [a], Di Yan [b], Josua Stuckelberger [a], Xinyu Zhang [c], Daniel Macdonald [a]

[a] School of Engineering, The Australian National University (ANU), Canberra, ACT, 2600, Australia
[b] Department of Electrical and Electronic Engineering, University of Melbourne, Melbourne, VIC, 3010, Australia
[c] Jinko Solar Co., Ltd, Shangrao, Jiangxi Province, China

ARTICLE INFO

Keywords:
Polysilicon
Degradation
Surface passivation
Firing
Silicon solar cells

ABSTRACT

We investigate the impact of firing treatments on n-type silicon samples passivated by ex-situ phosphorus-doped polysilicon (poly-Si)/SiO_x structures, and identify factors affecting the firing response. Our samples show stable surface passivation upon firing at temperatures from 600 °C to 750 °C but exhibit a substantial increase in the recombination current density parameter J_0 when the peak firing temperature reaches 800 °C. The extent of degradation is found to also be affected by various processing parameters, such as the means of oxide growth, the poly-Si deposition conditions, and the subsequent phosphorus diffusion. Particularly, the degradation extent appears to increase with poly-Si deposition temperature, possibly associated with changes in the crystal structure. Moreover, phosphorus diffusions performed at a lower temperature leads to stronger firing impact, which could be attributed to the lighter doping concentration in the poly-Si film. In addition, dielectric coatings show the most obvious influence on the firing behavior. Samples fired without the presence of dielectric capping layers suffered the most pronounced degradations in J_0, whereas samples coated with SiN_x/AlO_x stacks or SiN_x single layer with high refractive index above 2 exhibit minimum firing impact. It is speculated that hydrogen diffusion is responsible for the changes in surface passivation quality of the poly-Si/SiO_x passivating contacts. The hypothesis explains the stronger firing impact on samples with lighter doping and lower crystallinity, which determines the diffusion of hydrogen upon firing and hence the amount of hydrogen present in the poly-Si/SiO_x structure, and especially at the oxide interface.

1. Introduction

Recombination losses at the interface between metal contacts and silicon are a key factor limiting the efficiencies of crystalline silicon (c-Si) solar cells, particularly for industrial cell structures, such as the aluminum back surface field (Al-BSF) and passivated emitter and rear contact (PERC) [1]. Passivating contact structures consisting of doped polysilicon (poly-Si) and ultra-thin SiO_x interlayers can drastically reduce carrier recombination at the contact regions [2–5]. The structures utilize thin SiO_x layers to provide effective chemical passivation [6–9], while achieving good field-effect passivation via dopants within the poly-Si layer [10–12] and the diffused regions in the c-Si wafer [13]. Excellent surface passivation, with recombination current density parameter J_0 values of below 5 fA/cm^2, has been reported by using phosphorus-doped poly-Si passivating contacts [14–18].

Mass production of solar cells with phosphorus-doped poly-Si passivating contact technology is already underway, with PV manufacturers such as Jinko Solar [19] and LONGi [20] reaching an impressive efficiency of above 25.2% on large-area n-type c-Si solar cells. However, some challenges remain when transferring the poly-Si/SiO_x technology into the state-of-the-art industrial production, potentially limiting the throughput and the performance of poly-Si passivating contact solar cells. In particular, the high-temperature firing step used in the screen-printed metallization process has been reported to degrade both the contact resistance and the passivation quality of phosphorus-doped poly-Si structures in the passivated and contacted regions [15,21–24], with the extent of the degradation depending on the firing conditions [15,21] and the dielectric coating layers (such as AlO_x, SiN_x or AlO_x/-SiN_x) [22,24,25].

Although the firing impact on poly-Si passivating contacts has been

* Corresponding author.
E-mail address: di.kang@anu.edu.au (D. Kang).

https://doi.org/10.1016/j.solmat.2021.111407
Received 15 May 2021; Received in revised form 2 August 2021; Accepted 20 September 2021
Available online 30 September 2021

studied extensively, the underlying mechanisms and origins are not yet well understood. This work aims to provide a detailed overview of firing impact on the passivated regions of phosphorus-doped poly-Si passivating contact structures, and evaluate the firing response of surface passivation caused by various factors, including the peak firing temperature, the growth method of the interfacial SiO_x, the poly-Si deposition temperature, the phosphorus diffusion conditions, and the dielectric coating layer. The samples are characterized by effective lifetime (τ_{eff}), implied open circuit voltage (iV_{oc}) and recombination current density parameter (J_0), to demonstrate the degradation behavior and the corresponding changes in the surface passivation quality. Moreover, grazing incidence X-ray diffraction (GIXRD) and Fourier-transform infrared spectroscopy (FTIR) were applied to identify correlations with the thermal stability or the properties of the poly-Si/SiO_x layers, such as the crystal structure and the hydrogen bond density in the dielectric coatings. This study is valuable to develop optimum processing conditions for the fabrication of stable phosphorus-doped poly-Si/SiO_x passivating contact structures, potentially accelerating the industrial adoption, and at the same time helps to clarify the mechanisms behind the degradation in surface passivation quality after the firing step.

2. Experimental details

We used n-type phosphorus-doped Czochralski (Cz) wafers (~170 μm, 4 Ω cm) and float-zone (FZ) n-type phosphorus-doped (~300 μm, 100 Ω cm) wafers in this work. The Cz-Si wafers were chemically polished and processed in an industrial production line at Jinko Solar, whereas the FZ-Si wafers were TMAH etched and prepared in the laboratory at ANU. They were processed into symmetric lifetime samples with poly-Si passivating contact structures either using large-scale industrial tools or small-scale laboratory tools, based on a similar fabrication process. As demonstrated in Fig. 1, the key process flows involved oxide growth, intrinsic a-Si deposition, ex-situ $POCl_3$ diffusions, dielectric film deposition and firing. Note that a 400 °C forming gas anneal (FGA) was performed on the FZ samples for 30 min after phosphorus diffusion before the dielectric film deposition, which is a standard step when processing poly-Si passivating contacts in our lab, to achieve an excellent surface passivation. But the Cz samples were deposited with dielectric films directly after the diffusion in the industry. All the samples were fired with a rapid thermal annealing (RTA) tool, with the ramp-up and ramp-down rate of 30 and 60 °C/s respectively. During the firing treatment, samples were covered by a 180 μm dummy wafer on each side to avoid potential influence caused by the strong illumination from the lamps.

The samples were divided into different groups to explore the dependence of firing stability on various parameters, with the detailed processing conditions used for each group described in Table 1. The n-type Cz-Si wafers were used to investigate the influence of firing conditions (Section 3.1) and dielectric coatings (Section 3.5). These samples featured thermally grown SiO_x interface layers and 100 nm poly-Si films on both sides. The samples used to explore the influence of firing conditions (Section 3.1) were fired with industrially deposited SiN_x layers at various peak firing temperatures from 600 °C to 900 °C (temperature measured on the bottom dummy wafer by a thermocouple). The potential influence of dielectric capping layers (Section 3.5) was studied by comparing samples fired with AlO_x, SiN_x, and AlO_x/SiN_x stacks, as well as samples fired without the presence of any dielectric capping. The properties of the SiN_x films are shown in Table 3. To characterize the properties of the SiN_x films, ellipsometry was used to measure the thickness and refractive index (at a wavelength of 633 nm) of the SiN_x layers after the deposition. The AlO_x layers had a thickness of 20 nm, deposited with a Beneq TFS-200 thermal atomic layer deposition (ALD) system at ~200 °C, and the SiN_x films used for AlO_x/SiN_x stacks were 81 nm (measured by ellipsometry) and deposited using a Roth and Rau AK400 PECVD system. Different SiN_x films were also evaluated on the industrial poly-Si samples. They were deposited with different tools or at different deposition conditions, either using a Roth and Rau AK400 (SiN_x-A), or an Oxford PlasmaLab 100 (SiN_x-B to SiN_x-D). Additionally, Fourier-transform infrared spectroscopy (FTIR) was employed to estimate the bond densities in the SiN_x films before firing, using mechanically polished Si wafers from a separate batch. Three absorption peaks, including Si–N (880 cm^{-1}), Si–H (2200 cm^{-1}), and N–H (3340 cm^{-1}), were identified by FTIR, with their bond densities [A−B] being determined by the following equation [26]:

$$[A-B] = k_{A-B} \int \omega^{-1} \alpha(\omega) d\omega \quad (1)$$

Where $k_{A-B}$is the proportionality constant given by Ref. [27], and $\alpha(\omega)$ denotes the absorption coefficient at wavenumber ω. In this work, the total hydrogen bond density, [H], is defined by [Si–H] + [N–H].

The n-type FZ-Si samples were used to explore the influence of the oxide growth (Section 3.2), poly-Si deposition (Section 3.3), and diffusion conditions (Section 3.4) on their firing stability. All samples were fired with the presence of SiN_x-B films (95 nm, measured by ellipsometry) at 800 °C. Their SiO_x thin layers were either grown using chemical (68 wt% nitric acid bath at a temperature of ~90 °C for 30 min) or thermal (at 600 °C for 5 min in O_2) processes, with a thickness of ~1.4 nm and ~1.5 nm respectively, measured by ellipsometry. Within Section 3.2, the samples were deposited with ~50 nm poly-Si films on either chemical or thermal SiO_x layers. The phosphorus diffusion was carried out at 760 °C for deposition and 900 °C for drive-in, in a Tempress quartz tube furnace. The influence of poly-Si deposition (Section 3.3) was separately evaluated in three aspects, including deposition tool and

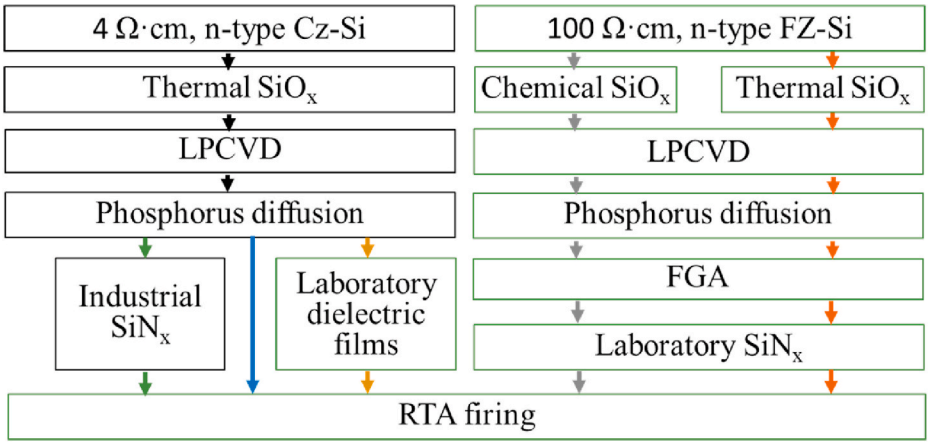

Fig. 1. Flowchart of experimental details.

Table 1
Descriptions of processing steps and degradation conditions studied in each section.

Section number and varied parameters	Si bulk	Growth of SiO_x	Deposition tool, temperature	Thickness of poly-Si	$POCl_3$ diffusion	Dielectric film	Firing temperature
3.1. Peak firing temperatures	n Cz	Thermal	LPCVD	100 nm	Industrial diffusion	Industrial SiN_x	600 °C, 700 °C, 750 °C, 800 °C, 900 °C
3.2. SiO_x growth	n FZ	Thermal Chemical	LPCVD, 520 °C	50 nm	760 °C deposition 900 °C drive-in	SiN_x-B (95 nm)	800 °C
3.3. Poly-Si deposition	n FZ	Chemical	PECVD, 250 °C LPCVD, 520 °C	50 nm	760 °C deposition 900 °C drive-in	SiN_x-B (95 nm)	800 °C
		Thermal	LPCVD, 500 °C LPCVD, 520 °C LPCVD, 550 °C		750 °C deposition 900 °C drive-in		
3.4. Diffusion conditions	n FZ	Chemical	LPCVD, 520 °C	50 nm	790 °C–810 °C deposition 850 °C–900 °C drive-in	SiN_x-B (95 nm)	800 °C
3.5. Dielectric coatings	n Cz	Thermal	LPCVD	100 nm	Industrial diffusion	No cappings, AlO_x, AlO_x/SiN_x-A, SiN_x-A, B, C, D	800 °C

deposition temperature. The samples used for exploring the dependence of deposition tool received 50 nm poly-Si film deposition, on chemical SiO_x, using an Oxford PlasmaLab 100 PECVD system at 450 °C or a Tempress LPCVD furnace at 520 °C, followed by a phosphorus diffusion in the same batch. The impact of the deposition temperature was evaluated on the Si wafers grown with thermal SiO_x interlayers. ~50 nm poly-Si films were separately deposited at 500 °C, 520 °C, or 550 °C, while keeping the gas flow and pressure constant. Subsequently, the samples were subjected into a phosphorus diffusion with 750 °C deposition and 900 °C drive-in steps. The crystalline properties were examined by GIXRD measurement, using a PANalytical X'Pert PRO MRD High Resolution X-ray diffractometer with CuKα radiation and a graphite monochromator. The average crystallite sizes were also calculated for the GIXRD peak at 28.5° (<111> orientation) using the Scherrer formula [28–30]:

$$Average\ crystallite\ size = \frac{k\lambda}{\beta\cos\theta} \quad (2)$$

Where k denotes a shape factor of 0.9, λ is the wavelength of the X-ray, β is the full-width-at-half-maximum in radians, and θ is the Bragg angle.

In addition, the dependence of firing stability on doping is investigated in Section 3.4, on samples with chemical SiO_x and 50 nm LPCVD poly-Si layers. We adjusted the temperature of deposition (from 790 °C to 810 °C) and drive-in (850 °C and 900 °C) steps for the phosphorus diffusion, while keeping the other parameters constant. It should be noted that the tube furnace used for the phosphorus diffusions studied in this section is different from that in Section 3.2 and 3.3. Table 2 provides the deposition and drive-in temperatures applied for the study within Section 3.4, as well as the corresponding sheet resistance, measured by a four-point-probe.

Lifetime values, τ_{eff}, were measured using a Sinton Instruments WCT-120 lifetime tester using the transient method [31], at an injection level of 1×10^{15} cm^{-3}. To monitor changes in the surface passivation quality of poly-Si passivation layers, recombination current density parameters, J_0, were extracted using the Kane and Swanson method [32], at injection levels of 7×10^{15} cm^{-3} and 4×10^{15} cm^{-3} for 4 Ω cm Cz-Si and 100 Ω cm FZ-Si wafers respectively. Note that, within the present work, the samples are assumed to have identical poly-Si films on the front and the rear side, and the single-side J_0 values were obtained by dividing the extracted J_0 by 2. Implied open-circuit voltage (iV_{oc}) was also used to demonstrate the potential influence on device performance.

Table 2
Diffusion conditions applied for samples shown in Fig. 6, and their corresponding sheet resistance measured by four-point probe.

	Deposition temperature	Deposition time	Drive-in temperature	Drive-in time	Sheet resistance (Ω/sq)
I	790 °C	25 min	850 °C	25 min	~1830
II	790 °C	25 min	900 °C	25 min	~840
III	810 °C	25 min	900 °C	25 min	~560
IV	810 °C	25 min	900 °C	50 min	~140
V[a]	760 °C	25 min	900 °C	25 min	~620

[a] The sample V is added here from Section 3.2 and 3.3 for easier comparison. Note, that its phosphorus diffusion was performed using a different tube.

Table 3
Properties of the laboratory SiN_x capping layers measured by ellipsometry and FTIR.

	Thickness (nm)	Refractive index (n)	[Si–N] (cm^{-3})	[H] (cm^{-3})
SiN_x-A	81	1.94	1.39×10^{23}	2.55×10^{22}
SiN_x-B	95	1.96	1.45×10^{23}	3.83×10^{22}
SiN_x-C	79	2.04	1.84×10^{23}	3.29×10^{22}
SiN_x-D	76	2.1	1.93×10^{23}	1.59×10^{22}

3. Results

3.1. Dependence on peak firing temperatures

Fig. 2 compares the changes in τ_{eff}, J_0 and iV_{oc} of the n-type CZ-Si samples fired at different peak firing temperatures ranging from 600 °C to 900 °C. As seen from Fig. 2 (a), the samples show only a slight decrease of τ_{eff} when fired at a temperature between 600 °C and 750 °C, but exhibit a considerable reduction in τ_{eff} fired at 800 °C or above. The change in lifetimes corresponds well with their J_0 values presented in Fig. 2 (b), suggesting a surface-related degradation. Specifically for the sample fired at 800 °C, the τ_{eff} decreased from 7.2 to 1.8 ms, with the corresponding J_0 value increasing from 8 to 32 fA/cm^2. The surface degradation would lead to a substantial loss in device performance, which is reflected in the reduction of iV_{oc}, dropping from 720 to 672 mV after the 800 °C firing treatment. Screen printed solar cells are typically fired at a peak temperature in a range from 750 °C to 800 °C [33–35], depending on the metallization paste. Our results imply that the high-temperature firing treatment used in screen-printing silicon solar cells could potentially impact the performance of poly-Si passivating contact based devices.

A similar correlation between the J_0 degradation and the peak firing temperature has been observed by Çiftpınar et al. [21] and Stodolny et al. [15]. However, van de Loo et al. [24] reported an increase of iV_{oc} from 730 to 740 mV after firing at ~800 °C, on symmetric lifetime samples passivated by phosphorus-doped poly-Si contacts coated with

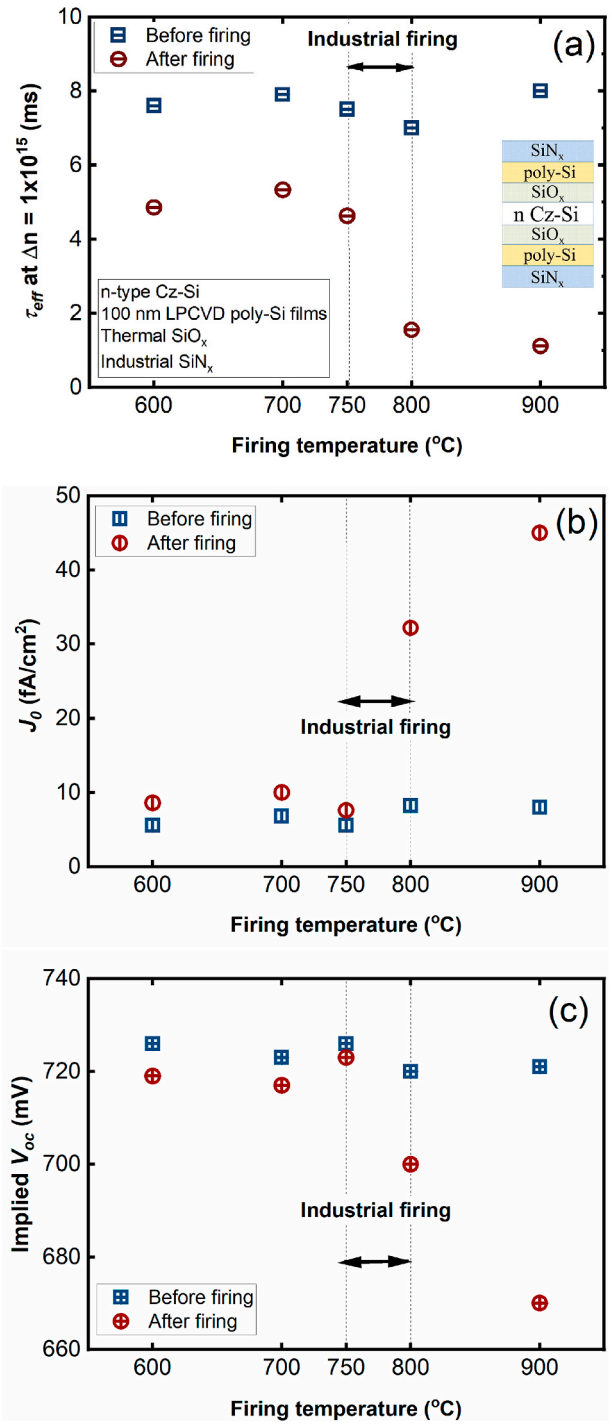

Fig. 2. (a) τ_{eff}, (b) J_0 and (c) iV_{oc} values measured in samples before and after RTA treatment at peak firing temperatures between 600 °C and 900 °C. The samples were prepared on 4 Ω cm n-type Cz-Si, and coated with 100 nm LPCVD poly-Si and ~80 nm industrial SiN_x films. J_0 values were determined at an injection level of 7 × 10^{15} cm^{-3}.

SiN_x films. The inconsistent results could indicate that the thermal stability of poly-Si/SiO_x stack is sensitive to the processing conditions. In the following sections, we will investigate factors influencing the firing stability of the poly-Si layers.

3.2. Dependence on oxide growth

The influence of the growth method of the interfacial SiO_x is evaluated in this section, while keeping the dielectric coatings (SiN_x-B) and firing profile (a peak firing temperature of 800 °C) consistent. Fig. 3 compares the firing behavior of samples with chemically or thermally grown SiO_x layers. While both samples degraded upon firing, the sample with chemical SiO_x was more resistant to firing impact, with the J_0 value only increasing slightly from 7 to 18 fA/cm^2, in comparison to the sample with thermal oxide where the J_0 value increased considerably from 10 to 40 fA/cm^2.

3.3. Dependence on poly-Si deposition

This subsection demonstrates the correlation between the firing response of poly-Si passivating contacts and the poly-Si deposition method or the deposition temperature. Fig. 4 compares the firing behavior for PECVD and LPCVD deposited poly-Si. The PECVD poly-Si started with a higher J_0 value than for the LPCVD poly-Si, as the profile of phosphorus diffusion was optimized for LPCVD poly-Si films, which may not be optimum for the PECVD poly-Si due to their different film properties. Nevertheless, both samples were impacted by firing with the J_0 value rising from 7 to 18 fA/cm^2 for LPCVD poly-Si and 25 to 38 fA/cm^2 for PECVD poly-Si, indicating that the firing impact is not limited to a particular deposition method. It should be also noted that the deposition step for LPCVD and PECVD were performed at 520 °C and 450 °C, which could result in uncertainties when comparing the degradation extent.

Firing behavior for poly-Si/SiO_x passivating contacts with the poly-Si films deposited, using LPCVD, at 500 °C, 520 °C and 550 °C are compared in Fig. 5 (a). All the poly-Si layers suffered a substantial increase in J_0 after firing, from 4 to 40 fA/cm^2, 7 to 50 fA/cm^2, and 14 to 66 fA/cm^2 respectively. The magnitude of J_0 rise (ΔJ_0), determined by J_0 (after firing) − J_0 (before firing), increases with deposition temperature. Fig. 5 (b) demonstrates the intensity of the <111>, <220> and <311> peaks in the poly-Si films measured, by GIXRD, after phosphorus diffusion. As can be observed, while the (111) reflex increases with deposition temperature, the (220) and (311) reflexes remained largely unchanged, in an agreement with the work by Chen et al. [36]. Also shown in Fig. 5 (b) are the average crystallite sizes calculated from the <111> peak detected at 28.5° using the Scherrer formula [29]. The poly-Si film deposited at 550 °C is found to feature the smallest average crystallite size, which, combined with the high crystallinity, could also indicate a high fraction of grain boundaries in the 550 °C deposited poly-Si. However, it is worth noting that the decrease of crystallite size or grain size with increasing deposition temperature may be detectable

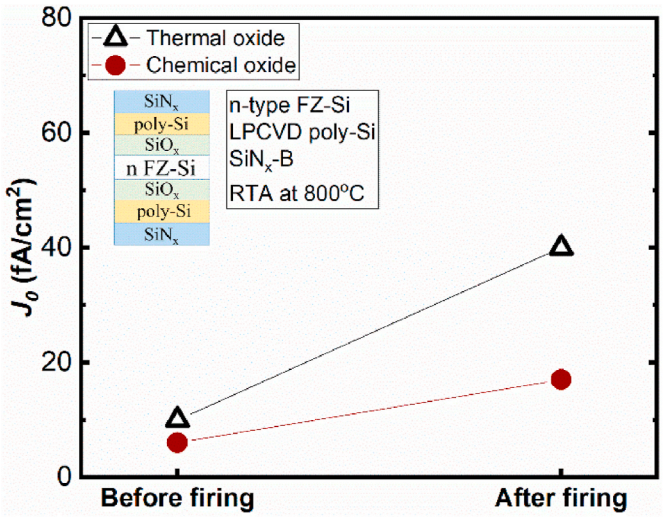

Fig. 3. Comparison of firing behavior for samples featuring thermally and chemically grown SiO_x interlayer. The lines are guides to the eye.

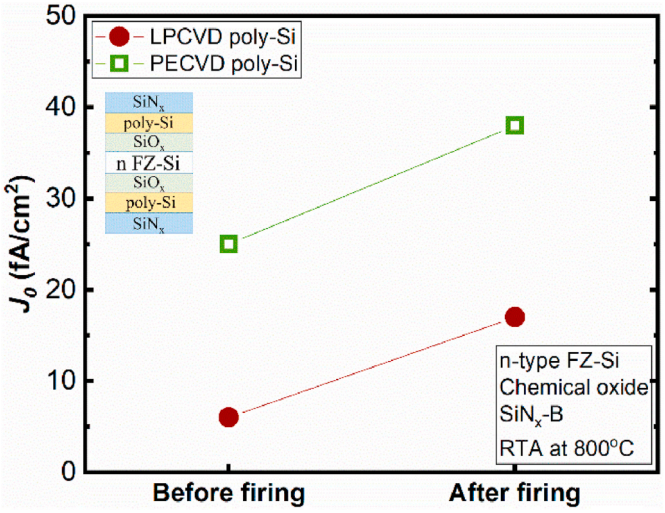

Fig. 4. Comparison of firing behavior for PECVD and LPCVD deposited poly-Si. The lines are guides to the eye.

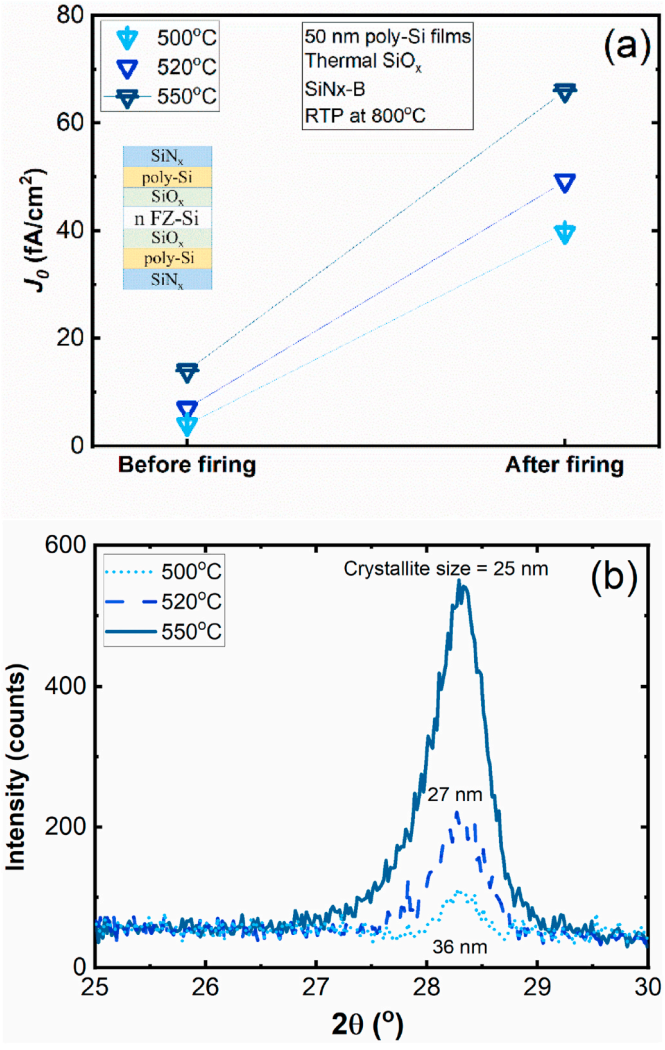

Fig. 5. (a) Comparison of firing behavior for samples passivated by poly-Si films deposited at 500 °C, 520 °C and 550 °C, while keeping pressure and gas flow constant, and their (b) GIXRD results for the <111>, <220> and <311> peaks, measured after phosphorus diffusion. Note that the samples received the same phosphorus diffusion. The lines are guides to the eye.

only in a certain temperature range, as there is also literature reporting that grain size increases with deposition temperature [37,38]. The experimental results suggest that the different firing behavior of the poly-Si films deposited at various temperatures could be potentially related to the difference in crystalline properties, such as crystallinity, crystallite size, and fraction of grain boundaries. Nevertheless, the crystallite size should not be affected by the firing treatment, as confirmed by GIXRD measurements.

3.4. Dependence on phosphorus diffusion

The influence of diffusion conditions on the firing stability is explored by adjusting the deposition and drive-in temperature and time. Details for the applied parameters, as well as the corresponding sheet resistance, measured by a four-point-probe, are given in Table 2. The Electrochemical capacitance-voltage (ECV) profiles presented in Fig. 6 (a) indicate that the diffusion process in which the deposition and drive-in steps were both performed at a low temperature, provides the highest sheet resistance (sample I), owing to the low doping level in the poly-Si film, as well as the shallow diffusion tail [39,40]. Increasing the drive-in temperature from 850 °C to 900 °C drove the phosphorus diffusion deeper into the wafer, resulting in a lower sheet resistance (sample II). When comparing the phosphorus diffusion with a deposition temperature of 790 °C (sample II) and 810 °C (sample III), the doping

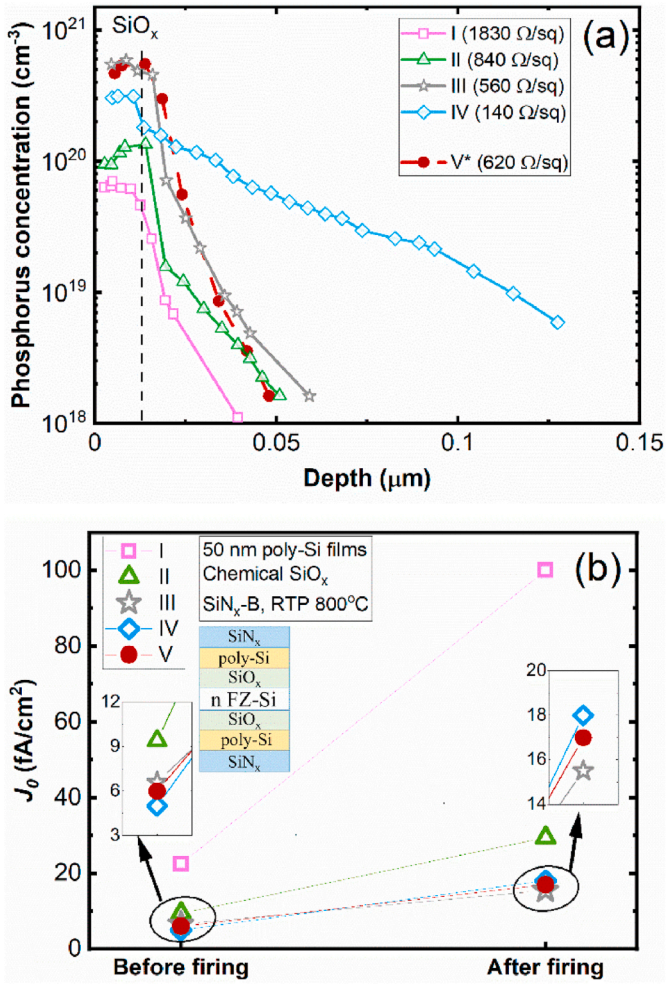

Fig. 6. (a) ECV profiles for the samples (sample I to V) subjected into different phosphorus diffusions (details shown in Table 2), and (b) comparison of firing behavior. Note that sample V is added here from Fig. 3 (chemical oxide) in Section 3.2 and Fig. 4 (LPCVD poly-Si) in Section 3.3 for easier comparison. The lines are guides to the eye.

concentration in the poly-Si film increased with the deposition temperature, resulting in a lower sheet resistance. Moreover, the sample with the lowest sheet resistance (sample IV) is found to show a substantially deeper in-diffusion tail compared to the other samples, possibly associated with the extended time for the drive-in step.

Fig. 6 (b) compares the changes in J_0 for poly-Si/SiO_x structures with different phosphorus diffusion profiles before and after firing at 800 °C. It is interesting to note that the samples (sample III and IV) subjected to phosphorus diffusions with a deposition temperature of 810 °C suffered a similar degradation in J_0, from 6.6 to 15.5 fA/cm^2 for sample III, and 5 to 18 fA/cm^2 for sample IV. In comparison, the phosphorus diffusion in which the deposition step was performed at 790 °C is more prone to firing damage, with the J_0 value increasing from 22.5 to 100 fA/cm^2 and 9.4 to 29.4 fA/cm^2 for sample I and II respectively. Also shown in Fig. 6 (red solid circle) is the sample with LPCVD poly-Si and chemical SiO_x (sample V) taken from Section 3.2 and 3.3, for which the phosphorus diffusion was performed using a different tube furnace. Sample V and III showed similar ECV profiles, and similar firing response.

This stronger degradation could be due to the lighter doping in these poly-Si films, since the surface passivation of poly-Si/SiO_x structures is provided by the combination of chemical passivation from the SiO_x interlayer and field-effect passivation from dopants [10,12]. The firing impact observed in this study are likely to be dominated by the degradation in chemical passivation, as the phosphorus doping profiles remained largely unchanged before and after the firing treatment (confirmed by ECV measurements). It is likely that, for poly-Si/SiO_x contacts with a higher doping level, the stronger field-effect passivation from dopants contributes to their improved firing stability [24]. Additionally, when comparing the heavily doped samples (sample III and IV), the sample with a lower doping concentration within the poly-Si film but a deeper in-diffusion tail (sample IV) exhibited a slightly higher degradation extent after firing, which might indicate that the doping concentration in the poly-Si film shows more impact than the in-diffusion regions in the c-Si wafer. Further research, however, is needed to understand the influence of the in-diffusion layer on the firing response of poly-Si/SiO_x samples.

3.5. Dependence on dielectric coatings

Fig. 7 (a) compares the effects of an 800 °C RTA anneal on industrially processed poly-Si (100 nm thick) passivated samples coated with various dielectric layers. The sample fired without any capping layer exhibits the most pronounced degradation in surface passivation, with J_0 values increasing from 27 to 300 fA/cm^2. Obvious degradation is also observed on samples fired with either a single layer of 20 nm ALD AlO_x or 80 nm SiN_x, but is not as severe as on the sample without coatings. Surprisingly, a stack of the two films allows the poly-Si passivation layers to maintain a low J_0 value after firing.

Fig. 7 (b) depicts the impact of firing on samples coated with four different SiN_x films deposited using a Roth and Rau AK400 (SiN_x-A) or an Oxford PlasmaLab 100 (SiN_x-B, C and D) PECVD tool. The degradation is very sensitive to the SiN_x films, possibly caused by their different properties, such as refractive index and Si–N bond density ([Si–N]) as shown in Table 3. Among the investigated SiN_x films, the degree of degradation decreases with increasing [Si–N], indicating that the firing induced degradation could depend on the film density, which has shown to be directly correlated with [Si–N] [41]. It has been reported that denser films tend to inject more hydrogen into the poly-Si/SiO_x [42] and also prevent the out-diffusion of hydrogen [43,44] during firing and high temperature annealing. In addition, samples fired with SiN_x films featuring a refractive index >2 exhibited an enhanced thermal stability, which is consistent with the observations by Steinhauser et al. [22]. On the other hand, the firing stability does not appear to show a correlation with the [H] in the SiN_x films. Our results agree with Hong et al. [45] who reported that the amount of hydrogen released from SiN_x layers into the Si wafer is determined by the process of in- and out-diffusion rather than [H] in the SiN_x film.

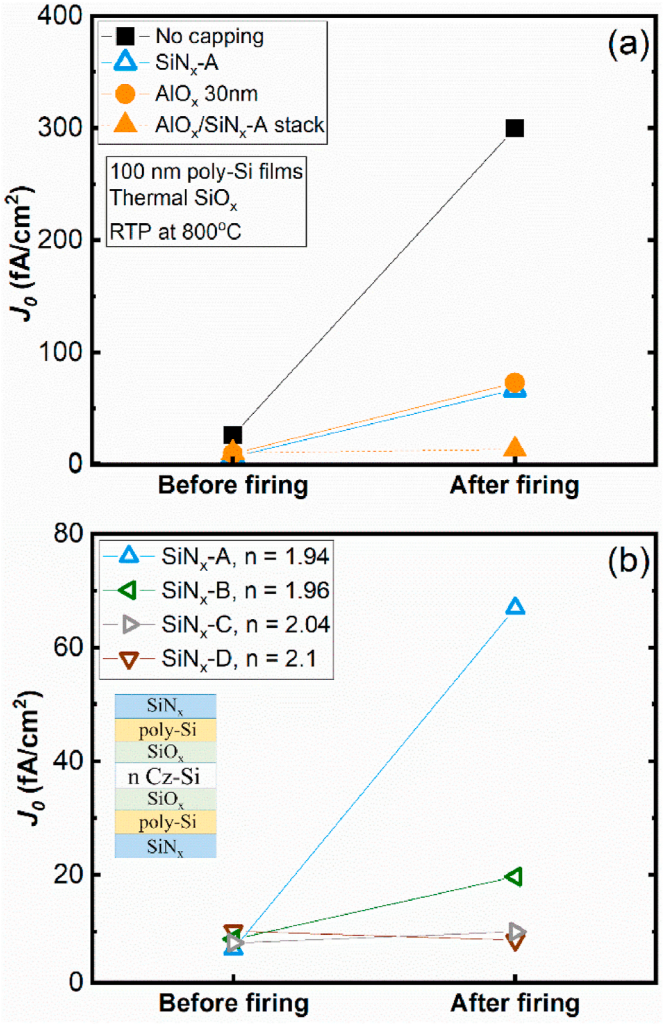

Fig. 7. Firing response of poly-Si passivated samples coated with (a) different dielectric coating layers, and (b) various SiN_x capping layers upon 800 °C RTA anneal. The poly-Si/SiO_x contacts were processed using industrial tools, on 4 Ω cm n-type Cz-Si wafers. Note that FTIR and ellipsometry measurements were performed separately, after SiN_x deposition, on mechanically polished wafers. The lines are guides to the eye.

4. Discussion

According to the experimental results, we propose that hydrogen is a possible candidate responsible for the changes in surface passivation quality of phosphorus poly-Si/SiO_x passivating contacts upon firing, in an agreement with the theory proposed in the literature [22,24]. The substantial increase of J_0 in the samples fired without dielectric coatings, in conjunction with the positive correlation between firing stability and the SiN_x film density, observed in Fig. 7 (b), suggest that the dielectric capping layers act either as a barrier to avoid out-diffusion of hydrogen from the poly-Si layers, or as a hydrogen source for hydrogenating the interfacial oxide during firing. This speculation is also supported by the possible dependence of firing behavior on the crystalline properties (shown in Fig. 5) and phosphorus diffusion conditions (shown in Fig. 6), as it has been reported in the literature that hydrogen diffusion can be influenced by crystal structure in the poly-Si film [46,47] and doping concentration in the heavily doped region [48,49]. The underlying mechanism of the hydrogen involvement in phosphorus doped poly-Si/SiO_x passivating contacts and the corresponding effects on the

changes of J_0 upon firing is explained in a separate work [50].

On the other hand, it should be also noted that the influence of the SiO_x properties cannot be excluded in this work. In Fig. 5, the dependence of firing behaviors on the temperature of poly-Si deposition was attributed to the crystalline properties, potentially affecting the diffusion of hydrogen during firing. However, varying the poly-Si deposition temperature could also affect properties of the SiO_x interlayer, as evidenced by the FTIR results shown in Ref. [36], where Si–O bonds were found to increase with the deposition temperature in phosphorus-doped PECVD poly-Si films. Similarly, samples subjected to different phosphorus diffusion conditions (shown in Fig. 6) could feature oxides with different properties [40].

In addition to the experiments presented above, we compared the firing stability of poly-Si with a film thickness of 150–230 nm. The different poly-Si thicknesses were achieved by subjecting samples to a TMAH solution after phosphorus diffusion, allowing to thin the poly-Si layer, while keeping the oxide properties and in-diffusion layers unchanged. The samples exhibited very similar firing response. However, the etched samples appeared to show a slightly different initial doping profile in the poly-Si films, which could potentially introduce uncertainties. To further study the influence of poly-Si film thickness and other factors, such as surface morphology of c-Si, that could also affect the firing stability of poly-Si, more experiments will be needed.

5. Conclusions

We observed an obvious loss of surface passivation on poly-Si samples after firing at 800 °C or above. The degradation can lead to a substantial reduction in iV_{oc}, indicating potential impacts on the cell performance when transferring the poly-Si/SiO_x passivating technology into industrial production. The firing stability appeared to be dependent on various parameters used for the fabrication of the poly-Si structures, including the growth of SiO_x interlayers, conditions applied for the poly-Si deposition and phosphorus diffusion, as well as the dielectric coatings. It was found that the dielectric coatings have the strongest impact on the firing stability. Samples fired without the presence of dielectric capping layers exhibited the most severe degradations in J_0, whereas samples coated with SiN_x/AlO_x stacks or SiN_x with more Si–N bonds showed minimum degradation after firing. It is hypothesized that the observed correlation of firing behavior with crystal property and sheet resistance could be potentially explained by the different hydrogen diffusivity in the doped poly-Si layer upon firing.

CRediT authorship contribution statement

Di Kang: Writing – original draft, Methodology, Conceptualization. **Hang Cheong Sio:** Supervision, Writing – review & editing. **Di Yan:** Formal analysis, Writing – review & editing, Investigation. **Josua Stuckelberger:** Data curation. **Xinyu Zhang:** Resources. **Daniel Macdonald:** Project administration, Writing – review & editing.

Declaration of competing interest

The authors declare that they have no known competing financial interests or personal relationships that could have appeared to influence the work reported in this paper.

Acknowledgements

This work has been supported by the Australian Renewable Energy Agency (ARENA) through projects RND017 and 1-A060. Access to the Australian National Fabrication Facility (ANFF) ACT node is gratefully acknowledged.

References

[1] A. Cuevas, P.A. Basore, G. Giroult-Matlakowski, C. Dubois, Surface recombination velocity of highly doped n-type silicon, J. Appl. Phys. 80 (6) (1996) 3370–3375.
[2] R. Peibst, U. Römer, Y. Larionova, H. Schulte-Huxel, T. Ohrdes, M. Häberle, B. Lim, J. Krügener, D. Stichtenoth, T. Wütherich, C. Schöllhorn, J. Graff, R. Brendel, Building Blocks for Back-Junction Back-Contacted Cells and Modules with Ion-Implanted Poly-Si Junctions, 2014 IEEE 40th Photovoltaic Specialist Conference, PVSC), 2014, 0852-0856.
[3] R. Basnet, S.P. Phang, C. Samundsett, D. Yan, W. Liang, C. Sun, S. Armand, R. Einhaus, J. Degoulange, D. Macdonald, 22.6% Efficient solar cells with polysilicon passivating contacts on n-type solar-grade wafers, Solar RRL 3 (11) (2019) 1900297.
[4] F. Haase, S. Schäfer, C. Klamt, F. Kiefer, J. Krügener, R. Brendel, R. Peibst, Perimeter Recombination in 25%-efficient IBC solar sells with passivating polo contacts for both polarities, IEEE Journal of Photovoltaics 8 (1) (2018) 23–29.
[5] F. Feldmann, M. Simon, M. Bivour, C. Reichel, M. Hermle, S.W. Glunz, Carrier-selective contacts for Si solar cells, Appl. Phys. Lett. 104 (18) (2014) 181105.
[6] A. Ingenito, G. Nogay, Q. Jeangros, E. Rucavado, C. Allebé, S. Eswara, N. Valle, T. Wirtz, J. Horzel, T. Koida, M. Morales-Masis, M. Despeisse, F.-J. Haug, P. Löper, C. Ballif, A passivating contact for silicon solar cells formed during a single firing thermal annealing, Nature Energy 3 (9) (2018) 800–808.
[7] R. Peibst, U. Römer, Y. Larionova, M. Rienäcker, A. Merkle, N. Folchert, S. Reiter, M. Turcu, B. Min, J. Krügener, D. Tetzlaff, E. Bugiel, T. Wietler, R. Brendel, Working principle of carrier selective poly-Si/c-Si junctions: is tunnelling the whole story? Sol. Energy Mater. Sol. Cell. 158 (2016) 60–67.
[8] D. Yan, A. Cuevas, Y. Wan, J. Bullock, Passivating contacts for silicon solar cells based on boron-diffused recrystallized amorphous silicon and thin dielectric interlayers, Sol. Energy Mater. Sol. Cell. 152 (2016) 73–79.
[9] S.W. Glunz, F. Feldmann, SiO2 surface passivation layers – a key technology for silicon solar cells, Sol. Energy Mater. Sol. Cell. 185 (2018) 260–269.
[10] A. Cuevas, Y. Wan, D. Yan, C. Samundsett, T. Allen, X. Zhang, J. Cui, J. Bullock, Carrier population control and surface passivation in solar cells, Sol. Energy Mater. Sol. Cell. 184 (2018) 38–47.
[11] A.S. Kale, W. Nemeth, S.P. Harvey, M. Page, D.L. Young, S. Agarwal, P. Stradins, Effect of silicon oxide thickness on polysilicon based passivated contacts for high-efficiency crystalline silicon solar cells, Sol. Energy Mater. Sol. Cell. 185 (2018) 270–276.
[12] F.A. Lindholm, A. Neugroschel, M. Arienzo, P.A. Iles, Heavily doped polysilicon-contact solar cells, IEEE Electron. Device Lett. 6 (7) (1985) 363–365.
[13] J. Stuckelberger, G. Nogay, P. Wyss, A. Ingenito, C. Allebé, J. Horzel, B.A. Kamino, M. Despeisse, F. Haug, P. Löper, C. Ballif, Recombination analysis of phosphorus-doped nanostructured silicon oxide passivating electron contacts for silicon solar cells, IEEE Journal of Photovoltaics 8 (2) (2018) 389–396.
[14] D. Yan, A. Cuevas, J.I. Michel, C. Zhang, Y. Wan, X. Zhang, J. Bullock, Polysilicon passivated junctions: the next technology for silicon solar cells? Joule 5 (4) (2021) 811–828.
[15] M.K. Stodolny, M. Lenes, Y. Wu, G.J.M. Janssen, I.G. Romijn, J.R.M. Luchies, L. J. Geerligs, n-Type polysilicon passivating contact for industrial bifacial n-type solar cells, Sol. Energy Mater. Sol. Cell. 158 (2016) 24–28.
[16] F. Haase, C. Hollemann, S. Schäfer, A. Merkle, M. Rienäcker, J. Krügener, R. Brendel, R. Peibst, Laser contact openings for local poly-Si-metal contacts enabling 26.1%-efficient POLO-IBC solar cells, Sol. Energy Mater. Sol. Cell. 186 (2018) 184–193.
[17] J. Schmidt, R. Peibst, R. Brendel, Surface passivation of crystalline silicon solar cells: present and future, Sol. Energy Mater. Sol. Cell. 187 (2018) 39–54.
[18] M. Hermle, F. Feldmann, M. Bivour, J.C. Goldschmidt, S.W. Glunz, Passivating contacts and tandem concepts: approaches for the highest silicon-based solar cell efficiencies, Appl. Phys. Rev. 7 (2) (2020), 021305.
[19] JinkoSolar, JinkoSolar Large-Area N-type Monocrystalline Silicon Solar Cell Reaches Record-Breaking New High Efficiency of 25.25%, 2021. "Press release" [Online] Available: http://jinkosolar.com.au/2021/05/jinkosolar-large-area-n-type-monocrystalline-silicon-solar-cell-reaches-record-breaking-new-high-efficiency-of-25-25/.
[20] LONGi, LONGi Breaks Three More World Records for Solar Cell Efficiency, 2021. "Press release" [Online] Available: https://en.longi-solar.com/home/events/press_detail/id/335.html.
[21] H.E. Çiftpınar, M.K. Stodolny, Y. Wu, G.J.M. Janssen, J. Löffler, J. Schmitz, M. Lenes, J.-M. Luchies, L.J. Geerligs, Study of screen printed metallization for polysilicon based passivating contacts, Energy Procedia 124 (2017) 851–861.
[22] B. Steinhauser, F. Feldmann, D. Ourinson, H. Nagel, T. Fellmeth, M. Hermle, On the influence of the SiNx composition on the firing stability of poly-Si/SiNx stacks, Phys. Status Solidi 217 (21) (2020) 2000333.
[23] F. Feldmann, T. Fellmeth, B. Steinhauser, H. Nagel, D. Ourinson, S. Mack, E. Lohmüller, J.-I. Polzin, J. Benick, J. Rentsch, M. Hermle, S. Glunz, Large Area TOPCon Cells Realized by a PECVD Tube Process, 36th European Photovoltaic Solar Energy Conference and Exhibition, 2019, pp. 304–308.
[24] B.W.H. van de Loo, B. Macco, M. Schnabel, M.K. Stodolny, A.A. Mewe, D.L. Young, W. Nemeth, P. Stradins, W.M.M. Kessels, On the hydrogenation of Poly-Si passivating contacts by Al2O3 and SiNx thin films, Sol. Energy Mater. Sol. Cell. 215 (2020) 110592.
[25] A. Mewe, M. Stodolny, J. Anker, M. Lenes, X. Pagès, Y. Wu, K. Tool, B. Geerligs, I. G. Romijn, Full wafer size IBC cell with polysilicon passivating contacts, AIP Conference Proceedings 2018 (1999), 040014.
[26] M. Cardona, Vibrational spectra of hydrogen in silicon and germanium, Phys. Status Solidi 118 (2) (1983) 463–481.

[27] F. Giorgis, F. Giuliani, C. Pirri, T. Elena, C. Summonte, R. Rizzoli, R. Galloni, A. Desalvo, P. Rava, Optical, structural and electrical properties of device-quality hydrogenated amorphous silicon-nitrogen films deposited by plasma-enhanced chemical vapur deposition, Phil. Mag. B 77 (1998) 925–944.
[28] J.I. Langford, A.J.C. Wilson, Scherrer after sixty years: a survey and some new results in the determination of crystallite size, J. Appl. Crystallogr. 11 (2) (1978) 102–113.
[29] P. Scherrer, Bestimmung der Größe und der inneren Struktur von Kolloidteilchen mittels Röntgenstrahlen.
[30] J. Dash, L. Chen, M. Topka, P. Dinolfo, L. Zhang, K. Kisslinger, T.-M. Lu, G.C. Wang, A simple growth method for Nb2O5 films and their optical properties, RSC Adv. 5 (2015).
[31] R.A. Sinton, A. Cuevas, M. Stuckings, Quasi-steady-state photoconductance, a new method for solar cell material and device characterization. Conference Record of the Twenty Fifth IEEE Photovoltaic Specialists Conference - 1996, 1996, pp. 457–460.
[32] D.E. Kane, R.M. Swanson, Measurement of the emitter saturation current by a contactless photoconductivity decay method, Proceedings of the IEEE 18th Photovoltaic Specialist Conference (1985) 578.
[33] D. Chen, Y. Chen, Z. Wang, J. Gong, C. Liu, Y. Zou, Y. He, Y. Wang, L. Yuan, W. Lin, R. Xia, L. Yin, X. Zhang, G. Xu, Y. Yang, H. Shen, Z. Feng, P.P. Altermatt, P. J. Verlinden, 24.58% total area efficiency of screen-printed, large area industrial silicon solar cells with the tunnel oxide passivated contacts (i-TOPCon) design, Sol. Energy Mater. Sol. Cell. 206 (2020) 110258.
[34] J. Benick, A. Richter, M. Hermle, S.W. Glunz, Thermal stability of the Al2O3 passivation on p-type silicon surfaces for solar cell applications, Phys. Status Solidi Rapid Res. Lett. 3 (7-8) (2009) 233–235.
[35] J.D. Fields, M.I. Ahmad, V.L. Pool, J. Yu, D.G. Van Campen, P.A. Parilla, M. F. Toney, M.F.A.M. van Hest, The formation mechanism for printed silver-contacts for silicon solar cells, Nat. Commun. 7 (1) (2016) 11143.
[36] W. Chen, T.N. Truong, H.T. Nguyen, C. Samundsett, S.P. Phang, D. MacDonald, A. Cuevas, L. Zhou, Y. Wan, D. Yan, Influence of PECVD deposition temperature on phosphorus doped poly-silicon passivating contacts, Sol. Energy Mater. Sol. Cell. 206 (2020) 110348.
[37] E.Y. Gusev, J.Y. Jityaeva, A.A. Geldash, O.A. Ageev, Effects of PECVD temperature and RF power on surface structure and refractive index of amorphous and polycrystalline silicon films, J. Phys. Conf. 917 (2017), 032029.
[38] M. Hatalis, D. Greve, Large grain polycrystalline silicon by low-temperature annealing of low-pressure chemical vapor deposited amorphous silicon films, J. Appl. Phys. 63 (1988) 2260–2266.
[39] A. Dastgheib-Shirazi, M. Steyer, G. Micard, H. Wagner, P.P. Altermatt, G. Hahn, Relationships between diffusion parameters and phosphorus precipitation during the POCl3 diffusion process, Energy Procedia 38 (2013) 254–262.
[40] D. Yan, S.P. Phang, Y. Wan, C. Samundsett, D. Macdonald, A. Cuevas, High efficiency n-type silicon solar cells with passivating contacts based on PECVD silicon films doped by phosphorus diffusion, Sol. Energy Mater. Sol. Cell. 193 (2019) 80–84.
[41] F. Chen, I.G. Romijn, A.W. Weeber, J. Tan, B. Hallam, J. Cotter, Relationship between PECVD Silicon Nitride Film Composition and Surface and Edge Passivation, 2007.
[42] M. Sheoran, D.S. Kim, A. Rohatgi, H.F.W. Dekkers, G. Beaucarne, M. Young, S. Asher, Hydrogen diffusion in silicon from PECVD silicon nitride, in: 2008 33rd IEEE Photovoltaic Specialists Conference, 2008, pp. 1–4.
[43] H.F.W. Dekkers, G. Beaucarne, M. Hiller, H. Charifi, A. Slaoui, Molecular hydrogen formation in hydrogenated silicon nitride, Appl. Phys. Lett. 89 (21) (2006) 211914.
[44] A.W. Weeber, H.C. Rieffe, I.G. Romijn, W. Sinke, W.J. Soppe, The Fundamental Properties of SiNx:H that Determine its Passivating Qualities, 2005 IEEE 31st Photovoltaic Specialist Conference, PVSC), 2005, pp. 1043–1046.
[45] J. Hong, W.M.M. Kessels, W.J. Soppe, A.W. Weeber, W.M. Arnoldbik, M.C. M.v. d. Sanden, Influence of the high-temperature “firing” step on high-rate plasma deposited silicon nitride films used as bulk passivating antireflection coatings on silicon solar cells, J. Vac. Sci. Technol. B: Microelectronics and Nanometer Structures Processing, Measurement, and Phenomena 21 (5) (2003) 2123–2132.
[46] N.M. Johnson, D.K. Biegelsen, M.D. Moyer, Deuterium passivation of grain-boundary dangling bonds in silicon thin films, Appl. Phys. Lett. 40 (10) (1982) 882–884.
[47] N.H. Nickel, W.B. Jackson, J. Walker, Influence of grain boundaries on hydrogen transport in polycrystalline silicon, J. Non-Cryst. Solids 227–230 (1998) 885–889.
[48] P. Hamer, B. Hallam, R.S. Bonilla, P.P. Altermatt, P. Wilshaw, S. Wenham, Modelling of hydrogen transport in silicon solar cell structures under equilibrium conditions, J. Appl. Phys. 123 (4) (2018), 043108.
[49] S.J. Pearton, J.W. Corbett, T.S. Shi, Hydrogen in crystalline semiconductors, Appl. Phys. A 43 (3) (1987) 153–195.
[50] D. Kang, H.C. Sio, J. Stuckelberger, R. Liu, D. Yan, X. Zhang, D. Macdonald, Optimum Hydrogen Injection in Phosphorus-Doped Polysilicon Passivating Contacts, 2021 submitted.

Chapter 4 – Optimum hydrogen injection in phosphorus-doped polysilicon passivating contacts

ACS APPLIED MATERIALS & INTERFACES

www.acsami.org

Research Article

Optimum Hydrogen Injection in Phosphorus-Doped Polysilicon Passivating Contacts

Di Kang,* Hang Cheong Sio, Josua Stuckelberger, Rong Liu, Di Yan, Xinyu Zhang, and Daniel Macdonald

Cite This: https://doi.org/10.1021/acsami.1c17342

Read Online

ACCESS | Metrics & More | Article Recommendations

ABSTRACT: It has previously been shown that ex situ phosphorus-doped polycrystalline silicon on silicon oxide (poly-Si/SiO_x) passivating contacts can suffer a pronounced surface passivation degradation when subjected to a firing treatment at 800 °C or above. The degradation behavior depends strongly on the processing conditions, such as the dielectric coating layers and the firing temperature. The current work further studies the firing stability of poly-Si contacts and proposes a mechanism for the observed behavior based on the role of hydrogen. Secondary ion mass spectrometry is applied to measure the hydrogen concentration in the poly-Si/SiO_x structures after firing at different temperatures and after removing hydrogen by an anneal in nitrogen. While it is known that a certain amount of hydrogen around the interfacial SiO_x can be beneficial for passivation, surprisingly, we found that the excess amount of hydrogen can deteriorate the poly-Si passivation and increase the recombination current density parameter J_0. The presence of excess hydrogen is evident in selected poly-Si samples fired with silicon nitride (SiN_x), where the injection of additional hydrogen to the SiO_x interlayer leads to further degradation in the J_0, while removing hydrogen fully recovers the surface passivation. In addition, the proposed model explains the dependence of firing stability on the crystallite properties and the doping profile, which determine the effective diffusivity of hydrogen upon firing and hence the amount of hydrogen around the interfacial SiO_x after firing.

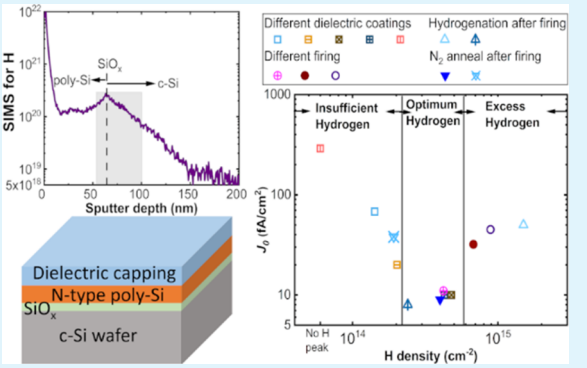

KEYWORDS: *hydrogen, firing, polysilicon, poly-Si, TOPCon, POLO*

1. INTRODUCTION

Doped polycrystalline silicon on silicon oxide (poly-Si/SiO_x) passivating contacts utilize the ultrathin oxide layers to passivate the dangling bonds at the c-Si/SiO_x interface[1−4] while effectively controlling the carrier population as a consequence of the dopants in the poly-Si films and the diffused regions in the c-Si substrate[5−7] and the diffused regions in the c-Si substrate.[8] To further improve the chemical passivation of SiO_x, hydrogenation treatment is commonly applied. The passivation quality of poly-Si/SiO_x structures is sensitive to the hydrogen content around the SiO_x interfacial layer.[9,10] The crystalline silicon (c-Si)/SiO_x interface state density (D_{it}) has been shown to be reduced by injecting hydrogen,[11,12] which can be achieved via forming gas anneal (FGA)[13,14] or by coating with a hydrogen-rich layer, such as silicon nitride (SiN_x)[15−17] or aluminum oxide (AlO_x),[10,18] followed by thermal annealing.

Remarkable efficiencies have been achieved with poly-Si/SiO_x passivating contact technology on laboratory-scale solar cells. The Institute for Solar Energy Research Hamelin (ISFH)[19] and Fraunhofer ISE[20] achieved efficiencies of 26.1 and 26% on interdigitated back contacted (IBC) solar cells with polycrystalline on oxide (POLO) passivating contacts and both-sides-contacted solar cells based on tunnel oxide passivated contact (TOPCon) technology, respectively. Poly-Si passivating contacts are currently being implemented in commercial solar cells, showing great promise toward excellent performance. Photovoltaic (PV) manufacturers, such as JinkoSolar[21] and LONGi,[22] have reported an impressive conversion efficiency above 25.2% on large-area n-type c-Si solar cells with a phosphorus-doped poly-Si/SiO_x passivating contact at the rear side.

However, the transfer of poly-Si/SiO_x technology to industrial manufacturing is challenging, with potential limitations on the performance of poly-Si passivating contact

Received: September 8, 2021
Accepted: November 3, 2021

solar cells. In particular, the high-temperature firing step used in the screen-printed metallization process can degrade the passivation quality of phosphorus-doped poly-Si structures in the passivated and contacted regions, as shown in our previous works[23,24] and the literature.[14,15,17,25−29] It was observed that the change in J_0 after firing increases with increasing firing temperature.[15,29] Moreover, the firing behavior of poly-Si coated with SiN_x films depends strongly on the SiN_x film density and the refractive index of the SiN_x coatings,[17,23] for which a refractive index >2 allows samples to be resistant to firing damage. In our previous work,[23] a pronounced degradation in the recombination current density parameter J_0 was detected on ex situ phosphorus-doped poly-Si/SiO_x passivating contacts after firing at 800 °C or above, and hydrogen was believed to play a role in the firing effects according to correlations between the firing response and the dielectric properties.

This paper is an extension of our former work[23] to further investigate the correlation between hydrogen and the firing impact on phosphorus-doped poly-Si. We applied secondary ion mass spectrometry (SIMS) to measure the hydrogen content in the poly-Si/SiO_x stacks and correlated the hydrogen concentration surrounding the SiO_x to the J_0 values on samples fired at different temperatures and with various dielectric coating layers. Based on these experimental results and by further manipulating the hydrogen concentration via the injection or removal of hydrogen during annealing, we propose a mechanism underlying the firing impact. Furthermore, our previous observations,[23] such as the dependence of firing behavior on the doping profile and the crystal properties, are further explored in this work. This study is valuable to identify the mechanisms behind the degradation in surface passivation quality after the firing step and to design optimal industrial processes for poly-Si passivating contacts.

2. EXPERIMENTAL DETAILS

Phosphorus-doped n-type Czochralski (Cz) wafers were used here, with a thickness of ∼170 μm and a resistivity of 4 Ω·cm. The Si wafers were chemically polished and processed in an industrial production line, following the process flows shown in Figure 1. The main process

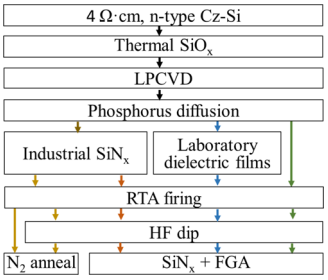

Figure 1. Flowchart of experimental details.

flows included thermal growth of the SiO_x thin layer (∼1.5 nm), deposition of the ∼100 nm poly-Si film using low-pressure chemical vapor deposition (LPCVD), and ex situ $POCl_3$ diffusions (sheet resistance of ∼200 Ω/sq, measured by a four-point probe). After phosphorus diffusion, phosphosilicate glass (PSG) was removed via a hydrogen fluoride (HF) dip. Then, the samples were either coated with dielectric films followed by firing or were fired directly without any capping layer. The firing treatment was performed using a rapid thermal annealing (RTA) tool, with ramp-up and ramp-down rates of 30 and 60 °C/s, respectively. During the firing treatment, both sides of the samples were covered by a 180 μm dummy wafer to prevent potential influence by the strong illumination from the lamps. The temperature was measured on the bottom dummy wafer by a thermocouple. The SiN_x capping layers were deposited either using a Roth and Rau AK400 (SiN_x-A), an Oxford PlasmaLab 100 (SiN_x-B and SiN_x-C), or a Centrotherm batch-type plasma-enhanced chemical vapor deposition (PECVD) tool (industrial SiN_x).

Selected samples coated with the industrial SiN_x films were subjected to a further hydrogenation and dehydrogenation treatment after firing at 800 °C, to inject additional hydrogen, or to reduce hydrogen in the poly-Si/SiO_x stacks. To inject more hydrogen, the samples had their original SiN_x films removed by the HF dip after firing followed by a fresh SiN_x deposition using a Roth and Rau AK400 PECVD system (SiN_x-A) and a subsequent forming gas anneal (FGA) at 400 °C. To remove hydrogen, the fired samples were annealed in N_2 after removing the fired SiN_x coatings via the HF dip. A sample was annealed with the fired SiN_x as a reference control.

SIMS characterization was applied to measure the concentration of hydrogen in the poly-Si/SiO_x passivating contacts after different processing steps using a Cameca IMS 5fE7 SIMS tool (Cameca, France). A primary ion beam of Cs^+ with an impact energy of 5.0 keV and beam current of 16 nA was employed to raster a 125 × 125 μm region of the sample surface, with a sputtering rate of 0.5 nm/s. Note that the dielectric coating layers were removed before the SIMS measurements. In addition to the hydrogen profiles acquired by measuring H^+, a separate SIMS profiling was obtained by measuring complex HCs_2^+ ions to avoid measurement artifacts caused by the higher ion yield of H^+ in oxides than in poly-Si or c-Si.[30] The two measurements showed similar hydrogen peaks around the SiO_x, confirming that the hydrogen peaks surrounding the SiO_x acquired with H^+ are not due to measurement artifacts.

Lifetime values, τ_{eff}, were measured with a Sinton Instruments WCT-120 lifetime tester using the transient mode,[31] at an injection level of 1×10^{15} cm^{-3}. To monitor changes in the surface passivation quality of poly-Si passivation layers, the corresponding recombination current density parameters, J_0, were extracted using the slope method by Kane and Swanson[32] (at an injection level of 7×10^{15} cm^{-3}).

3. RESULTS AND DISCUSSION

3.1. Impact of Additional Hydrogenation after Firing.

This subsection compares the impact of an 800 °C firing step and a subsequent hydrogenation treatment, achieved through SiN_x deposition and FGA after firing, for the n-type poly-Si contacts with and without SiN_x coatings. As shown in Figure 2, the sample fired without any SiN_x coating suffered pronounced degradation in both τ_{eff} (from 2.4 to 0.3 ms) and J_0 (from 26 to 290 fA/cm^2). After the hydrogenation process, the τ_{eff} (5.7 ms) and J_0 (8 fA/cm^2) were fully recovered and improved even further compared to those before firing. The recovery of surface passivation degradation by hydrogenation is consistent with the results reported by Feldmann *et al.*[25]

Hydrogen concentrations in the poly-Si/SiO_x passivated samples were assessed by SIMS. As observed in Figure 2b, for the samples after diffusion and after firing, there were no clear hydrogen signals near the interfacial SiO_x. By contrast, after SiN_x deposition and FGA, the sample showed an increase in hydrogen around the SiO_x, which could contribute to the recovery of surface passivation.[14,25,33]

As observed in Figure 3a, the poly-Si contacts capped with industrial SiN_x films exhibited a degradation in τ_{eff} and J_0 after firing, changing from 3.6 to 2.9 ms and 13 to 32 fA/cm^2, respectively. The extent of the degradation is less severe than the samples fired without SiN_x, as shown in Figure 2. However, in contrast to the samples fired without SiN_x, the subsequent hydrogenation treatment, surprisingly, did not recover the surface passivation but caused a further degradation, with the

https://doi.org/10.1021/acsami.1c17342
ACS Appl. Mater. Interfaces XXXX, XXX, XXX−XXX

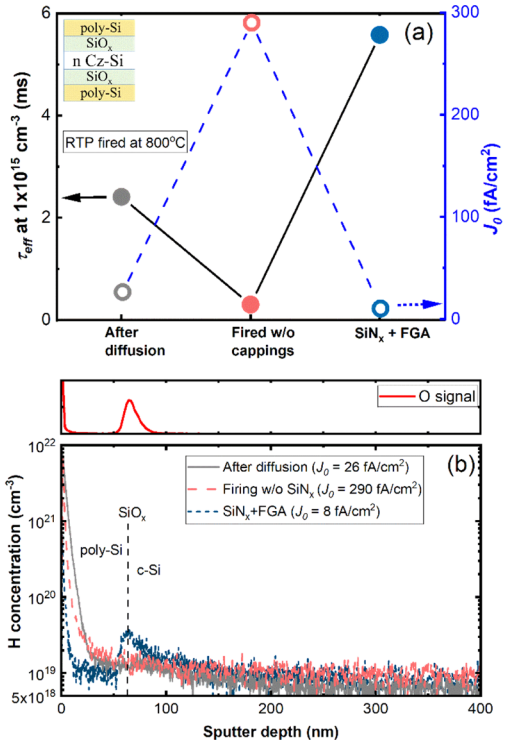

Figure 2. (a) Effective lifetimes, τ_{eff}, recombination current density parameters, J_0, and (b) the corresponding SIMS profiles for hydrogen, measured after various processing steps, including phosphorus diffusion, firing, and subsequent hydrogenation by SiN_x deposition and FGA. The raw signal for oxygen is shown in panel (b) as a reference to identify the position of the SiO_x interlayer. Note that the SiN_x capping layers were removed prior to the SIMS measurements.

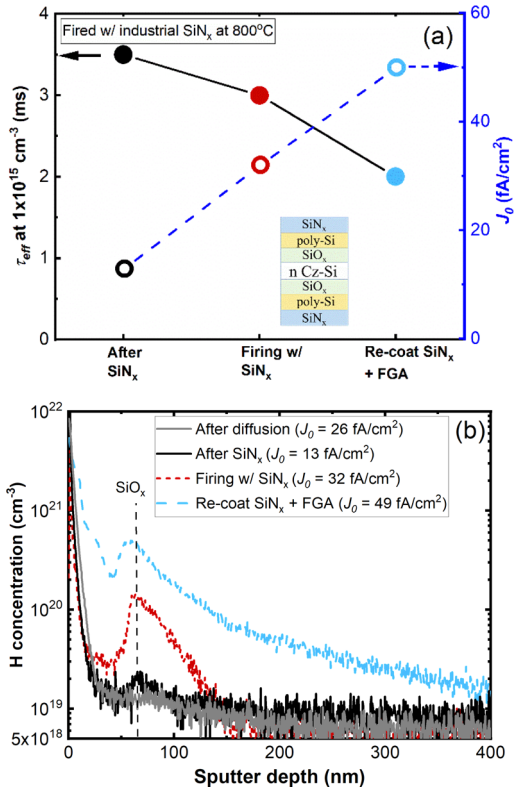

Figure 3. (a) Effective lifetimes, τ_{eff}, and recombination current density parameters, J_0, and (b) the corresponding SIMS profiles for hydrogen, measured after various processing steps, including SiN_x deposition, 800 °C firing, and subsequent rehydrogenation by SiN_x deposition and FGA after removing the fired SiN_x films. Note that the SiN_x capping layers were removed prior to the SIMS measurements.

τ_{eff} dropping from 2.9 to 1.9 ms and the J_0 value increasing from 32 to 49 fA/cm^2.

The SIMS profiles (Figure 3b) indicate a small hydrogen peak around the oxide on the sample after coating with SiN_x, reflecting the injection of a small amount of hydrogen into the SiO_x interlayer during the SiN_x deposition. After firing, the hydrogen signal increased considerably, supporting our previous speculation that the dielectric capping layers act as a source for injecting hydrogen into the interfacial oxide during firing.[23] Upon an additional hydrogenation treatment (removal and redeposition of SiN_x and FGA), there was a further increase in the hydrogen concentration surrounding the interfacial oxide, which further extended into the poly-Si layer and the c-Si.

The results depicted in Figures 2 and 3 indicate that the quality of surface passivation does not monotonically increase with the amount of hydrogen near the interlayer of SiO_x, which appears to be inconsistent with the well-established theory that hydrogenation improves the surface passivation of poly-Si/SiO_x structures.[10,14,15,33−35] Therefore, further study is performed to understand the role of hydrogen in poly-Si/SiO_x passivating contacts, and the possible mechanism will be proposed in Section 3.4.

3.2. Impact of the Capping Layer and Firing Temperature. In our previous work, the degradation in J_0 after firing was found to correlate to the dielectric capping layers and the firing temperature.[23] Thus, the hydrogen concentration in these poly-Si/SiO_x contacts was measured by SIMS and correlated to the J_0 value, with the results shown in Figure 4a in the case of different capping layers and in Figure 4b for various firing temperatures. Detailed characterization results for SiN_x-A, SiN_x-B, and SiN_x-C were reported in the former work, with SiN_x-C showing a larger refractive index (n) and a higher density of Si−N bonds than SiN_x-A and SiN_x-B,[23] reflecting a higher film density of SiN_x-C.[36,37] The SIMS results given in Figure 4a support our former speculation that the observed dependence of firing stability on the refractive index (n) and the density of Si−N bonds of the SiN_x capping films could be related to the film density.[23] Denser SiN_x layers could be more effective in preventing the out-diffusion of hydrogen from the wafer upon high-temperature annealing,[38,39] resulting in more hydrogen near the SiO_x interlayer, as evidenced by the higher hydrogen content around the SiO_x in the sample fired with SiN_x-C.

Also given in Figure 4a are the hydrogen profiles for samples fired with AlO_x (~20 nm)/SiN_x-A stacks or industrial SiN_x films. Comparing AlO_x/SiN_x-A stacks with SiN_x-A single films, improved firing stability and a higher hydrogen content around the SiO_x were detected on the sample fired with AlO_x/SiN_x-A stacks. All the samples coated with laboratory dielectric films (SiN_x-A, SiN_x-B, SiN_x-C, and AlO_x) appear to show that J_0 increases with a decreasing amount of hydrogen surrounding the SiO_x.

For samples fired at a temperature of 700−900 °C shown in Figure 4b, the hydrogen concentration around the SiO_x increases with the peak firing temperature, most likely because the SiN_x films release an increasing amount of hydrogen with higher annealing temperature.[40,41] Interestingly, the J_0 value of

https://doi.org/10.1021/acsami.1c17342
ACS Appl. Mater. Interfaces XXXX, XXX, XXX−XXX

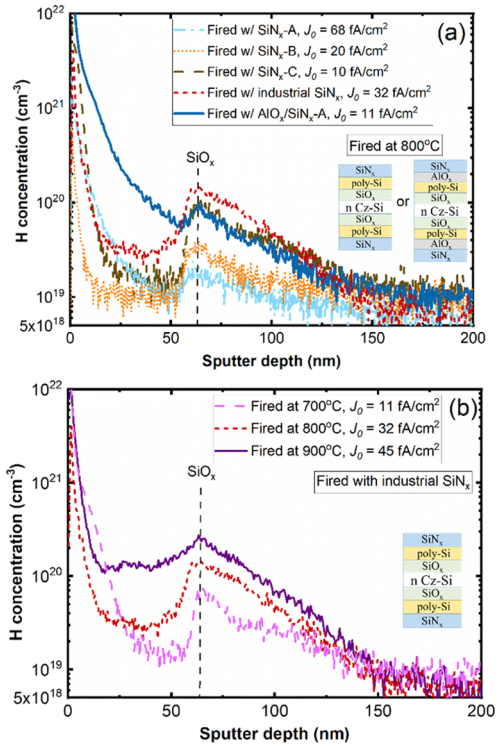

Figure 4. (a) Hydrogen profiles measured by SIMS for samples fired with different dielectric capping layers at 800 °C and (b) samples fired with industrial SiN_x at a temperature from 700 to 900 °C. SiN_x-A, SiN_x-B, and SiN_x-C in the current study correspond to SiN_x-A, SiN_x-B, and SiN_x-D, respectively, in our previous work.[23]

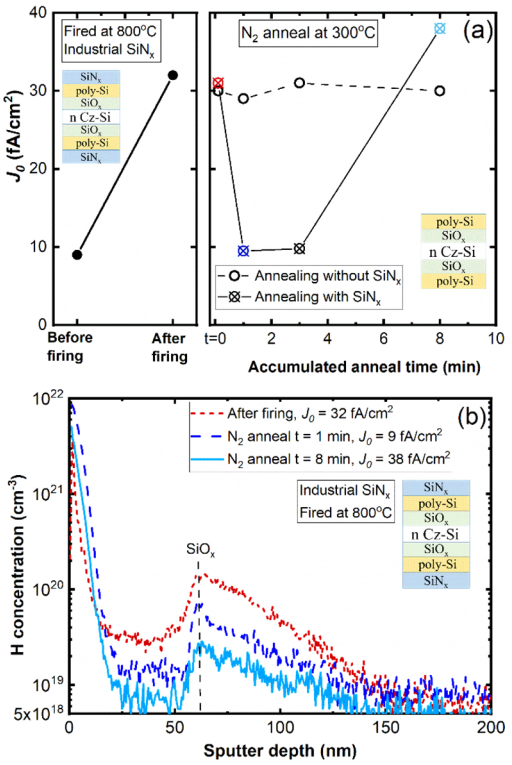

Figure 5. (a) Evolution of J_0 values in poly-Si-passivated samples during firing and the subsequent N_2 anneal for samples annealed with and without removing the fired SiN_x films. (b) SIMS profiles of hydrogen for the samples fired at 800 °C with industrial SiN_x films measured after various treatments, including firing, and the 300 °C N_2 anneal for 1 and 8 min with the removal of SiN_x films.

these samples increases with the peak intensity of hydrogen near the thin SiO_x. The results presented in Figures 3 and 4 reveal a possibility that an excess amount of hydrogen around the interfacial SiO_x after firing could cause increased surface recombination.

3.3. Impact of Dehydrogenation after Firing. It is surprising to observe in the previous section that hydrogen can be detrimental for poly-Si passivation. To confirm this finding, the role of hydrogen is further investigated by annealing the 800 °C fired samples in N_2 at 300 °C after removing the SiN_x capping layer. Figure 5a depicts the evolution of J_0 values during the N_2 anneal for the sample with the fired SiN_x films removed. Interestingly, the deterioration of surface passivation after firing at 800 °C was fully recovered by the 1 min N_2 anneal (J_0 dropped from 31 to 9 fA/cm^2). After an additional 2 min N_2 anneal, the surface passivation was largely unchanged (J_0 = 10 fA/cm^2). After the annealing reaches 8 min, there was a substantial increase in the J_0 value again (J_0 = 38 fA/cm^2). The corresponding SIMS profiles of hydrogen measured on samples before the N_2 anneal and after the 1 and 8 min N_2 anneal are compared in Figure 5b, showing the release of hydrogen from the poly-Si/SiO_x structure during the N_2 anneal. These results indicate that removing excess hydrogen in fired poly-Si passivating contacts can improve the passivation quality. For the sample annealed for 8 min, a significant amount of hydrogen effused from the poly-Si/SiO_x passivating contact structure to the ambient, making the lack of hydrogen around the SiO_x a possible reason for the reduction in passivation quality. Also shown as reference in Figure 5a is a poly-Si sample fired at 800 °C with industrial SiN_x but annealed without removing the fired SiN_x films. The J_0 was largely unchanged during the anneal, indicating that SiN_x could act as a barrier preventing the effusion of hydrogen.[42]

3.4. Proposed Mechanism: An Optimum Amount of Hydrogen. To better assess the relationship between the J_0 of fired poly-Si and the hydrogen concentration near the SiO_x, we integrated the area under the hydrogen curves, from a sputter depth of 55−100 nm to reflect the hydrogen density around the SiO_x interlayer. Following this procedure, the J_0 values of all the fired samples shown in Figures 2−5 are plotted in Figure 6 as a function of hydrogen density. Samples fired without dielectric films (Figure 2b) and fired with SiN_x-A and SiN_x-B (Figure 4a) as well as the sample with additional dehydrogenation treatment (via the N_2 anneal for 8 min after removing the fired SiN_x, as shown in Figure 5b) indicate that a low hydrogen content surrounding the interfacial SiO_x leads to a strong surface recombination, with J_0 increasing with decreasing hydrogen concentration. This is consistent with the literature,[10,14,15,33−35] confirming the benefits of hydrogen incorporation. Surprisingly, for samples fired with industrial SiN_x at 800 and 900 °C (Figure 4b) and samples treated with additional hydrogenation after firing with SiN_x (Figure 3b), our results reveal that excess hydrogen near the SiO_x is also detrimental to the surface passivation of poly-Si, as observed from the increased J_0 with higher hydrogen density. Therefore, it is speculated that an optimum amount of hydrogen is needed for the best surface passivation. Note that the proposed model should not be limited to the poly-Si passivating contact studied herein. J_0 degradation due to the presence of excess hydrogen was also observed on poly-Si structures fabricated with different processing, including ex situ doped PECVD and

https://doi.org/10.1021/acsami.1c17342
ACS Appl. Mater. Interfaces XXXX, XXX, XXX−XXX

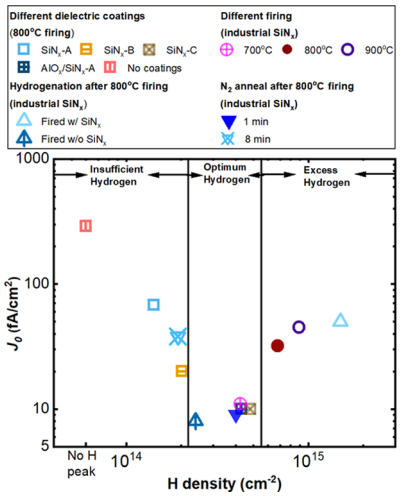

Figure 6. J_0 values measured after firing as a function of hydrogen density estimated by integrating the hydrogen signal between sputter depths of 50 and 150 nm. Note that all the samples are taken from Figures 2–4. Samples fired at different temperatures were coated with industrial SiN_x films; 800 °C firing was performed on all samples, unless stated otherwise in the legend.

LPCVD poly-Si, LPCVD poly-Si deposited at various temperatures, and LPCVD poly-Si deposited on chemical and thermal oxide.[23,43] Therefore, it is anticipated that the proposed model can also be applied to differently processed poly-Si.

The negative impact of excess hydrogen on surface passivation observed in this work agrees with the literature.[44,45] Hollemann *et al.*[44] performed firing experiments on n-type poly-Si/SiO_x passivated lifetime samples with AlO_x and SiN_x stacks by varying the AlO_x thickness and the peak firing temperature and compared the interface defect density (D_{it}) calculated by the MarcoPOLO model and the hydrogen concentration measured by time-of-flight secondary ion mass spectrometry (ToF-SIMS). It was observed that a high-temperature firing at 863 °C can lead to excessive hydrogenation, in which the hydrogen concentration was several times higher than the corresponding D_{it},[44] implying the presence of hydrogen-related defects. In addition, Gotoh *et al.*[45] studied the influence of the deposition temperature on the passivation performance and the hydrogen concentration in a-Si:H/c-Si heterojunctions with hydrogen depth profiling by nuclear reaction analysis. They found that the passivation performance can decrease with an increasing hydrogen level at the a-Si:H/c-Si interface.[45]

In the literature, while hydrogenation has been proven to be effective in improving the performance of solar cells,[34,46–48] hydrogen has been shown to cause recombination in multiple ways, such as formation of structural defects or platelets,[49,50] deactivation of phosphorus dopants,[51] formation of powerful recombination centers composed of carbon, oxygen, and hydrogen,[51,52] and creation of vacancy-hydrogen complexes.[53] It was also suggested that hydrogen itself could cause recombination, potentially resulting in a reduction in the carrier lifetime,[54] which might also be a possible explanation for the impact of excess hydrogen observed herein.

Based on our experimental results, the following mechanism for the firing effect on phosphorus-doped poly-Si is proposed. A large temperature gradient during the rapid firing treatment could result in thermal stress in poly-Si/SiO_x structures and create or activate defects that act as recombination centers, degrading the J_0.[26] The generated dangling bonds can be terminated by the hydrogen atoms released by dielectric coating layers; therefore, poly-Si fired with SiN_x (shown in Figure 3a) exhibits a lower J_0 value than samples fired without SiN_x (shown in Figure 2a). However, once all the dangling bonds are saturated, the accumulation of excess hydrogen surrounding SiO_x becomes detrimental to the surface passivation (Sections 3.2 and 3.3). Therefore, the overall passivation quality of the poly-Si/SiO_x structure is determined by the diffusion of hydrogen during firing and its interaction with defects at the oxide interface.

4. INFLUENCE OF CRYSTAL PROPERTIES AND THE DOPING CONCENTRATION

In addition to the influence of the firing temperature and the dielectric capping layers, the firing behavior depends on the diffusion conditions and poly-Si deposition temperature, possibly due to different hydrogen diffusivities caused by the changes in the crystallite properties and the doping concentration of the poly-Si film, as shown in our previous work.[23] This finding is further investigated here based on the proposed model and the evolution of J_0 in the fired samples during the N_2 anneal at 300 °C (with the fired SiN_x removed, similar to Section 3.3). Note that the samples shown in this section were laboratory ex situ doped n-type LPCVD poly-Si on 100 Ω·cm n-type FZ-Si wafers that were used in our former study.[23]

Figure 7 compares the poly-Si films deposited at temperatures of 500–550 °C, showing a different behavior upon firing

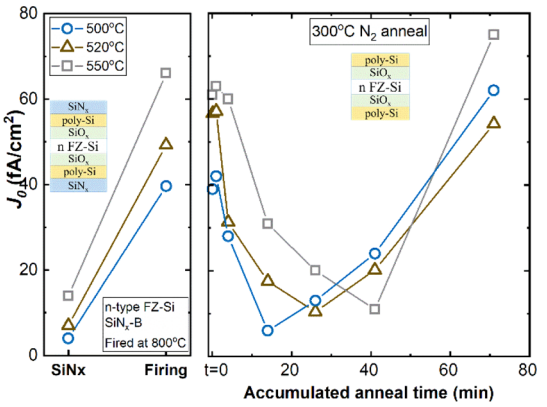

Figure 7. Changes in J_0 upon firing and the subsequent 300 °C N_2 anneal (with SiN_x removed after firing) for poly-Si deposited at 500, 520, and 550 °C.

and the subsequent N_2 anneal. During the N_2 anneal, all the samples showed a recovery of the J_0, implying that these samples could have an excess amount of hydrogen near the SiO_x. Interestingly, the samples recovered at different rates, possibly explained by the different amounts of hydrogen around the SiO_x after firing, as a result of the different effective diffusivities of hydrogen in the poly-Si layers upon firing. The different hydrogen diffusivities in these samples are likely to be related to the difference in the crystallite properties. Oudriss *et al.*[55] reported that the hydrogen diffusion can be accelerated in the vicinity of grain boundaries. The previous grazing incidence X-ray and neutron diffraction (GIXRD) measurements reveal that the poly-Si deposited at 550 °C featured the highest fraction of grain boundaries;[23] hence, the sample is

https://doi.org/10.1021/acsami.1c17342
ACS Appl. Mater. Interfaces XXXX, XXX, XXX–XXX

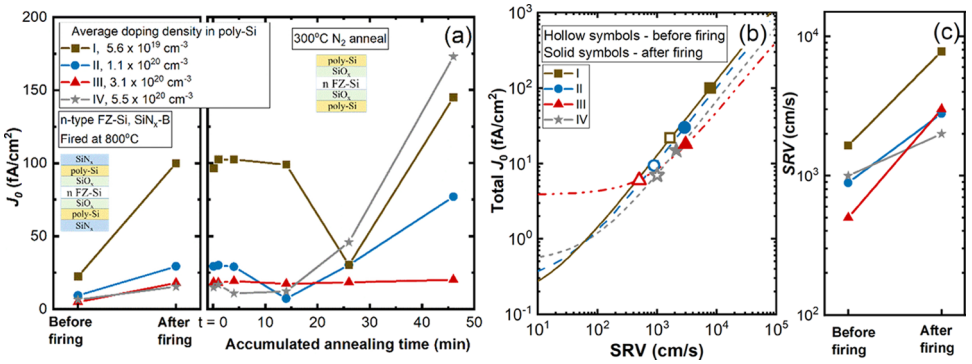

Figure 8. (a) Changes in the J_0 values in poly-Si with different doping concentrations after firing and during the subsequent N_2 anneal with the removal of SiN_x films. Also given are the average doping concentrations in the poly-Si film estimated based on the ECV profiles. (b) Total recombination current density parameter for the measured doping profiles as a function of the SRV at the c-Si/SiO_x interface. (c) Corresponding SRV values before and after firing for the investigated samples.

expected to contain the highest amount of hydrogen after firing (showing the strongest firing degradation) and therefore requires the longest time for the excess hydrogen to effuse during the subsequent N_2 anneal.

Figure 8a compares the firing response of poly-Si doped using different phosphorus diffusion conditions. Sample III remained stable upon the N_2 anneal within the studied time frame, whereas samples I, II, and IV showed a full recovery of J_0, indicating that the deterioration of surface passivation after firing could be associated with excess hydrogen near the SiO_x. It is also observed that the recovery rate inversely correlates to the doping concentration.

To isolate the influence of doping, which affects the carrier concentration at the SiO_x/c-Si interface, field-effect passivation, and Auger recombination,[8,56] from the chemical passivation that is dominated by interfacial defect density, we applied EDNA 2[57] simulations to extract the effective surface recombination velocity (SRV) of the c-Si/SiO_x interface, and following the approach of Stuckelberger *et al.*,[8] Figure 8b presents the total recombination current density parameter J_0 for the measured doping profiles as a function of the SRV at the c-Si/SiO_x interface, which represents the chemical passivation quality of the poly-Si/SiO_x stack, and is expected to be strongly related to the hydrogen concentration. Recombination in sample III is dominated by the Auger recombination due to the large in-diffusion depth observed in the previous work,[23] thus drastically reducing the susceptibility of J_0 to changes in SRV.[8] Figure 8c summarizes the changes in SRV before and after firing for samples I to IV. When comparing samples I, II, and IV, the general trend is that the magnitude of SRV changes increases with decreasing doping concentration in poly-Si, possibly due to the different hydrogen diffusivities in doped poly-Si layers. The poly-Si with a lower doping level could enable more hydrogen to be injected into the interfacial SiO_x, supported by Hamer *et al.*[58] While samples I, II, and IV all contained excess hydrogen, the most lightly doped poly-Si (sample I) could have the highest hydrogen level around the SiO_x, therefore the most pronounced surface passivation degradation after firing and also a longer timescale to reach the full recovery of J_0 during the N_2 anneal.

5. CONCLUSIONS

This work proposes a mechanism for the changes in poly-Si passivation after firing. The overall passivation quality of the fired poly-Si/SiO_x structure could be determined by the diffusion of hydrogen during firing and its interaction with defects surrounding the oxide interface. The presence of hydrogen is beneficial to passivate the defects, but excess hydrogen can deteriorate poly-Si passivation. The negative impact of excessive hydrogen is evidenced by the trend that the J_0 value increases with the hydrogen concentration near the SiO_x when increasing the peak firing temperature or using denser SiN_x coating layers. For poly-Si with a surplus of hydrogen after firing, injecting additional hydrogen to the SiO_x interlayer via an additional hydrogenation treatment leads to further degradation in the J_0, while removing hydrogen by the N_2 anneal after removing the fired SiN_x can fully recover the surface passivation. The plot for the J_0 of all the fired samples as a function of hydrogen density indicates that excellent surface passivation after firing can be achieved with an optimum amount of hydrogen surrounding the interfacial SiO_x, whereas insufficient or excessive hydrogen can both attribute to surface passivation degradation. The proposed model can also explain the dependence of the firing behavior on the poly-Si deposition temperature and the diffusion conditions, which determine the effective diffusivity of hydrogen upon firing and hence the amount of hydrogen at the interfacial SiO_x and the surface passivation after firing.

AUTHOR INFORMATION

Corresponding Author

Di Kang − *School of Engineering, The Australian National University (ANU), Canberra 2601, Australia;* orcid.org/0000-0002-9441-5201; Email: di.kang@anu.edu.au

Authors

Hang Cheong Sio − *School of Engineering, The Australian National University (ANU), Canberra 2601, Australia;* orcid.org/0000-0002-5872-9254

Josua Stuckelberger − *School of Engineering, The Australian National University (ANU), Canberra 2601, Australia*

Rong Liu − *SIMS and Microscopy Facility, Western Sydney University, Sydney, NSW 2753, Australia;* Present Address: CAMECA SAS, 29, quai des Grésillons, 92230 Gennevilliers Cedex, France (R.L.)

Di Yan − *Department of Electrical and Electronic Engineering, University of Melbourne, Melbourne, VIC 3010, Australia*

Xinyu Zhang − *Jinko Solar Co., Ltd., Shangrao, Jiangxi Province 334100, China*

https://doi.org/10.1021/acsami.1c17342
ACS Appl. Mater. Interfaces XXXX, XXX, XXX−XXX

Daniel Macdonald − *School of Engineering, The Australian National University (ANU), Canberra 2601, Australia*

Complete contact information is available at: https://pubs.acs.org/10.1021/acsami.1c17342

Funding

This work is supported by the Australian Renewable Energy Agency (ARENA) through projects RND017 and 1-A060. H.C.S. and J.S. are supported by the Australian Centre for Advanced Photovoltaics (ACAP) Postdoctoral Fellowship scheme.

Notes

The authors declare no competing financial interest.

■ ACKNOWLEDGMENTS

Access to the Australian National Fabrication Facility (ANFF) ACT node is gratefully acknowledged. The authors would like to thank Dr. Sieu Pheng Phang for helpful discussions.

■ REFERENCES

(1) Ingenito, A.; Nogay, G.; Jeangros, Q.; Rucavado, E.; Allebé, C.; Eswara, S.; Valle, N.; Wirtz, T.; Horzel, J.; Koida, T.; Morales-Masis, M.; Despeisse, M.; Haug, F.-J.; Löper, P.; Ballif, C. A Passivating Contact for Silicon Solar Cells Formed During a Single Firing Thermal Annealing. *Nat. Energy* **2018**, *3*, 800−808.

(2) Peibst, R.; Römer, U.; Larionova, Y.; Rienäcker, M.; Merkle, A.; Folchert, N.; Reiter, S.; Turcu, M.; Min, B.; Krügener, J.; Tetzlaff, D.; Bugiel, E.; Wietler, T.; Brendel, R. Working Principle of Carrier Selective Poly-Si/C-Si Junctions: Is Tunnelling the Whole Story? *Sol. Energy Mater. Sol. Cells* **2016**, *158*, 60−67.

(3) Yan, D.; Cuevas, A.; Wan, Y.; Bullock, J. Passivating Contacts for Silicon Solar Cells Based on Boron-Diffused Recrystallized Amorphous Silicon and Thin Dielectric Interlayers. *Sol. Energy Mater. Sol. Cells* **2016**, *152*, 73−79.

(4) Glunz, S. W.; Feldmann, F. Sio2 Surface Passivation Layers − a Key Technology for Silicon Solar Cells. *Sol. Energy Mater. Sol. Cells* **2018**, *185*, 260−269.

(5) Cuevas, A.; Wan, Y.; Yan, D.; Samundsett, C.; Allen, T.; Zhang, X.; Cui, J.; Bullock, J. Carrier Population Control and Surface Passivation in Solar Cells. *Sol. Energy Mater. Sol. Cells* **2018**, *184*, 38−47.

(6) Kale, A. S.; Nemeth, W.; Harvey, S. P.; Page, M.; Young, D. L.; Agarwal, S.; Stradins, P. Effect of Silicon Oxide Thickness on Polysilicon Based Passivated Contacts for High-Efficiency Crystalline Silicon Solar Cells. *Sol. Energy Mater. Sol. Cells* **2018**, *185*, 270−276.

(7) Lindholm, F. A.; Neugroschel, A.; Arienzo, M.; Iles, P. A. Heavily Doped Polysilicon-Contact Solar Cells. *IEEE Electron Device Lett.* **1985**, *6*, 363−365.

(8) Stuckelberger, J.; Nogay, G.; Wyss, P.; Ingenito, A.; Allebé, C.; Horzel, J.; Kamino, B. A.; Despeisse, M.; Haug, F. J.; Löper, P.; Ballif, C. Recombination Analysis of Phosphorus-Doped Nanostructured Silicon Oxide Passivating Electron Contacts for Silicon Solar Cells. *IEEE J. Photovoltaics* **2018**, *8*, 389−396.

(9) Park, H. J.; Bae, S.; Park, S. J.; Hyun, J. Y.; Lee, C. H.; Choi, D.; Kang, D.; Han, H.; Kang, Y.; Lee, H.-S.; Kim, D. Role of polysilicon in poly-Si/SiOx passivating contacts for high-efficiency silicon solar cells. *RSC Adv.* **2019**, *9*, 23261−23266.

(10) van de Loo, B. W. H.; Macco, B.; Schnabel, M.; Stodolny, M. K.; Mewe, A. A.; Young, D. L.; Nemeth, W.; Stradins, P.; Kessels, W. M. M. On the Hydrogenation of Poly-Si Passivating Contacts by Al2o3 and Sinx Thin Films. *Sol. Energy Mater. Sol. Cells* **2020**, *215*, 110592.

(11) Hezel, R.; Jaeger, K. Low-Temperature Surface Passivation of Silicon for Solar Cells. *J. Electrochem. Soc.* **1989**, *136*, 518−523.

(12) Kerr, M. J.; Schmidt, J.; Cuevas, A.; Bultman, J. H. Surface Recombination Velocity of Phosphorus-Diffused Silicon Solar Cell Emitters Passivated with Plasma Enhanced Chemical Vapor Deposited Silicon Nitride and Thermal Silicon Oxide. *J. Appl. Phys.* **2001**, *89*, 3821−3826.

(13) Truong, T. N.; Yan, D.; Chen, W.; Tebyetekerwa, M.; Young, M.; Al-Jassim, M.; Cuevas, A.; Macdonald, D.; Nguyen, H. T. Hydrogenation Mechanisms of Poly-Si/Siox Passivating Contacts by Different Capping Layers. *Sol. RRL* **2020**, *4*, 2070033.

(14) Schnabel, M.; Van De Loo, B. W. H.; Nemeth, W.; Macco, B.; Stradins, P.; Kessels, W. M. M.; Young, D. L. Hydrogen Passivation of Poly-Si/Siox Contacts for Si Solar Cells Using Al2o3 Studied with Deuterium. *Appl. Phys. Lett.* **2018**, *112*, 203901.

(15) Stodolny, M. K.; Lenes, M.; Wu, Y.; Janssen, G. J. M.; Romijn, I. G.; Luchies, J. R. M.; Geerligs, L. J. N-Type Polysilicon Passivating Contact for Industrial Bifacial N-Type Solar Cells. *Sol. Energy Mater. Sol. Cells* **2016**, *158*, 24−28.

(16) Truong, T. N.; Yan, D.; Samundsett, C.; Basnet, R.; Tebyetekerwa, M.; Li, L.; Kremer, F.; Cuevas, A.; Macdonald, D.; Nguyen, H. T. Hydrogenation of Phosphorus-Doped Polycrystalline Silicon Films for Passivating Contact Solar Cells. *ACS Appl. Mater. Interfaces* **2019**, *11*, 5554−5560.

(17) Steinhauser, B.; Feldmann, F.; Ourinson, D.; Nagel, H.; Fellmeth, T.; Hermle, M. On the Influence of the Sinx Composition on the Firing Stability of Poly-Si/Sinx Stacks. *Phys. Status Solidi A* **2020**, *217*, 2000333.

(18) Nemeth, B.; Young, D. L.; Page, M. R.; LaSalvia, V.; Johnston, S.; Reedy, R.; Stradins, P. Polycrystalline Silicon Passivated Tunneling Contacts for High Efficiency Silicon Solar Cells. *J. Mater. Res.* **2016**, *31*, 671−681.

(19) Hollemann, C.; Haase, F.; Schäfer, S.; Krügener, J.; Brendel, R.; Peibst, R. 26.1%-efficient POLO-IBC cells: Quantification of electrical and optical loss mechanisms. *Prog. Photovolt.: Res. Appl.* **2019**, *27*, 950−958.

(20) Fraunhofer Ise Sets New World Record of 26 Percent Efficiency for Both-Sides-Contacted Solar Cell. "Press release" [Online] Available: https://www.ise.fraunhofer.de/en/press-media/press-releases/2021/fraunhofer-ise-sets-new-world-record-of-26-percent-efficiency-for-both-sides-contacted-solar-cell.html, April 2021.

(21) JinkoSolar, Jinkosolar Large-Area N-Type Monocrystalline Silicon Solar Cell Reaches Record-Breaking New High Efficiency of 25.25%. "Press release" [Online] Available: http://jinkosolar.com.au/2021/05/jinkosolar-large-area-n-type-monocrystalline-silicon-solar-cell-reaches-record-breaking-new-high-efficiency-of-25-25/, May 2021.

(22) LONGi, Longi Breaks Three More World Records for Solar Cell Efficiency. "Press release" [Online] Available: https://en.longi-solar.com/home/events/press_detail/id/335.html, June 2021.

(23) Kang, D.; Sio, H. C.; Yan, D.; Stuckelberger, J.; Zhang, X.; Macdonald, D. Firing Stability of Phosphorus-Doped Polysilicon Passivating Contacts: Factors Affecting the Degradation Behavior. *Sol. Energy Mater. Sol. Cells* **2022**, *234*, 111407.

(24) Kang, D.; Sio, H. C.; Yan, D.; Stuckelberger, J.; Truong, T. N.; Phang, S. P.; Liu, R.; Macdonald, D., Firing Stability of Polysilicon Passivating Contacts: The Role of Hydrogen. In *48th IEEE Photovoltaic Specialists (PVSC)*, IEEE: 2021.

(25) Feldmann, F.; Fellmeth, T.; Steinhauser, B.; Nagel, H.; Ourinson, D.; Mack, S.; Lohmüller, E.; Polzin, J.-I.; Benick, J.; Rentsch, J.; Hermle, M.; Glunz, S., Large Area Topcon Cells Realized by a Pecvd Tube Process. In *36th European Photovoltaic Solar Energy Conference and Exhibition*, 2019; pp. 304−308.

(26) Hollemann, C.; Haase, F.; Krügener, J.; Brendel, R.; Peibst, R., Firing Stability of N-Type Poly-Si on Oxide Junctions Formed by Quartz Tube Annealing. In *2020 47th IEEE Photovoltaic Specialists Conference (PVSC)*, 2020; pp. 1274−1278.

(27) Lehmann, M.; Valle, N.; Horzel, J.; Pshenova, A.; Wyss, P.; Döbeli, M.; Despeisse, M.; Eswara, S.; Wirtz, T.; Jeangros, Q.; Hessler-Wyser, A.; Haug, F.-J.; Ingenito, A.; Ballif, C. Analysis of Hydrogen Distribution and Migration in Fired Passivating Contacts (Fpc). *Sol. Energy Mater. Sol. Cells* **2019**, *200*, 110018.

(28) Stöhr, M.; Aprojanz, J.; Brendel, R.; Dullweber, T. Firing-Stable Pecvd Sioxny/N-Poly-Si Surface Passivation for Silicon Solar Cells. *ACS Appl. Energy Mater.* **2021**, *4*, 4646−4653.
(29) Çiftpınar, H. E.; Stodolny, M. K.; Wu, Y.; Janssen, G. J. M.; Löffler, J.; Schmitz, J.; Lenes, M.; Luchies, J.-M.; Geerligs, L. J. Study of Screen Printed Metallization for Polysilicon Based Passivating Contacts. *Energy Procedia* **2017**, *124*, 851−861.
(30) Gnaser, H.; Oechsner, H. Hydrogen Analysis by Secondary Ion Mass Spectrometry Using Hcs+ Ions. *Nucl. Instrum. Methods Phys. Res., Sect. B* **1992**, *64*, 646−649.
(31) Sinton, R. A.; Cuevas, A.; Stuckings, M., Quasi-Steady-State Photoconductance, a New Method for Solar Cell Material and Device Characterization. In *Conference Record of the Twenty Fifth IEEE Photovoltaic Specialists Conference - 1996*, 1996; pp. 457−460.
(32) Kane, D. E.; Swanson, R. M., Measurement of the Emitter Saturation Current by a Contactless Photoconductivity Decay Method. *Proceedings of the IEEE 18th Photovoltaic Specialist Conference* 1985, 578.
(33) Truong, T. N.; Yan, D.; Samundsett, C.; Liu, A.; Harvey, S. P.; Young, M.; Ding, Z.; Tebyetekerwa, M.; Kremer, F.; Al-Jassim, M.; Cuevas, A.; Macdonald, D.; Nguyen, H. T. Hydrogen-Assisted Defect Engineering of Doped Poly-Si Films for Passivating Contact Solar Cells. *ACS Appl. Energy Mater.* **2019**, *2*, 8783−8791.
(34) Feldmann, F.; Bivour, M.; Reichel, C.; Hermle, M.; Glunz, S. W. Passivated Rear Contacts for High-Efficiency N-Type Si Solar Cells Providing High Interface Passivation Quality and Excellent Transport Characteristics. *Sol. Energy Mater. Sol. Cells* **2014**, *120*, 270−274.
(35) Yan, D.; Cuevas, A.; Bullock, J.; Wan, Y.; Samundsett, C. Phosphorus-Diffused Polysilicon Contacts for Solar Cells. *Sol. Energy Mater. Sol. Cells* **2015**, *142*, 75−82.
(36) Lelièvre, J. F.; Fourmond, E.; Kaminski, A.; Palais, O.; Ballutaud, D.; Lemiti, M. Study of the Composition of Hydrogenated Silicon Nitride Sinx:H for Efficient Surface and Bulk Passivation of Silicon. *Sol. Energy Mater. Sol. Cells* **2009**, *93*, 1281−1289.
(37) Yoshinaga, S.; Ishikawa, Y.; Kawamura, Y.; Nakai, Y.; Uraoka, Y. The Optical Properties of Silicon-Rich Silicon Nitride Prepared by Plasma-Enhanced Chemical Vapor Deposition. *Mater. Sci. Semicond. Process.* **2019**, *90*, 54−58.
(38) Dekkers, H. F. W.; Beaucarne, G.; Hiller, M.; Charifi, H.; Slaoui, A. Molecular Hydrogen Formation in Hydrogenated Silicon Nitride. *Appl. Phys. Lett.* **2006**, *89*, 211914.
(39) Weeber, A. W.; Rieffe, H. C.; Romijn, I. G.; Sinke, W.; Soppe, W. J., The Fundamental Properties of Sinx:H That Determine Its Passivating Qualities. In *2005 IEEE 31st Photovoltaic Specialist Conference (PVSC)*, 2005; pp. 1043−1046.
(40) Martínez, F. L.; del Prado, A.; Mártil, I.; González-Diaz, G.; Bohne, W.; Fuhs, W.; Röhrich, J.; Selle, B.; Sieber, I. Molecular models and activation energies for bonding rearrangement in plasma-deposited a− SiN x: H dielectric thin films treated by rapid thermal annealing. *Phys. Rev. B* **2001**, *63*, 245320.
(41) Wilking, S.; Ebert, S.; Herguth, A.; Hahn, G. Influence of Hydrogen Effusion from Hydrogenated Silicon Nitride Layers on the Regeneration of Boron-Oxygen Related Defects in Crystalline Silicon. *J. Appl. Phys.* **2013**, *114*, 194512.
(42) Holt, J. K.; Goodwin, D. G.; Gabor, A. M.; Jiang, F.; Stavola, M.; Atwater, H. A. Hot-Wire Chemical Vapor Deposition of High Hydrogen Content Silicon Nitride for Solar Cell Passivation and Anti-Reflection Coating Applications. *Thin Solid Films* **2003**, *430*, 37−40.
(43) Kang, D.; Sio, H. C.; Stuckelberger, J.; Yan, D.; Phang, S. P.; Nguyen, H. T.; Truong, T. N.; Le, T.; Zhang, X.; Liu, R.; Macdonald, D., *Comparison of Firing Stability of P- and N-Type Polysilicon Passivating Contacts*. 2021 (**Submitted**).
(44) Hollemann, C.; Folchert, N.; Harvey, S. P.; Stradins, P.; Young, D. L.; Salles de Souza, C. L.; Rienäcker, M.; Haase, F.; Brendel, R.; Peibst, R. Changes in Hydrogen Concentration and Defect State Density at the Poly-Si/Siox/C-Si Interface Due to Firing. *Sol. Energy Mater. Sol. Cells* **2021**, *231*, 111297.
(45) Gotoh, K.; Wilde, M.; Kato, S.; Ogura, S.; Kurokawa, Y.; Fukutani, K.; Usami, N. Hydrogen Concentration at a-Si:H/C-Si Heterointerfaces—the Impact of Deposition Temperature on Passivation Performance. *AIP Adv.* **2019**, *9*, No. 075115.
(46) Schmidt, J.; Werner, F.; Veith, B.; Zielke, D.; Steingrube, S.; Altermatt, P. P.; Gatz, S.; Dullweber, T.; Brendel, R. Advances in the Surface Passivation of Silicon Solar Cells. *Energy Procedia* **2012**, *15*, 30−39.
(47) Yan, D.; Phang, S. P.; Wan, Y.; Samundsett, C.; Macdonald, D.; Cuevas, A. High Efficiency N-Type Silicon Solar Cells with Passivating Contacts Based on Pecvd Silicon Films Doped by Phosphorus Diffusion. *Sol. Energy Mater. Sol. Cells* **2019**, *193*, 80−84.
(48) Yang, Y.; Altermatt, P. P.; Cui, Y.; Hu, Y.; Chen, D.; Chen, L.; Xu, G.; Zhang, X.; Chen, Y.; Hamer, P.; Bonilla, R. S.; Feng, Z.; Verlinden, P. J. Effect of Carrier-Induced Hydrogenation on the Passivation of the Poly-Si/Siox/C-Si Interface. *AIP Conf. Proc.* **2018**, *1999*, No. 040026.
(49) Nickel, N. H.; Anderson, G. B.; Walker, J. Hydrogen-Induced Platelets in Disordered Silicon. *Solid State Commun.* **1996**, *99*, 427−431.
(50) Steingrube, S.; Altermatt, P. P.; Steingrube, D. S.; Schmidt, J.; Brendel, R. Interpretation of Recombination at C-Si/Sinx Interfaces by Surface Damage. *J. Appl. Phys.* **2010**, *108*, No. 014506.
(51) Vaqueiro-Contreras, M.; Markevich, V. P.; Halsall, M. P.; Peaker, A. R.; Santos, P.; Coutinho, J.; Öberg, S.; Murin, L.; Falster, R.; Binns, J.; Monakhov, E. V.; Svensson, B. G. Powerful Recombination Centers Resulting from Reactions of Hydrogen with Carbon-Oxygen Defects in N-Type Czochralski-Grown Silicon. *Phys. Status Solidi RRL* **2017**, *11*, 1700133.
(52) Santos, P.; Coutinho, J.; Öberg, S.; Vaqueiro-Contreras, M.; Markevich, V. P.; Halsall, M. P.; Peaker, A. R. Theory of a Carbon-Oxygen-Hydrogen Recombination Center in N-Type Si. *Phys. Status Solidi A* **2017**, *214*, 1700309.
(53) Roberson, M. A.; Estreicher, S. K. Vacancy and Vacancy-Hydrogen Complexes in Silicon. *Phys. Rev. B* **1994**, *49*, 17040−17049.
(54) née Wenham, A. C.; Wenham, S.; Chen, R.; Chan, C.; Chen, D.; Hallam, B.; Payne, D.; Fung, T.; Kim, M.; Liu, S.; Wang, S.; Kim, K.; Samadi, A.; Sen, C.; Vargas, C.; Varshney, U.; Stefani, B. V.; Hamer, P.; Bourret-Sicotte, G.; Nampalli, N.; Hameiri, Z.; Chong, C.; Abbott, M., Hydrogen-Induced Degradation. In *2018 IEEE 7th World Conference on Photovoltaic Energy Conversion (WCPEC) (A Joint Conference of 45th IEEE PVSC, 28th PVSEC & 34th EU PVSEC)*, 2018; pp. 0001−0008.
(55) Oudriss, A.; Creus, J.; Bouhattate, J.; Savall, C.; Peraudeau, B.; Feaugas, X. The Diffusion and Trapping of Hydrogen Along the Grain Boundaries in Polycrystalline Nickel. *Scr. Mater.* **2012**, *66*, 37−40.
(56) Battaglia, C.; Cuevas, A.; De Wolf, S. High-Efficiency Crystalline Silicon Solar Cells: Status and Perspectives. *Energy Environ. Sci.* **2016**, *9*, 1552−1576.
(57) "EDNA2" [online] Available: https://www2.pvlighthouse.com.au/calculators (accessed 10 Aug 2021).
(58) Hamer, P.; Hallam, B.; Bonilla, R. S.; Altermatt, P. P.; Wilshaw, P.; Wenham, S. Modelling of Hydrogen Transport in Silicon Solar Cell Structures under Equilibrium Conditions. *J. Appl. Phys.* **2018**, *123*, No. 043108.

https://doi.org/10.1021/acsami.1c17342
ACS Appl. Mater. Interfaces XXXX, XXX, XXX−XXX

Chapter 5 – Comparison of firing stability between p- and n-type polysilicon passivating contacts

Di Kang[1], Hang Cheong Sio[1], Josua Stuckelberger[1], Di Yan[2], Sieu Pheng Phang[1], Rong Liu[3], Thien N. Truong[1], Tien Le[1], Hieu T. Nguyen[1], Xinyu Zhang[4], Daniel Macdonald[1]

[1]School of Engineering, The Australian National University (ANU), Canberra, ACT, 2601

[2]Department of Electrical and Electronic Engineering, University of Melbourne, Melbourne, VIC 3010, Australia

[3]SIMS and Microscopy Facility, Western Sydney University, Sydney, NSW, Australia

[4]Jinko Solar Co., Ltd, Shangrao, Jiangxi Province, China

Submitted to Progress in Photovoltaics in July 2021, under review

Abstract

This work compares the firing response of ex-situ doped p- and n-type polysilicon (poly-Si) passivating contacts, and identifies possible mechanisms underlying their distinct firing behavior. P-type poly-Si shows greater firing stability than n-type poly-Si, particularly at a higher firing temperature, which results in a substantial increase in the recombination current density parameter J_0 from 9 to 96 fA/cm^2 upon firing at 900°C for n-type poly-Si, in comparison to an increase from 11 to 30 fA/cm^2 for p-type poly-Si. It is observed that p-type poly-Si contacts only suffer a slight degradation or even exhibit a small improvement in J_0 after firing at 800°C, depending on the boron diffusion temperature. Secondary ion mass spectrometry (SIMS) results demonstrate that the hydrogen concentration near the interfacial SiO_x increases with the peak firing temperature in n-type poly-Si, whereas the hydrogen profile remains unchanged for p-type poly-Si upon firing at various temperatures. Moreover, we observe that injecting additional hydrogen into the poly-Si/SiO_x stacks fired with SiN_x coating layers further degrades n-type poly-Si, but recovers the J_0 of p-type poly-Si to the value before firing. In contrast, removing hydrogen from the fired poly-Si/SiO_x stacks leads to an initial recovery and then a second degradation of J_0 in n-type poly-Si, but no substantial impact on p-type poly-Si. It is hypothesized that the distinct difference in the firing impact on p- and n-type poly-Si is related to the different effective hydrogen diffusivity, which determines the hydrogen content surrounding the SiO_x layer, and hence the passivation quality after firing.

Introduction

Passivating contacts consisting of doped polysilicon (poly-Si) and ultra-thin SiO_x layers have been developed to reduce carrier recombination at the metal/Si interface. Extremely low recombination current density parameter J_0 values have been reported, below 5 fA/cm^2 for n-type poly-Si passivating contacts and below 10 fA/cm^2 for p-type poly-Si passivating contacts.[1-5] N-type poly-Si passivating contacts are being introduced in mass production, with photovoltaics (PV) manufacturers, such as Jinko Solar and LONGi reaching an impressive efficiency above 25.2%.[6, 7] Although p-type poly-Si passivating contacts have not yet been widely implemented in the PV industry, the potential has been demonstrated on lab-processed POLO-IBC solar cells with an efficiency as high as 26.1%.[8] In mass production, a high-temperature firing treatment is of great importance for the fabrication of screen-printed solar cells. However, it has been found that the firing process could potentially affect the contact resistance and passivation quality of the poly-Si structures in passivated and contacted regions.[9-11]

The firing influence on n-type ex-situ phosphorus-doped poly-Si contacts has been investigated in our recent work.[12] A pronounced surface degradation was observed on samples fired either with or without the presence of SiN_x capping layers at above 800°C, with the degradation extent depending on various processing parameters, such as the growth of interfacial SiO_x, the poly-Si deposition temperature, the phosphorus diffusion conditions, and the dielectric capping layer. In other work,[13] we proposed a hypothesis that an excessive amount of hydrogen released from the dielectric capping layer to the poly-Si/SiO_x structure, particularly surrounding the interfacial SiO_x, causes the degradation after firing.

In addition to our own work, the firing stability of n-type poly-Si passivating contacts has been studied by a number of research groups.[11, 14-20] However, few studies have been performed on the firing influence of p-type poly-Si contacts. This paper evaluates the firing stability of p-type poly-Si passivating contacts, and then compares the response of p- and n-type poly-Si to rapid firing and subsequent thermal treatments. Moreover, secondary ion mass spectrometry (SIMS) and Fourier-transform infrared spectroscopy (FTIR) are employed, to identify possible root causes for the different firing behavior in samples passivated by p- and n-type poly-Si. The results extend our understanding of the firing effect on poly-Si/SiO_x structures, which may help to further improve the performance of doped poly-Si contacts.

Experimental details

Planar 100 Ω·cm n-type float-zone (FZ) Si wafers, with a thickness of ~300 µm, were processed into symmetric lifetime samples passivated by 80 nm n- or p-type poly-Si/SiO_x contacts. As shown in Figure 1, the main process flows included growth of SiO_x, deposition of poly-Si, ex-situ BBr_3 or $POCl_3$ diffusions, forming gas anneal (FGA), SiN_x deposition (~80 nm, measured by ellipsometry), and firing. The thin SiO_x layers were grown either using a thermal process at 600℃ for 5 min in O_2 (thickness of ~1.5 nm, measured by ellipsometry) or through a chemical method by immersing the wafers in 68 wt% nitric acid at a temperature of ~90℃ for 30 min (~1.4 nm). Poly-Si films were deposited using a low-pressure chemical vapor deposition (LPCVD) system at 520℃. After diffusion, samples received a 30 min FGA at 400℃ prior to SiN_x deposition as part of our standard process in our lab to identify and remove any low-quality samples prior to further processing steps. The SiN_x films were deposited with an Oxford PlasmaLab 100 plasma-enhanced chemical vapor deposition (PECVD) tool. The firing treatment was performed using a rapid thermal annealing (RTA) furnace, with a ramp-up and ramp-down rate of 30 and 60 ℃/s respectively. During the firing treatment, the samples were sandwiched between two 180 µm thick dummy wafers, to avoid potential influence, such as ultraviolet (UV)-induced degradation of the surface passivation,[21, 22] caused by the strong illumination from the lamps. There is a small temperature difference between the actual temperature of poly-Si samples and the temperature measured on the bottom dummy wafer (± 30℃ measured by an additional thermocouple). However, this should not affect the overall conclusions, as this study aims to investigate the trend in the firing response over a large range of temperature from 700℃ to 900℃.

Regarding the samples with chemically grown oxide (green part in Figure 1), the temperature for boron diffusion was varied from 900℃ to 980℃, and the firing process was performed at 800℃ (temperature measured on the bottom dummy wafer by a thermocouple), to explore the influence of diffusion conditions on subsequent firing behavior.

Regarding the thermal SiO_x split in Figure 1 (blue part), the wafers received either a $POCl_3$ (deposition at 780℃, drive-in at 900℃) or a BBr_3 diffusion (980℃ for both deposition and drive-in) and were divided afterwards into various groups, for comparing firing effects on n- and p-type poly-Si/SiO_x passivating contacts. It is worth noting that the high temperature for boron diffusion also allowed the n- and p-type poly-Si to feature similar crystallinity and crystallite size measured by grazing incidence X-ray diffraction. The crystallite size of these samples was estimated to be ~27 nm applying the Scherrer

formula on the (111) orientation.[12] Some samples were then subjected to a FGA and SiN_x deposition and fired at various peak firing temperatures from 700℃ to 900℃, while others were fired directly after the diffusion without subjecting to FGA and SiN_x deposition. After firing, all samples had their fired SiN_x films removed by HF dip before selected samples were re-coated with fresh SiN_x films and then annealed in forming gas to inject more hydrogen into the fired poly-Si/SiO_x stack, while others were annealed in N_2 at 300℃ without SiN_x coatings. The deposition of SiN_x after the firing step was performed using a Roth and Rau AK400 PECVD system.

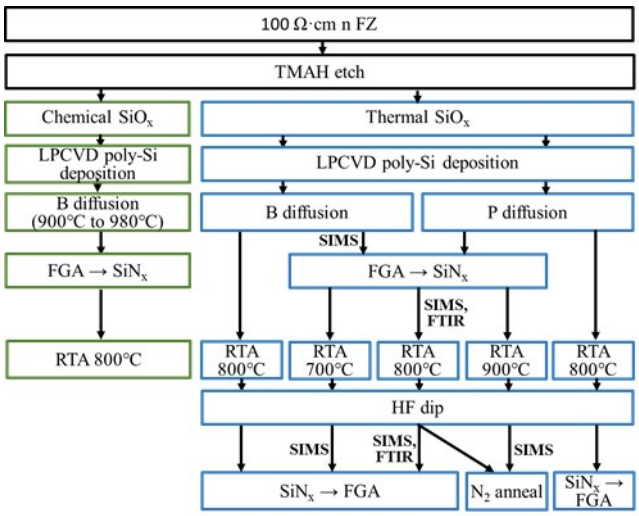

Figure 1. Flowchart of experimental details.

P-type poly-Si contacts were characterized by SIMS after various processing steps, including boron diffusion, FGA and SiN_x deposition (before firing), firing at various temperatures from 700℃ to 900℃. The SiN_x capping layers were removed by HF dip before SIMS measurement. A Cameca IMS 5fE7 SIMS tool (Cameca, France) was employed to acquire the depth profile for hydrogen. A primary ion beam of Cs^+ with an impact energy of 5.0 keV and beam current of 16 nA was employed to raster a 125 × 125 μm region of the sample surface, with a sputtering rate of 0.5 nm/s. The H^+ intensity was measured to estimate the hydrogen level in the poly-Si samples. Additionally, FTIR absorbance spectra were acquired by a Bruker VERTEX 80v vacuum spectrometer, to assess changes of chemical bonds in the n- and p-type poly-Si contacts caused by firing. Dopant profiles in the doped poly-Si films were determined by a Wafer Profiler CVP21 electrochemical capacitance voltage (ECV) system.

Lifetime values, τ_{eff}, were measured using a Sinton Instruments WCT-120 lifetime tester using the transient method,[23] at an injection level of 1×10^{15} cm^{-3}. To monitor changes in the surface passivation quality of poly-Si passivation layers, recombination

current density parameters, J_0, were extracted using the Kane and Swanson method,[24] at an injection level of 4×10^{15} cm^{-3}. Within the present work, the samples are assumed to have identical poly-Si films on the front and the rear side, and the single-side J_0 values were obtained by dividing the extracted J_0 by 2. Implied open-circuit voltage (iV_{oc}) was also used to demonstrate the potential influence on device performance.

Results and discussion

Firing response of p-type poly-Si

Figure 2 (a) shows the stability of p-type poly-Si passivating contacts fabricated at different boron diffusion temperatures (900℃, 950℃ and 980℃), before and after firing at 800℃. The samples started with different τ_{eff} and J_0 values before the firing treatment (after FGA and SiN_x deposition), due to differences in the doping profile. The samples subjected to a boron diffusion at 980℃ had the best performance before firing, followed by the samples diffused at 950℃ and 900℃. After the firing treatment, the 980℃ diffused poly-Si contacts exhibited a slight improvement in the τ_{eff} (from 6.8 to 7.2 ms) and J_0 (from 13 to 11 fA/cm^2), which was also reflected in a small improvement of the iV_{oc} (from 704 to 707 mV). While firing damage was detected in both boron diffusions performed at 950℃ and 900℃, the 950℃ diffused sample was more resistant to firing impact, showing only a slight decrease in τ_{eff} (from 6.7 to 6.4 ms) and a small increase in J_0 (from 18 to 22 fA/cm^2), in comparison to the 900℃ diffused poly-Si for which the degradation in τ_{eff} (from 6.2 to 2.5 ms) and J_0 (from 24 to 31 fA/cm^2) was more pronounced. This surface degradation could potentially affect the device performance, as observed from the reduction in iV_{oc}, dropping from 701 to 698 mV in the poly-Si with 950℃ diffusion, and 696 to 688 mV in the poly-Si treated with 900℃ boron diffusion.

Figure 2 (b) presents the corresponding ECV profiles and sheet resistance (measured by four-point probe), demonstrating that increasing the diffusion temperature at both deposition and drive-in steps drove the boron diffusion deeper into the wafer without significantly affecting the doping level in the poly-Si film. In general, increasing the diffusion temperature improves the firing stability of p-type poly-Si/SiO_x contacts. This is similar to what was observed in n-type poly-Si in our previous work [12], where increasing the deposition temperature from 790℃ to 810℃ (keeping the drive-in temperature constant), or increasing the drive-in temperature from 850℃ to 900℃ (keeping the deposition temperature constant) allowed the samples to be more resistant to firing damage. However, adjusting the diffusion temperature appears to show a lesser

impact on p-type poly-Si than on n-type poly-Si. In contrast to the severe firing impact on lightly doped n-type poly-Si,[12] only small surface degradation was detected on lowly doped p-type poly-Si after 800℃ firing.

The measured ECV profiles and the J_0 values are also used to estimate the effective surface recombination velocity (SRV) at the interface between c-Si and SiO_x, using EDNA 2 simulations,[25] based on the approach applied by Stuckelberger *et al.*.[26] Figure 2 (c) shows the total J_0 corresponding to the measured doping profiles as a function of the SRV that reflects the chemical passivation quality of the poly-Si/SiO_x stack. The simulation results indicate that the J_0 is not limited by the Auger recombination in the in-diffusion regions, and reflect changes in the passivation quality of the interfacial oxide (represented by the SRV). Figure 2 (d) summarizes the changes in the SRV before and after firing, which corresponds well to the J_0 values.

It is noted that the dopant source (phosphorus or boron) and the variation of diffusion conditions does not only lead to different doping concentration in the poly-Si film and in-diffusion depth in the c-Si substrate, but also affects the crystal properties,[27] making a direct comparison between n- and p-type poly-Si contacts rather difficult. In the following sections of this work, we have chosen to compare samples (780℃ deposition and 900℃ drive-in for phosphorus diffusion, 980℃ deposition and drive-in for boron diffusion) with similar crystal properties and surface passivation quality before firing, while keeping other parameters constant, such as the growth method for the interfacial SiO_x and SiN_x films, to reduce the impact of other process factors when comparing the firing stability for n- and p-type poly-Si contacts. The potential influence caused by different doping profiles and sheet resistance will be elaborated in the discussion section.

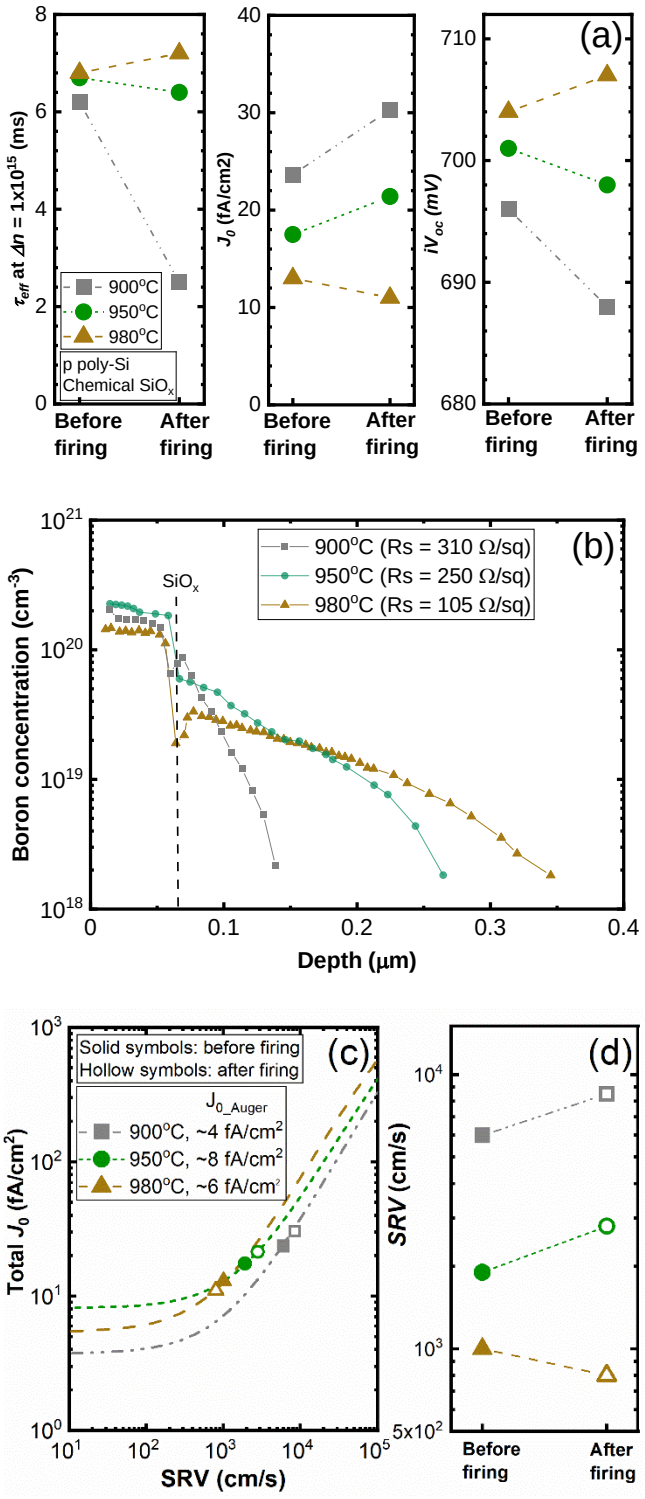

Figure 2. Comparison of firing behavior for p-type poly-Si samples diffused at 900°C, 950°C or 980°C - (a) τ_{eff}, single-side J_0 and 1 sun iV_{oc} values measured in samples before and after RTA treatment at a peak firing temperature of 800°C and (b) dopant profiles and sheet resistance values measured after boron diffusion. (c) The total recombination current density parameter for the measured doping profiles as a function of the SRV at the c-Si/SiO$_x$ interface. (d) The corresponding SRV values before and after firing. Also given in Figure 2 (c) are contribution of Auger recombination to the total J_0 values (J_{0_Auger}).

Impact of firing temperature on n- and p-type poly-Si

This subsection explores the influence of the peak firing temperature on firing response of n- and p-type poly-Si/SiO_x contacts. Figure 3 compares changes in the J_0 values of samples passivated by n-type and p-type poly-Si/SiO_x stacks, after firing at a temperature of 700℃ to 900℃. As observed, the firing response of both n- and p-type poly-Si passivating contacts is sensitive to the peak firing temperature. The n-type poly-Si contacts were not strongly impacted by firing at 700℃, but exhibited substantial degradation in J_0, increasing from 8 to 40 fA/cm^2 and 9 to 96 fA/cm^2 after firing at 800℃ and 900℃ respectively. On the other hand, the surface passivation of the p-type poly-Si did not change significantly upon firing at 700℃ and 800℃. Although the 900℃ firing process caused an increase in the J_0 value, from 11 to 30 fA/cm^2, in the p-type poly-Si, the degradation extent is considerably lower compared to the n-type poly-Si. In general, the p-type poly-Si/SiO_x samples appear to show better firing stability than n-type, which agrees with the work by Çiftpınar, *et al*. who reported that firing was slightly detrimental to n-type poly-Si passivation but helped to improve the passivation of p-type poly-Si.[10] The improvement of p-type poly-Si passivation after firing was also reported by van de Loo *et al*. and Mack *et al*., further supporting the excellent firing stability of p-type poly-Si passivating contacts.[28, 29]

It is noted that the p-type poly-Si (thermal SiO_x, 980℃ boron diffusion) studied in this section showed a small degradation in J_0, increasing from 12 to 15 fA/cm^2 after firing at 800℃, different to the observation in Figure 2, where J_0 decreased from 13 to 11 fA/cm^2 for the sample fired at 800℃ (chemical SiO_x, 980℃ boron diffusion). The small difference in their behavior might be related to the different growth method of the interfacial SiO_x.

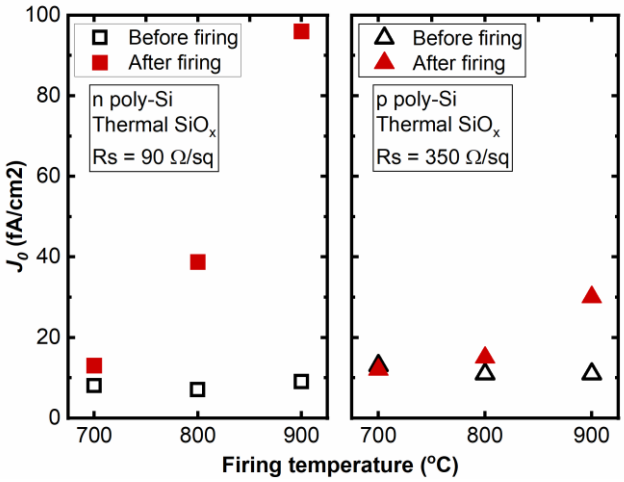

Figure 3. Comparison of firing behavior for n- and p-type poly-Si/SiO_x passivating contacts measured before and after RTA treatment at peak firing temperatures from 700℃ to 900℃.

To explore the possible role of hydrogen, we compare the hydrogen content in both n- and p-type poly-Si contacts measured by SIMS, for samples before and after coating with SiN_x layers, and after firing at temperatures in a range of 700°C to 900°C, as depicted in Figure 4. Note that the hydrogen profiles for n-type poly-Si contacts demonstrated in Figure 4 (a) are taken from our recent work,[13] whereas the SIMS data for p-type poly-Si given in Figure 4 (b) are the actual measurements performed on p-type poly-Si samples shown in Figure 3. The 100 nm n-type poly-Si/SiO_x stacks were prepared on chemically polished n-type Cz-Si wafers (180 µm), and deposited with SiN_x directly after phosphorus diffusion, while the 80 nm p-type poly-Si films were deposited on planar n-type FZ-Si wafers and received FGA prior to SiN_x deposition. The n-type poly-Si used for the SIMS measurements exhibited similar firing behavior as the n-type poly-Si samples processed in this work, showing similar dependence on the firing temperature (Figure 3), and the same response to the subsequent hydrogenation (Figure 6) and de-hydrogenation treatments (Figure 7) discussed below. Therefore, the samples processed in the two batches are expected to show similar variation of hydrogen profiles upon firing at different temperatures. Also note that the presented SIMS data are the uncalibrated H^+ secondary ion count signal, which cannot be used to directly compare the hydrogen concentrations between n- and p-type poly-Si, but to compare within one dopant type, due to the difference in the p- and n-type poly-Si samples such as their surface roughness. The different surface roughness of Cz-Si and FZ-Si wafers resulted in a different depth resolution of the SIMS measurement of hydrogen or oxygen in n- and p-type poly-Si, due to measurement artifacts (e.g. knock-on effects) induced by surface roughness. In addition, the uncertainties introduced by different thickness of Cz-Si and FZ-Si wafers, due to the slight difference in actual wafer temperature (± 10°C), should not affect our conclusion. In Figure 4, we focus on the overall trend of hydrogen changes in n- or p-type poly-Si fired at various temperatures from 700°C to 900°C.

The n-type poly-Si films demonstrated in Figure 4 (a) was covered by 80 nm SiN_x films, all processed using industrial facilities. When comparing the samples before and after SiN_x deposition, the samples coated with SiN_x films have a slightly stronger hydrogen signal near the oxide interlayer, indicating that hydrogen was injected into the poly-Si layer and the interfacial SiO_x during the SiN_x deposition. Moreover, increased hydrogen signals were detected in all fired n-type poly-Si contacts, particularly surrounding the thin SiO_x layer, in comparison with the non-fired sample (after SiN_x deposition), reflecting a further in-diffusion of hydrogen during the firing treatment,

which suggests that dielectric coatings could perform as a hydrogen source upon firing. Regarding the fired samples, the hydrogen density accumulated around the SiO_x increases with the peak firing temperature, possibly associated with the phenomenon that SiN_x films release an increasing amount of hydrogen with higher annealing temperature.[30, 31] In the meantime, the passivation quality reduces with increasing firing temperature.

As observed in Figure 4 (b), a very small hydrogen peak was detected in laboratory p-type poly-Si. This could be due to a small amount of residual hydrogen from the a-Si deposition or measurement artifacts from SIMS due to matrix effects that are measured on samples with mixed layers composed of matrices of different nature. P-type poly-Si also showed increased hydrogen concentration in the poly-Si film and interfacial SiO_x after SiN_x deposition. Note that, in comparison with n-type poly-Si, p-type poly-Si received an additional FGA prior to SiN_x deposition, leading to a more significant increase in the hydrogen peak. However, this should not be responsible for the distinct variation of hydrogen profiles in fired n- and p-type poly-Si. Comparing the p-type poly-Si contacts after firing at various temperatures, there are no obvious changes in hydrogen concentration as the peak firing temperature increases, which contrasts with the n-type poly-Si.

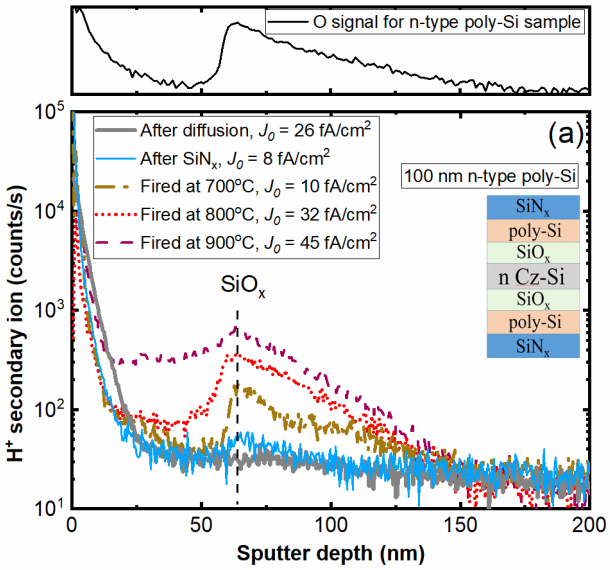

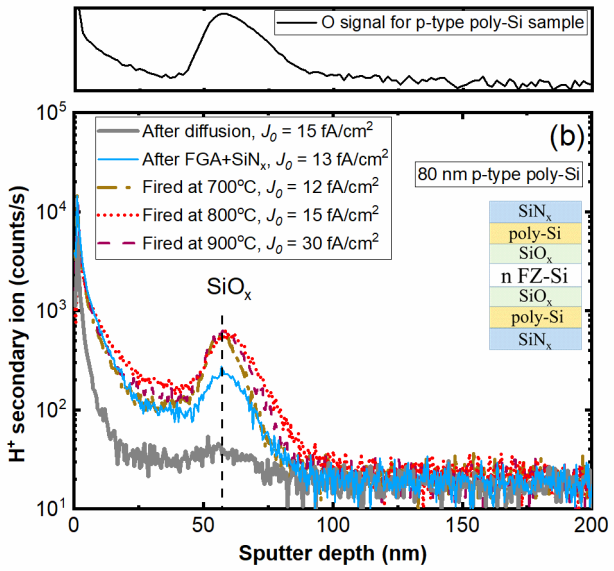

Figure 4. SIMS data for hydrogen profiles measured in (a) n- and (b) p-type poly-Si contacts after various processing steps, including phosphorus or boron diffusion, SiN_x deposition (n-type poly-Si) or FGA followed by SiN_x deposition (p-type poly-Si), and firing at various temperatures from 700°C to 900°C (both n- and p-type poly-Si samples were sandwiched during firing). The hydrogen profiles measured in n-type poly-Si were taken from our previous study.[13] Also given in Figure 4 (a) and (b) are the O signals measured by SIMS as a reference to identify the position of SiO_x. The SiN_x capping layers were removed by HF dip before SIMS measurement. Note that the sputter depth is a nominal value calculated based on the sputter rate determined in a separate c-Si calibration wafer using a profilometer, hence does not precisely reflect the actual poly-Si thickness and the location of the SiOx interfacial layer. The steep decay in the first 10 nm is an artefact caused by the residual hydrogen in the chamber and surface adsorbate, therefore the difference of the slope can be neglected in this study.

In addition to SIMS, FTIR was applied to identify the impact of 800°C firing on the properties of n- and p-type poly-Si. The changes in FTIR absorbance spectra upon firing for n- and p-type poly-Si passivating contacts are shown in Figure 5 (a) and (b) respectively, from which information on molecular interactions, such as hydrogen bonding, can be deduced. Note that different scales are used for the region between 700-1200 cm^{-1} and for the region between 2300-2400 cm^{-1}. For n-type poly-Si contacts, the absorption peaks located at ~890 cm^{-1} (Si–H bond) [32, 33] and ~970 cm^{-1} (Si–O–H bond) [34, 35] slightly increased in intensity after firing, while the height of the peaks at 2330 to 2360 cm^{-1} (Si–H$_x$ (x = 1, 2, 3) bonds) increased substantially.[36, 37] It is also noted that peak intensity of the Si–O–Si bonds detected at 1120 cm^{-1} was unchanged upon firing,[38-40] suggesting that the stoichiometry of the interfacial SiO_x layers were not significantly altered by the 800°C firing treatment.[37, 41] In contrast to n-type poly-Si, p-type poly-Si/SiO_x passivating contacts showed nearly identical FTIR spectra before and after firing. The distinct FTIR results for n- and p-type poly-Si contacts yield information about the

different molecular interactions occurring during the firing process. The different characteristics from SIMS and FTIR indicate that hydrogen may be responsible for the distinct firing behavior in n- and p-type poly-Si.

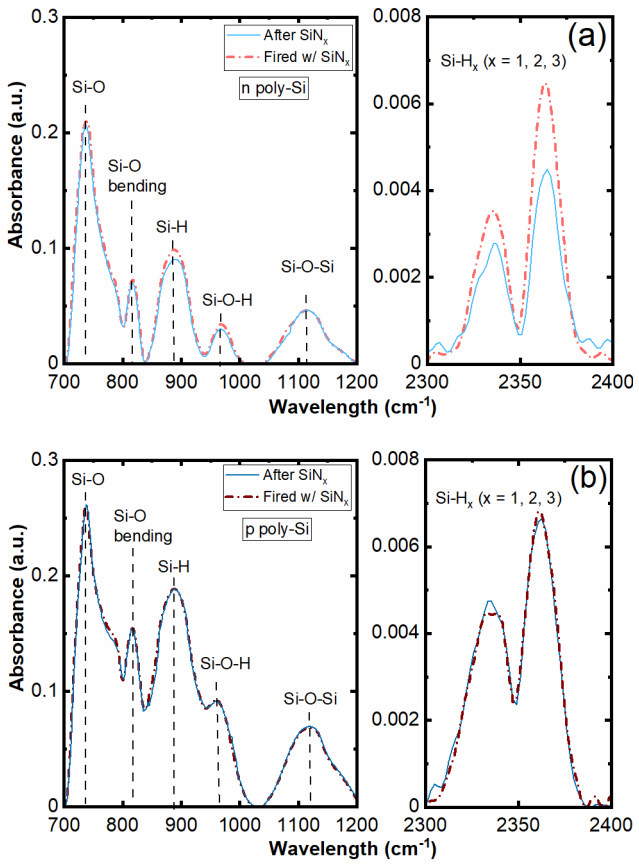

Figure 5. FTIR absorption spectrum measured in (a) n- and (b) p-type poly-Si fired with SiN_x at 800℃. Note that different scales are used for the region between 700-1200 cm^{-1} and for the region between 2300-2400 cm^{-1}. The fired SiN_x films were removed by HF dip prior to FTIR measurements.

Hydrogenation and de-hydrogenation after firing

To further understand the role of hydrogen, we also investigate the behavior of the fired poly-Si samples during a subsequent hydrogenation, in which more hydrogen was injected into the poly-Si/SiO_x stacks via deposition of SiN_x and FGA. The effect of hydrogenation was firstly evaluated on the samples fired at 800℃ without SiN_x coating films. As shown in Figure 6 (a), while both n- and p-type poly-Si passivation degraded after firing, p-type poly-Si was more resistant to firing damage, with the J_0 value only increasing slightly from 15 to 28 fA/cm^2, in comparison to the n-type poly-Si contacts where the J_0 value increased considerably from 22 to 320 fA/cm^2. Upon a subsequent hydrogenation, the samples showed a regeneration of J_0 values, to 13 fA/cm^2 for p-type poly-Si and 10 fA/cm^2 for n-type poly-Si.

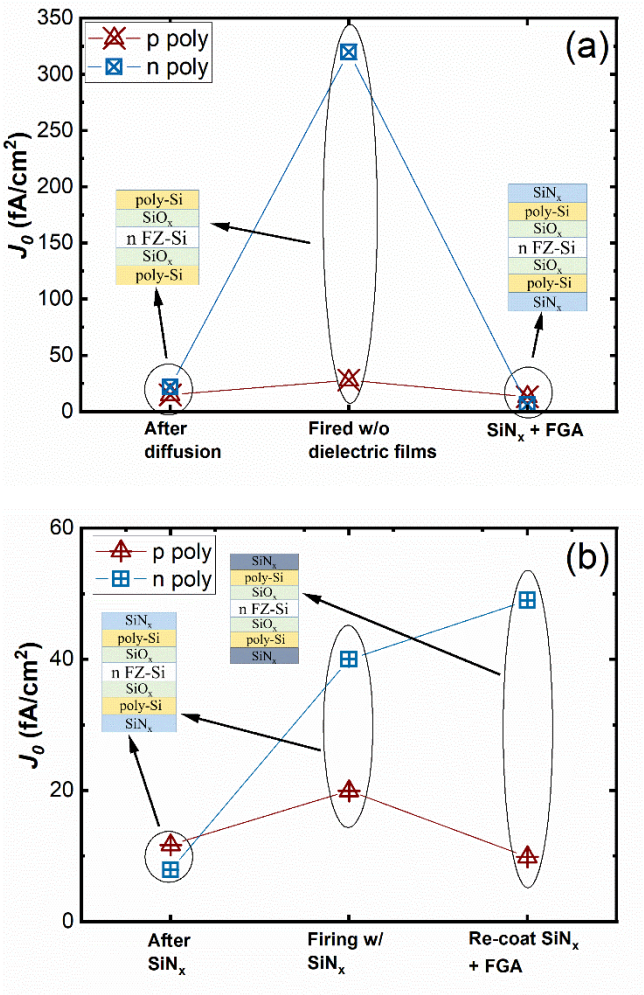

Figure 6. Changes in the J_0 values of n- and p-type poly-Si passivating contacts caused by a subsequent hydrogenation treatment after firing (a) without SiN_x and (b) with SiN_x films. Note that, in Figure 6 (a), the samples after diffusion did not receive FGA treatment.

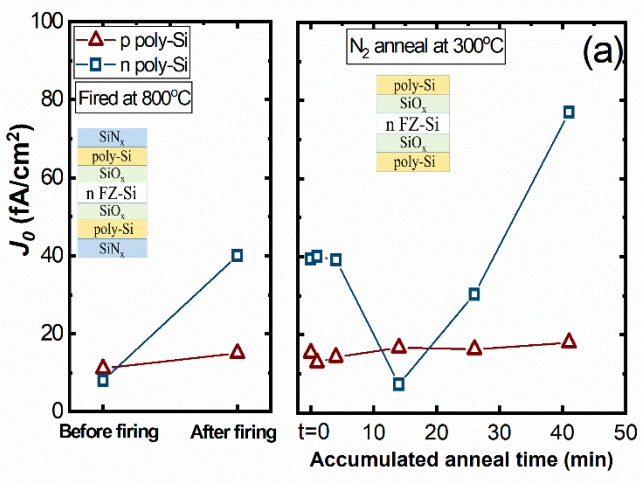

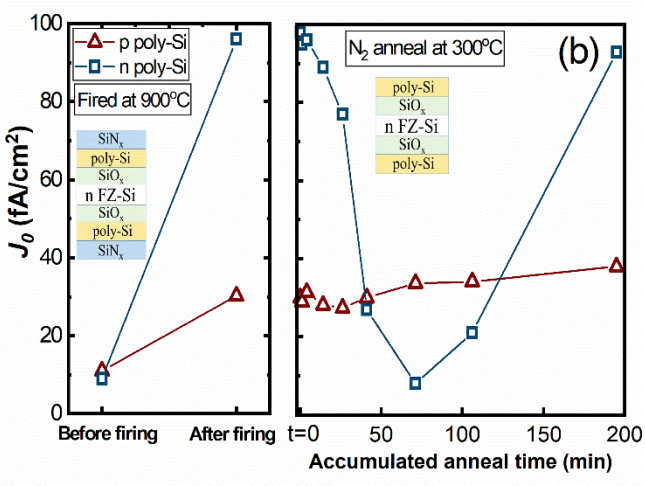

Figure 7. Evolution of J_0 during the N_2 anneal at 300°C, after the removal of fired SiN_x layers, after firing at (a) 800°C and (b) 900°C. Please note the different timescales used in Figure 7 (a) and (b).

Figure 6 (b) illustrates the influence of the subsequent hydrogenation treatment on the samples fired with SiN_x films, showing a different trend comparing to the samples fired without SiN_x. While the fired n-type poly-Si suffered a further degradation after the re-deposition of SiN_x and FGA, the degraded surface passivation of p-type poly-Si upon firing recovered upon the subsequent re-hydrogenation process and improved to the extent that the J_0 value is lower than before firing.

The behavior of the fired poly-Si samples after de-hydrogenation process was also tested. The effect of de-hydrogenation was examined on the samples fired with SiN_x at 800°C and 900°C via a N_2 anneal at 300°C after removing the originally fired SiN_x capping layers. Figure 7 (a) demonstrates evolution of the J_0 values during N_2 anneal for the 800°C fired n- and p-type poly-Si contacts. Interestingly, the firing-induced degradation in n-type poly-Si passivation was fully recovered after a 13 min N_2 anneal, while an additional 27 min N_2 anneal resulted in a significant increase in the J_0 value again. By contrast, we did not observe any obvious changes in the surface passivation of the p-type poly-Si/SiO_x structure upon the N_2 anneal. Changes in J_0 upon N_2 anneal for the n- and p-type poly-Si fired at 900°C are presented in Figure 7 (b), showing a similar trend compared to the samples fired at 800°C (Figure 7 (a)). However, the full recovery of 900°C fired n-type poly-Si was detected on a longer timescale (taking around 70 min to fully recover the J_0). In contrast, the surface degradation of p-type poly-Si after firing at 900°C, cannot be recovered by the 300°C N_2 anneal.

Discussion

The reversibility of surface passivation observed on n- and p-type poly-Si, in conjunction with the unchanged Si–O–Si bonds measured by FTIR after firing, indicate that the firing treatment at 800℃ is unlikely to cause a break-down of the SiO_x thin layer. The distinct hydrogen signals measured by SIMS and FTIR suggest the possible role of hydrogen for the different firing behavior of n- and p-type poly-Si.

In our recent work,[13] industrially processed n-type poly-Si/SiO_x contacts fired at 800℃ or above were found to suffer severe degradation in J_0, with the degradation extent depending on the dielectric capping film and the peak firing temperature. Based on the hydrogen profiles measured by SIMS for industrial poly-Si fired at different temperatures or fired with various dielectric coating layers, samples with more hydrogen content around SiO_x also exhibited a higher J_0 value.[13] Our previous results indicate that the passivation quality after firing could be determined by the amount of hydrogen released from the dielectric films to the SiO_x interlayer, and excess hydrogen around the SiO_x can be detrimental to the surface passivation, explaining the pronounced firing impact on industrially processed n-type poly-Si. This speculation was also supported by the increased degradation extent after injecting more hydrogen, as well as the recovered J_0 after reducing the hydrogen content around the SiO_x thin layer via a 300℃ N_2 anneal after the removal of fired SiN_x,[13] similar to what can be found in this work (Figure 6 and 7), which suggests that the hypothesis proposed in our previous work for industrial samples could be also applied to the n-type poly-Si investigated in the current work.

The impact of excess hydrogen can explain the observation in Figure 7 (a) and (b), where the recovery of J_0 in n-type poly-Si fired at 900℃ was detected on a longer timescale than that for the sample fired at 800℃. While the samples fired at 800℃ and 900℃ are likely to have a similar rate of hydrogen effusion during the N_2 anneal, the 900℃ fired sample is expected to take longer to release the excess hydrogen and to reach the optimum amount, owing to the higher amount of hydrogen injected into the SiO_x upon firing, which could require more time to release the excess hydrogen and to reach the optimum amount.

In contrast to n-type poly-Si, the J_0 of p-type poly-Si was recovered after injecting more hydrogen to the poly-Si/SiO_x stack by the re-hydrogenation treatment (shown in Figure 6 (b)), which could possibly indicate that there was no excess hydrogen in p-type poly-Si/SiO_x, possibly attributed to the lower effective diffusivity of atomic hydrogen in p-type materials.[42-45] Particularly, Hamer *et al*. reported that, for n-type Si wafers with a heavily phosphorus- or boron-doped layer with a similar doping profile, the hydrogen in-

diffusion is significantly lower in the boron-doped region, as the transport of hydrogen across the boron-doped region is opposed by the electric field.[46] It is speculated that the lower effective diffusivity of hydrogen in p-type poly-Si prevented the accumulation of excess hydrogen at the oxide interface upon firing, stopping it from degrading the surface passivation as otherwise observed in n-type poly-Si. During the subsequent N_2 anneal (shown in Figure 7), the stable J_0 in p-type poly-Si could be also related to the lower effective hydrogen diffusivity, preventing the out-diffusion of hydrogen from the interfacial SiO_x. The effective diffusivity of hydrogen could be affected by several factors, such as the charge state of hydrogen,[46-49] and different mechanisms for hydrogen trapping in n- and p-type Si.[45, 46, 50] The difference of these factors in n- and p-type poly-Si could also cause the different trend for hydrogen concentration in n- and p-type poly-Si fired at various temperatures (shown in Figure 4).

In this work, the comparison between n- and p-type poly-Si was implemented using samples with comparable surface passivation quality, and similar crystal properties. The investigated n- and p-type poly-Si films (shown in Figure 3, 6 and 7) had different doping profiles, as depicted in Figure 8. The p-type poly-Si had a lower doping concentration in the poly-Si film and a larger in-diffusion depth in the c-Si wafer, compared to the n-type poly-Si. Based on our previous study on the firing stability of n-type poly-Si,[13] the lower doping concentration in p-type poly-Si films should, in principle, cause a stronger firing impact than the more heavily doped n-type poly-Si film. This is, however, not observed in the current study, suggesting that the difference in doping concentration in p- and n-type poly-Si films does not contribute to their distinct firing stability. Moreover, we observe a different firing response in p- and n-type poly-Si with similar in-diffusion depth (n-type poly-Si in Figure 8 and p-type poly-Si in Figure 2 (b)). While the p-type poly-Si contacts exhibited only a slight degradation in J_0, increasing from 24 to 31 fA/cm^2, the J_0 value of the n-type poly-Si increased from 8 to 40 fA/cm^2.

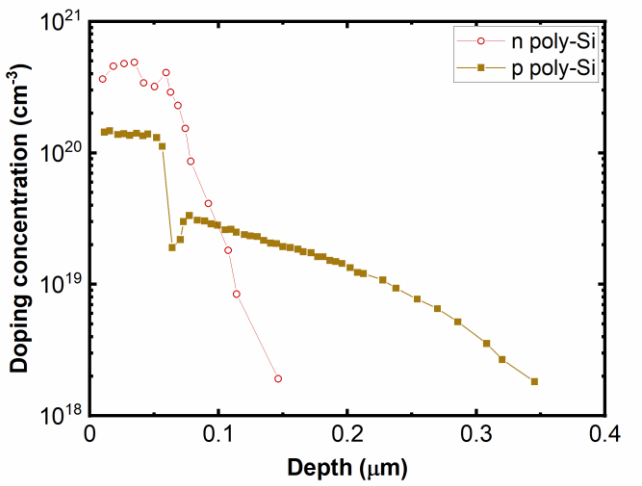

Figure 8. ECV profiles measured in n- and p-type poly-Si demonstrated in Figure 3, 6 and 7.

It should be noted that p-type poly-Si passivation degraded after firing at 900℃ (shown in Figure 3), potentially attributed to the defects, likely to be stress-induced, activated by firing. Our previous work has reported that a clear a-Si:H peak can be detected by photoluminescence spectroscopy after hydrogenation by FGA and SiN_x deposition, but disappeared after firing.[51] The result suggests a possibility that, upon firing, defects were activated by the increased stress in the poly-Si/SiO_x structure during the fast ramp-up step, and then were associated with the atomic hydrogen that was originally bonded with the Si atoms in the amorphous phase. The generation of defects could also affect the thin interfacial oxide layer, leading to enhanced surface recombination after firing. More evidence, however, is required to confirm our speculation. It is also worth noting that we did not observe any noticeable blisters on the fired samples by visual inspection,

Conclusions

We observed different firing response in samples passivated by n- and p-type poly-Si passivating contacts. While both n- and p-type poly-Si passivating contacts exhibited increasing degradation with firing temperature, p-type poly-Si was more resistant to firing impact. In n-type poly-Si/SiO_x structure, the hydrogen profiles measured by SIMS showed that hydrogen concentration surrounding the interfacial SiO_x increases with the peak firing temperature. This is in contrast to p-type poly-Si, in which similar hydrogen profiles were independent of the firing temperature. In addition, fired n- and p-type poly-Si exhibited different behavior during the subsequent hydrogenation and de-hydrogenation treatment. After injecting more hydrogen into the passivating contacts, p-type poly-Si fired with SiN_x showed improved surface passivation, whilst the n-type

counterpart further degraded in J_0. During a 300°C N_2 anneal after firing and removal of the SiN_x layer, the passivation quality was stable in p-type poly-Si, in comparison with a recovery of J_0 and a second degradation in n-type poly-Si.

In this work, it is hypothesized that the different behavior in n- and p-type poly-Si/SiO_x upon firing and the subsequent annealing are attributed to differences in the effective diffusivity of hydrogen. The diffusivity of hydrogen in p-type poly-Si might be lower than in n-type, preventing the accumulation of excess hydrogen around the oxide which deteriorates the passivation quality.

Acknowledgements

This work has been supported by the Australian Renewable Energy Agency (ARENA) through projects RND017 and 1-A060. Access to the Australian National Fabrication Facility (ANFF) ACT node is gratefully acknowledged. H.C.S, J.S., and H.T.N. acknowledge fellowship support from the Australian Centre for Advanced Photovoltaics (ACAP).

References

[1] M. Hermle, F. Feldmann, M. Bivour, J. C. Goldschmidt, and S. W. Glunz, "Passivating contacts and tandem concepts: Approaches for the highest silicon-based solar cell efficiencies," *Appl. Phys. Reviews*, vol. 7, no. 2, p. 021305, 2020.

[2] D. Yan, A. Cuevas, J. I. Michel, C. Zhang, Y. Wan, X. Zhang, and J. Bullock, "Polysilicon passivated junctions: The next technology for silicon solar cells?," *Joule*, vol. 5, no. 4, pp. 811-828, 2021.

[3] J. Schmidt, R. Peibst, and R. Brendel, "Surface passivation of crystalline silicon solar cells: Present and future," *Sol. Energy Mater. Sol. Cells*, vol. 187, pp. 39-54, 2018.

[4] M. Stodolny, J. Anker, C. Tool, M. Koppes, A. Mewe, P. Manshanden, M. Lenes, and I. G. Romijn, "Novel schemes of p+ polysi hydrogenation implemented in industrial 6" bifacial front-and-rear passivating contacts solar cells," in *35th European Photovoltaic Solar Energy Conference and Exhibition*, 2018, pp. 414 - 417.

[5] F. Haase, F. Kiefer, S. Schäfer, C. Kruse, J. Krügener, R. Brendel, and R. Peibst, "Interdigitated back contact solar cells with polycrystalline silicon on oxide passivating contacts for both polarities," *Jpn. J. Appl. Phys.*, vol. 56, no. 8S2, p. 08MB15, 2017.

[6] JinkoSolar. "Jinkosolar large-area n-type monocrystalline silicon solar cell reaches record-breaking new high efficiency of 25.25%." "Press release" [Online]. Available:"http://jinkosolar.com.au/2021/05/jinkosolar-large-area-n-type-monocrystalline-silicon-solar-cell-reaches-record-breaking-new-high-efficiency-of-25-25/" (accessed 31/05/2021).

[7] LONGi. "Longi breaks three more world records for solar cell efficiency." "Press release" [Online]. Available:"https://en.longi-solar.com/home/events/press_detail/id/335.html" (accessed 03/06/2021).

[8] C. Hollemann, F. Haase, S. Schäfer, J. Krügener, R. Brendel, and R. Peibst, "26.1%-efficient polo-ibc cells: Quantification of electrical and optical loss mechanisms," *Prog. Photovoltaics Res. Appl.*, vol. 27, no. 11, pp. 950-958, 2019.

[9] A. Mewe, M. Stodolny, J. Anker, M. Lenes, X. Pagès, Y. Wu, K. Tool, B. Geerligs, and I. G. Romijn, "Full wafer size ibc cell with polysilicon passivating contacts," in *AIP Conference Proceedings 1999*, 2018, vol. 1999, p. 040014.

[10] H. E. Çiftpınar, M. K. Stodolny, Y. Wu, G. J. M. Janssen, J. Löffler, J. Schmitz, M. Lenes, J.-M. Luchies, and L. J. Geerligs, "Study of screen printed metallization for polysilicon based passivating contacts," *Energy Procedia*, vol. 124, pp. 851-861, 2017.

[11] M. K. Stodolny, M. Lenes, Y. Wu, G. J. M. Janssen, I. G. Romijn, J. R. M. Luchies, and L. J. Geerligs, "N-type polysilicon passivating contact for industrial bifacial n-type solar cells," *Sol. Energy Mater. Sol. Cells*, vol. 158, pp. 24-28, 2016.

[12] D. Kang, H. C. Sio, D. Yan, J. Stuckelberger, X. Zhang, and D. Macdonald, "Firing stability of phosphorus-doped polysilicon passivating contacts: Factors affecting the degradation behavior," *Sol. Energy Mater. Sol. Cells*, vol. 234, p. 111407, 2021.

[13] D. Kang, H. C. Sio, J. Stuckelberger, R. Liu, D. Yan, X. Zhang, and D. Macdonald, "Optimum hydrogen injection in phosphorus-doped polysilicon passivating contacts," *ACS Appl. Mater. Interfaces*, DOI: 10.1021/acsami.1c17342, Accepted on 03/11/2021.

[14] B. Steinhauser, F. Feldmann, D. Ourinson, H. Nagel, T. Fellmeth, and M. Hermle, "On the influence of the sinx composition on the firing stability of poly-si/sinx stacks," *Phys. Status Solidi A*, vol. 217, no. 21, p. 2000333, 2020.

[15] F. Feldmann, T. Fellmeth, B. Steinhauser, H. Nagel, D. Ourinson, S. Mack, E. Lohmüller, J.-I. Polzin, J. Benick, J. Rentsch, M. Hermle, and S. Glunz, "Large area topcon cells realized by a pecvd tube process," in *36th European Photovoltaic Solar Energy Conference and Exhibition*, 2019, pp. 304-308.

[16] A. Ingenito, G. Nogay, Q. Jeangros, E. Rucavado, C. Allebé, S. Eswara, N. Valle, T. Wirtz, J. Horzel, T. Koida, M. Morales-Masis, M. Despeisse, F.-J. Haug, P. Löper, and C. Ballif, "A passivating contact for silicon solar cells formed during a single firing thermal annealing," *Nat. Energy*, vol. 3, no. 9, pp. 800-808, 2018.

[17] C. Hollemann, F. Haase, J. Krügener, R. Brendel, and R. Peibst, "Firing stability of n-type poly-si on oxide junctions formed by quartz tube annealing," presented at the 2020 47th IEEE Photovoltaic Specialists Conference (PVSC), 2020.

[18] M. Schnabel, B. Van de Loo, W. Nemeth, B. Macco, P. Stradins, W. M. M. Kessels, and D. Young, "Hydrogen passivation of poly-si/siox contacts for si solar cells using al2o3 studied with deuterium," *Appl. Phys. Lett.*, vol. 112, p. 203901, 2018.

[19] M. Lehmann, N. Valle, J. Horzel, A. Pshenova, P. Wyss, M. Döbeli, M. Despeisse, S. Eswara, T. Wirtz, Q. Jeangros, A. Hessler-Wyser, F.-J. Haug, A. Ingenito, and C. Ballif, "Analysis of hydrogen distribution and migration in fired passivating contacts (fpc)," *Sol. Energy Mater. Sol. Cells*, vol. 200, p. 110018, 2019.

[20] M. Stöhr, J. Aprojanz, R. Brendel, and T. Dullweber, "Firing-stable pecvd sioxny/n-poly-si surface passivation for silicon solar cells," *ACS Appl. Energy Mater.*, vol. 4, no. 5, pp. 4646-4653, 2021.

[21] R. Witteck, B. Veith-Wolf, H. Schulte-Huxel, A. Morlier, M. R. Vogt, M. Köntges, and R. Brendel, "Uv-induced degradation of perc solar modules with uv-transparent encapsulation materials," *Prog. Photovoltaics Res. Appl.*, vol. 25, no. 6, pp. 409-416, 2017.

[22] T. Lauinger, J. Moschner, A. G. Aberle, and R. Hezel, "Optimization and characterization of remote plasma-enhanced chemical vapor deposition silicon nitride for the passivation of p-type crystalline silicon surfaces," *J. Vac. Sci. Technol.*, vol. 16, no. 2, pp. 530-543, 1998.

[23] R. A. Sinton, A. Cuevas, and M. Stuckings, "Quasi-steady-state photoconductance, a new method for solar cell material and device characterization," presented at the Conference Record of the Twenty Fifth IEEE Photovoltaic Specialists Conference - 1996, 1996.

[24] D. E. Kane and R. M. Swanson, "Measurement of the emitter saturation current by a contactless photoconductivity decay method," *IEEE 18th Photovoltaic Specialist Conference*, p. 578, 1985.

[25] "EDNA2". [Online] Available: https://www2.pvlighthouse.com.au/calculators (accessed 10/08/2021).

[26] J. Stuckelberger, G. Nogay, P. Wyss, A. Ingenito, C. Allebé, J. Horzel, B. A. Kamino, M. Despeisse, F. J. Haug, P. Löper, and C. Ballif, "Recombination analysis of phosphorus-doped nanostructured silicon oxide passivating electron contacts for silicon solar cells," *IEEE J. Photovoltaics*, vol. 8, no. 2, pp. 389-396, 2018.

[27] S. Kalainathan, R. Dhanasekaran, and P. Ramasamy, "Grain size and size distribution in heavily phosphorus doped polycrystalline silicon," *Journal of Crystal Growth*, vol. 104, no. 2, pp. 250-256, 1990.

[28] B. W. H. van de Loo, B. Macco, M. Schnabel, M. K. Stodolny, A. A. Mewe, D. L. Young, W. Nemeth, P. Stradins, and W. M. M. Kessels, "On the hydrogenation of poly-si passivating contacts by al2o3 and sinx thin films," *Sol. Energy Mater. Sol. Cells*, vol. 215, p. 110592, 2020.

[29] S. Mack, J. Schube, T. Fellmeth, F. Feldmann, M. Lenes, and J.-M. Luchies, "Metallisation of boron-doped polysilicon layers by screen printed silver pastes," *Phys. Status Solidi RRL*, vol. 11, no. 12, p. 1700334, 2017.

[30] F. L. Martínez, A. del Prado, I. Mártil, G. González-Diaz, W. Bohne, W. Fuhs, J. Röhrich, B. Selle, and I. Sieber, "Molecular models and activation energies for bonding rearrangement in plasma-deposited dielectric thin films treated by rapid thermal annealing," *Phys. Rev. B*, vol. 63, no. 24, p. 245320, 2001.

[31] S. Wilking, S. Ebert, A. Herguth, and G. Hahn, "Influence of hydrogen effusion from hydrogenated silicon nitride layers on the regeneration of boron-oxygen related defects in crystalline silicon," *J. Appl. Phys.*, vol. 114, no. 19, p. 194512, 2013.

[32] F. Ay and A. Aydinli, "Comparative investigation of hydrogen bonding in silicon based pecvd grown dielectrics for optical waveguides," *Opt. Mater.*, vol. 26, no. 1, pp. 33-46, 2004.

[33] P. G. Pai, S. S. Chao, Y. Takagi, and G. Lucovsky, "Infrared spectroscopic study of siox films produced by plasma enhanced chemical vapor deposition," *J. Vac. Sci. Technol.*, vol. 4, no. 3, pp. 689-694, 1986.

[34] T. Oh, "Comparison between sioc thin film by plasma enhance chemical vapor deposition and sio2 thin film by fourier transform infrared spectroscopy," *Journal of The Korean Physical Society*, vol. 56, 2010.

[35] R. Sazonov, G. Kholodnaya, D. Ponomarev, G. Remnev, and I. Khailov, "Features of silicon-containing coatings deposition from ablation plasma formed by a powerful ion beam," *J. Phys. Conf. Ser.*, vol. 552, p. 012025, 2014.

[36] M. A. Vásquez-A, G. Águila Rodríguez, G. García-Salgado, G. Romero-Paredes, and R. Peña-Sierra, "Ftir and photoluminescence studies of porous silicon layers oxidized in controlled water vapor conditions," (in Inglés), *Revista Mexicana de Física*, vol. 53, no. 6, pp. 431-435, 2007.

[37] M. Bouzerdoum and B. Birouk, "Characterization by sem and ftir of b-lpcvd polysilicon films after thermal oxidation," in *2012 24th International Conference on Microelectronics (ICM)*, 2012, pp. 1-4.

[38] L. Johnson, L. Gao, C. Shields Iv, M. Smith, K. Efimenko, K. Cushing, J. Genzer, and G. López, "Elastomeric microparticles for acoustic mediated bioseparations," *J. Nanobiotechnology*, vol. 11, p. 22, 2013.

[39] A. Nandiyanto, R. Oktiani, and R. Ragadhita, "How to read and interpret ftir spectroscope of organic material," *Indones. J. Sci. Technol.*, vol. 4, pp. 97-118, 2019.

[40] U. Künzelmann and H. Schumacher, "Characterization of surface processes during oxide cmp by in situ ftir spectroscopy," in *Advances in chemical mechanical planarization (cmp)*, S. Babu Ed.: Woodhead Publishing, 2016, pp. 359-396.

[41] G. Kaur, Z. Xin, T. Dutta, R. Sridharan, R. Stangl, and A. Danner, "Improved silicon oxide/polysilicon passivated contacts for high efficiency solar cells via optimized tunnel layer annealing," *Sol. Energy Mater. Sol. Cells*, vol. 217, p. 110720, 2020.

[42] P. Hamer, C. Chan, R. S. Bonilla, B. Hallam, G. Bourret-Sicotte, K. A. Collett, S. Wenham, and P. R. Wilshaw, "Hydrogen induced contact resistance in perc solar cells," *Sol. Energy Mater. Sol. Cells*, vol. 184, pp. 91-97, 2018.

[43] A. Van Wieringen and N. Warmoltz, "On the permeation of hydrogen and helium in single crystal silicon and germanium at elevated temperatures," *Physica*, vol. 22, no. 6, pp. 849-865, 1956.

[44] B. J. Hallam, A. M. Ciesla, C. C. Chan, A. Soeriyadi, S. Liu, A. M. Soufiani, M. Wright, and S. Wenham, "Overcoming the challenges of hydrogenation in silicon solar cells," *Aust. J. Chem.*, vol. 71, no. 10, pp. 743-752, 2018.

[45] D. Mathiot, "Modeling of hydrogen diffusion in n- and p-type silicon," *Phys. Rev. B*, vol. 40, no. 8, pp. 5867-5870, 1989.

[46] P. Hamer, B. Hallam, R. S. Bonilla, P. P. Altermatt, P. Wilshaw, and S. Wenham, "Modelling of hydrogen transport in silicon solar cell structures under equilibrium conditions," *J. Appl. Phys.*, vol. 123, no. 4, p. 043108, 2018.

[47] K. J. Chang and D. J. Chadi, "Hydrogen bonding and diffusion in crystalline silicon," *Phys. Rev. B*, vol. 40, no. 17, pp. 11644-11653, 1989.

[48] S. J. Pearton, J. W. Corbett, and T. S. Shi, "Hydrogen in crystalline semiconductors," *Appl. Phys. A*, vol. 43, no. 3, pp. 153-195, 1987.

[49] R. Rizk, P. de Mierry, D. Ballutaud, M. Aucouturier, and D. Mathiot, "Hydrogen diffusion and passivation processes in p- and n-type crystalline silicon," *Phys. Rev. B*, vol. 44, no. 12, pp. 6141-6151, 1991.

[50] C. P. Herrero, M. Stutzmann, A. Breitschwerdt, and P. V. Santos, "Trap-limited hydrogen diffusion in doped silicon," *Phys. Rev. B*, vol. 41, no. 2, pp. 1054-1058, 1990.

[51] D. Kang, H. C. Sio, D. Yan, J. Stuckelberger, T. N. Truong, S. P. Phang, R. Liu, and D. Macdonald, "Firing stability of polysilicon passivating contacts: The role of hydrogen," in *48th IEEE Photovoltaic Specialists (PVSC)*, 2021,

Chapter 6 – Long-term stability study of the passivation quality of polysilicon-based passivation layers for silicon solar cells

Solar Energy Materials & Solar Cells 215 (2020) 110691

Contents lists available at ScienceDirect

Solar Energy Materials and Solar Cells

journal homepage: http://www.elsevier.com/locate/solmat

Long-term stability study of the passivation quality of polysilicon-based passivation layers for silicon solar cells

Di Kang [a,*], Hang Cheong Sio [a], Di Yan [a], Wenhao Chen [a], Jie Yang [b], Jingsheng Jin [b], Xinyu Zhang [b], Daniel Macdonald [a]

[a] Research School of Electrical, Energy and Materials Engineering, The Australian National University (ANU), Canberra, ACT, 0200, Australia
[b] Jinko Solar Co., Ltd, Shangrao, Jiangxi Province, China

ARTICLE INFO

Keywords:
Polysilicon
Degradation
Surface passivation
Czochralski silicon (Cz-Si)
Float zone silicon (FZ-Si)
Silicon solar cells

ABSTRACT

We investigate the stability of the effective lifetime τ_{eff} and the recombination current density parameter J_0 in n-type silicon samples with symmetric phosphorus doped poly-Si/SiO_x structures, and identify factors that contribute to the passivation degradation behavior. It is found that the surface passivation quality of phosphorus doped polysilicon passivating contacts degrades upon dark annealing and light soaking at temperatures between 75 °C and 200 °C, which can lead to a pronounced increase of the recombination current density parameter J_0 (one-side) from below 10 fA/cm^2 to 50 fA/cm^2 or above. The degradation is only detected on fired wafers, whereas the surface passivation quality is found to be stable in the non-fired sister samples. Surprisingly, a recovery of τ_{eff} and J_0 is observed after the degradation. The degradation and regeneration behaviors depend strongly on temperature and light intensity, and the presence of silicon nitride (SiN_x) capping layers during the light soaking. Increasing the annealing temperature dramatically increases the rate of the degradation and the regeneration process, and at the same time reduces the magnitude of the degradation. The regeneration process appears to be affected by the presence of SiN_x films during the light soaking treatment. Samples with SiN_x films removed after firing suffer a significantly larger degradation upon light soaking without any lifetime regeneration. Grazing incidence X-ray diffraction measurements reveal negligible change in the structural property and crystalline quality of the polysilicon layer during the degradation.

1. Introduction

Recombination losses at metal-silicon interfaces are a key factor limiting the efficiencies of industrial crystalline silicon (c-Si) solar cells [1]. One approach to limit this loss mechanism is to reduce the contact fraction using local contacts. Devices with such structures, such as the passivated emitter and rear cells (PERC), show improved performance [2]. Alternatively, passivating contact structures have been found to be efficient in reducing carrier recombination at the contact regions, while allowing effective carrier-selective contacts for solar cells [3,4].

Among the various passivating contact technologies, polysilicon (poly-Si) passivating contacts, consisting of an ultra-thin SiO_x layer capped with a doped poly-Si film, show great potential to be used for high efficiency devices in mass production [5,6]. It has been demonstrated that the application of phosphorus poly-Si and SiO_x as a carrier selective full-area rear contact can lead to a significant efficiency improvement in n-type solar cells [7–9]. Mass production of solar cells with $POCl_3$ diffused poly-Si passivating rear contacts is already underway, and it is expected that the technology will gain significant market share in the near future [10].

Although poly-Si passivating technologies have been extensively studied, the majority of previous work has been focused on their electrical performance directly after fabrication [3,11–15]. Unlike the reliability studies on passivated emitter and rear cells (PERC) [16–20], few studies have been performed on the longer-term stability of poly-Si passivation structures upon illumination and annealing. An exception is the study by Winter et al. [21] who recently reported that phosphorus doped poly-Si passivation layers applied on both p- and n-type Czochralski silicon (Cz-Si) substrates exhibit a firing-related degradation and recovery phenomenon when subjected to either illumination or dark annealing. Moreover, Yang et al. [22] reported changes in surface passivation in Cz-Si samples featuring phosphorus doped poly-Si upon light soaking or dark annealing at above 150 °C, and an improvement in surface passivation was observed on samples light soaked or annealed at

* Corresponding author.
E-mail address: di.kang@anu.edu.au (D. Kang).

https://doi.org/10.1016/j.solmat.2020.110691
Received 21 April 2020; Received in revised form 29 June 2020; Accepted 1 July 2020
Available online 13 July 2020

temperatures above 250 °C.

This work further investigates the long-term stability (up to 100,000 min or 70 days) of phosphorus doped poly-Si passivation layers on n-type silicon substrates under illumination at elevated temperature, and explores the impact of several factors, including the degradation conditions (temperature and light intensity), poly-Si fabrication processes, firing profile, the properties of SiN_x films, and the presence or absence of SiN_x capping layers during the light soaking. The samples were characterized by effective lifetime (τ_{eff}), recombination current density parameter (J_0) and implied open-circuit voltages (iV_{oc}), to respectively demonstrate the overall electronic degradation behavior, the corresponding changes in the surface passivation quality, and the potential influence on device performance. A room temperature super-acid passivation technique [23] was applied to monitor any variations in the bulk lifetimes of the samples during the stability experiments. Finally, we compare the degradation behaviors of *ex-situ* doped (through $POCl_3$ diffusion) poly-Si passivation layers fabricated via two different silicon film deposition approaches, the Plasma Enhanced Chemical Vapor Deposition (PECVD) approach and the Low Pressure Chemical Vapor Deposition (LPCVD) approach. Those two approaches are considered as the two main technologies for silicon films deposition in industrial mass production [10,24].

2. Experimental details

Fig. 1 shows a flowchart outlining the experimental details. The samples feature a symmetric phosphorus doped poly-Si/SiO_x structure and SiN_x capping layers on both surfaces. PECVD and LPCVD poly-Si layers were separately prepared on n-type phosphorus doped float-zone (FZ) and Cz-Si wafers. Samples passivated by PECVD poly-Si layers were prepared in our lab at ANU, using processes outlined in our previous works [15,25] for manufacturing high-efficiency poly-Si devices. The FZ-Si wafers had a resistivity of 2 Ω cm and a thickness of 300 ± 10 μm. After saw damage etching, thin thermal oxide layers were grown on the FZ samples by submerging them in boiling nitric acid solution for 30 min. A 50 nm thick intrinsic a-Si layer was then deposited on both sides of the wafers using a Roth and Rau AK400 PECVD tool, followed by a thermal $POCl_3$ diffusion at 840 °C to dope and crystallize the poly-Si film, and then a forming gas anneal at 400 °C for 30 min. Afterwards, the FZ-Si samples were coated with SiN_x films deposited using an Oxford PlasmaLab 100 PECVD system, and fired in a rapid thermal process (RTP) furnace at 700 °C (actual temperature) for 5 s with a ramp up and cool down rate of 20 °C/s and 70 °C/s (average rate from peak firing temperature to 400 °C) respectively. The n-type Cz-Si wafers had a resistivity of 4 Ω cm and a thickness of 180 ± 5 μm. The planar Cz-Si wafers were processed similarly to the FZ-Si samples described above, but with different equipment in an industrial production line. In particular, 100 nm intrinsic a-Si layers were deposited on the Cz-Si samples with an LPCVD tool and doped by phosphorus diffusion, as compared to the PECVD tool used for the FZ-Si samples. Three different SiN_x films were deposited on the LPCVD deposited poly-Si films samples, either using an Oxford PlasmaLab 100, a Roth and Rau AK400, or a Centrotherm batch-type PECVD tool, to study the potential influence of the SiN_x capping layer. The samples with LPCVD poly-Si were then fired at various temperatures either in a conveyor belt furnace (with a measured peak temperature of 770 ± 30 °C) or in an RTP furnace (with actual peak firing temperature of 600 °C, 700 °C, or 750 °C). In order to identify the factors affecting degradation behaviors, samples were divided into several groups according to the fabrication methods and degradation conditions. Table 1 summarizes the key differences in processing steps of samples in each group.

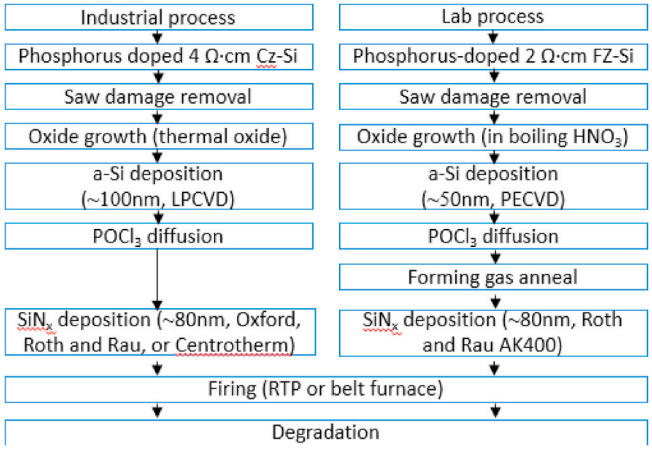

Fig. 1. Flowchart of experimental details.

The degradation tests were performed on a hotplate at various temperatures under illumination by a white light emitting diode (LED) light source with illumination intensity varying between 0.1 and 1 sun. During the tests, τ_{eff} and iV_{oc} values were measured using a Sinton Instruments WCT-120 QSSPC at room temperature [26]. J_0 values were also extracted using the Kane and Swanson method [27] to monitor changes in the surface passivation quality of poly-Si passivation layers. To evaluate the bulk lifetimes of the samples, a super-acid passivation technique was employed [23,28]. We selected various samples at different degradation stages, removed their surface films (SiN_x and poly-Si/SiO_x) via HF dip and TMAH etch, and then measured the lifetimes of the samples with a room-temperature passivation treatment using a super-acid solution mixed by bis(trifluoromethane)sulfonimide (TFSI) and hexane. It is noted that the heavily doped phosphorus diffused region in the crystalline silicon bulk near the surface was also removed during the TMAH etch, which removed around 5 μm from each surface of the wafers.

The structural properties of the poly-Si thin films before and after the degradation tests were examined by grazing incidence X-ray diffraction (GIXRD) measurement. The SiN_x layers were removed from the samples by hydrogen fluoride (HF) solution prior to the GIXRD characterization. A PANalytical X'Pert PRO MRD High Resolution X-ray diffractometer with CuKα radiation and a graphite monochromator was used.

3. Results and discussion

3.1. Overall degradation behaviors

Fig. 2 shows the evolution of τ_{eff} measured at an injection level of 1×10^{15} cm^{-3}, and the corresponding J_0 values (for one side) in the industrially-processed LPCVD poly-Si passivated n-type Cz-Si samples under 1-sun illumination at 140 °C. The J_0 values were extracted using the Kane and Swanson method [27], based on lifetime values at injection levels between 3.5×10^{15} and 9.5×10^{15} cm^{-3}. Fig. 2 (b) shows examples for J_0 fittings measured at initial (before degradation) and maximum degradation stages. A linear correlation between ($1/\tau_{eff} - 1/\tau_{Auger}$) and Δn was observed, demonstrating the accuracy of the extracted J_0 values [31]. Note that the samples are assumed to have identical poly-Si films on the front and the rear side, and the single-side J_0 values were obtained by dividing the extracted J_0 by 2. As seen in Fig. 2 (a) and (b), an obvious reduction in τ_{eff} and a corresponding increase in J_0 is detected in the sample. Interestingly, a partial recovery in τ_{eff} and J_0 can be observed after 10,000 min of illumination. The reduction and recovery of J_0 correlate well with the changes of effective lifetimes, indicating that the degradation is likely to be due to variations in surface passivation quality.

To differentiate the bulk contribution to the observed degradation phenomena, we measured lifetimes with room-temperature super-acid passivation treatment [23], on sister samples collected at different degradation stages during the light soaking under 1 sun at 140 °C (show in Fig. 2 (a)), after removing their surface films (SiN_x and poly-Si/SiO_x). It is notable that lifetimes measured with super-acid treatment are not

Table 1
Descriptions of processing steps and degradation conditions studied in this work.

	Process [a]	SiN_x films [b]	Firing condition	Degradation temperature	Light intensity
Overall degradation behaviors (**Section 3.1**)	Industrial	III	Belt furnace [c]	140°C	1 sun
Dependence on degradation temperatures (**Section 3.2**)	Industrial	III	Belt furnace [c]	75°C, 140°C, or 200°C	1 sun
Dependence on illumination intensities (**Section 3.3**)	Industrial	III	Belt furnace [c]	200°C	0.1 suns, 0.5 suns, 1 sun, or dark anneal
Dependence on fabrication processes (**Section 3.4**)	Industrial	III	Belt furnace [c]	140°C	1 sun
	Lab	II	RTP 700°C		
Dependence on firing profiles (**Section 3.5**)	Industrial	III	RTP: 600°C, 700°C, or 750°C; Belt furnace [c]	140°C	1 sun
Dependence on SiN_x films (**Section 3.6**)	Industrial	I, II, III	RTP 750°C	140°C	1 sun
		II	RTP 750°C	200°C	

[a] The processing steps are outlined in Fig. 1. Note that, as illustrated in Fig. 1, different Si wafers were used for industrial and lab processed samples.
[b] SiN_x I, II and III denotes silicon nitride films deposited using an Oxford PlasmaLab 100, a Roth and Rau AK400, or a Centrotherm batch-type PECVD tool respectively.
[c] Belt furnace firing process denotes a conventional industrial firing profile with an actual peak firing temperature of 770 ± 30°C.

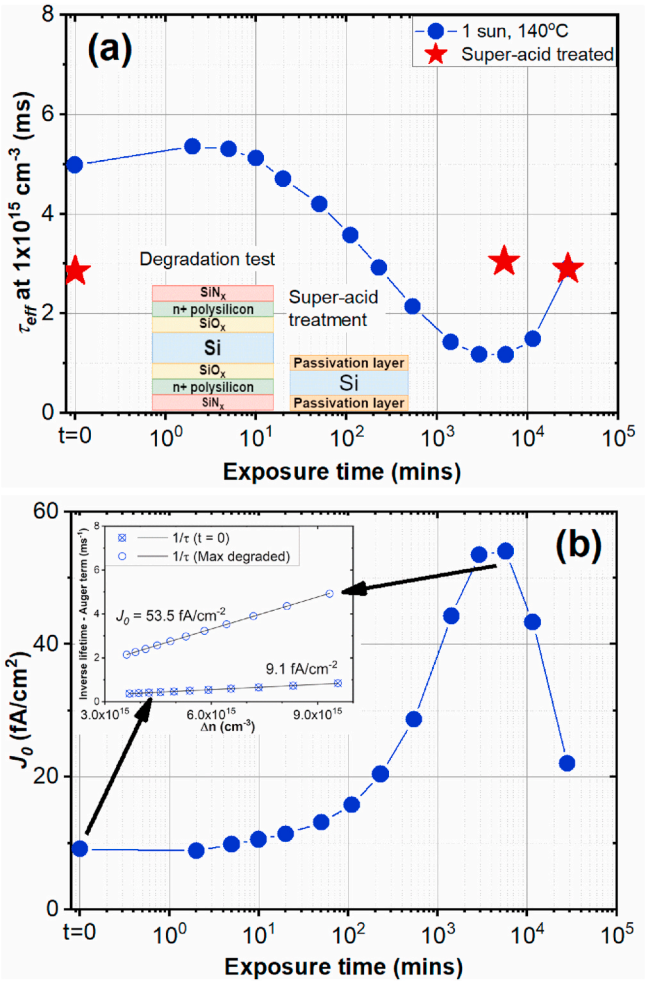

Fig. 2. Evolution of (a) τ_{eff} and (b) J_0 for samples illuminated under 1 sun at 140 °C. Also presented in Fig. 2 (a) are lifetimes measured by super-acid treatment [23] on samples collected at various degradation stages, including before light soaking, at the maximum degradation stage, and after a slight recovery. Inverse lifetimes ($1/\tau_{eff} - 1/\tau_{Auger}$) as a function of excess carrier density Δn for the sample measured at two different degradation stages are shown in Fig. 2 (b), and J_0 values are determined from the slope of the fit (Δn ranging from 3.5 × 10^{15} to 9.5 × 10^{15} cm^{-3}). The samples, as shown in Table 1, were industrially sourced and fired by belt furnace at a peak firing temperature of 770 ± 30 °C (actual temperature). The lines are guides to the eye.

necessarily the actual bulk lifetime of the wafers, as they are partly limited by the passivation quality of the super-acid solution, limiting τ_{eff} to around 3 ms in this case. However, comparing the lifetime values of samples passivated from the same batch of super-acid treatment can reveal changes in the bulk properties. As shown in Fig. 2 (a), the measured lifetimes are almost constant during the light soaking, confirming that the observed degradation in the effective lifetimes of the sample is caused by changes in the surface passivation quality. A further evidence for the degradation to occur in surface passivation rather than in the bulk is that the injection dependence of the τ_{eff} after degradation is consistent with a change in the J_0 parameter, with minimum lifetime reduction detected at low-injections. This leads to a conclusion that this degradation phenomenon is different from the widely reported light and elevated temperature induced degradation (LeTID), which is known to be a bulk-related degradation [20,29,30].

We compare the structural properties and crystalline quality of the poly-Si films before and after light soaking with GIXRD, to investigate its potential correlation with the observed degradation behaviors. The degraded sample was exposed to 1 sun illumination at 140 °C conditions for around 5000 min to achieve the maximum degraded state. As shown in Fig. 3, there is negligible change in the diffraction pattern from samples before and after the degradation, suggesting the degradation is not likely due to changes in the degree of crystallization, such as an increase in crystal grain size.

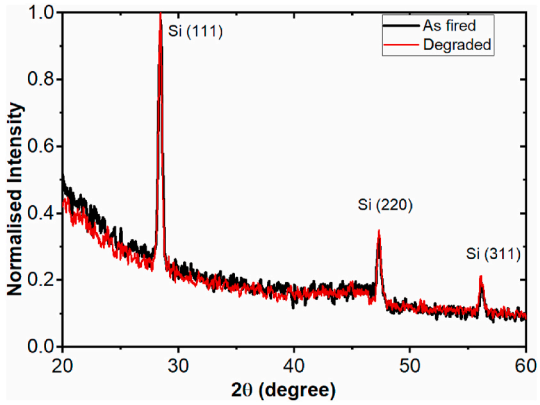

Fig. 3. Normalized GIXRD spectra of as-fired and degraded samples. SiN_x films on both samples were removed by HF dip before GIXRD. The degraded sample was exposed under 1 sun at 140 °C for around 5000 min, reaching the maximum degradation condition.

3.2. Correlation between degradation behaviors and degradation temperatures

Fig. 4 compares the samples subjected to light soaking at different temperatures. Samples illuminated at higher temperature (e.g. 200 °C) exhibit faster degradation, but with lower magnitude. The degradation can already be observed on the sample illuminated at 75 °C. However, due to the slow degradation rate at 75 °C, the tested sample does not appear to have reached its maximum degraded state within our experimental timeframe (more than 1500 h). The observed degradation phenomenon in the poly-Si structures can potentially affect the long-term performance of PV modules, and due to its slow reaction rate, might not be detected with standard degradation tests. On the other hand, for the sample degraded under 1 sun at 200 °C, a full recovery of lifetime and J_0 (Fig. 4 (b)) can be observed after 2000 min of light soaking. For further investigation in this work, we employed 140 °C and 200 °C for the degradation tests to accelerate the degradation and regeneration process.

It is notable that there is a slight variation in the initial lifetimes and J_0 values in the samples, potentially due to non-uniformity in the processing, such as the phosphorus diffusion. After the first few minutes of illumination, a small lifetime improvement can be also observed in samples, most likely due to the variation in bulk properties, which is evident from stable J_0 values, and the injection dependence of the lifetimes where a larger difference of τ_{eff} is detected at low injection (shown in Fig. 4 (a)). It is found that the magnitude of the τ_{eff} improvement within the first few minutes varies with the degradation conditions. The underlying mechanism for the bulk lifetime improvement remains unclear and is still under investigation.

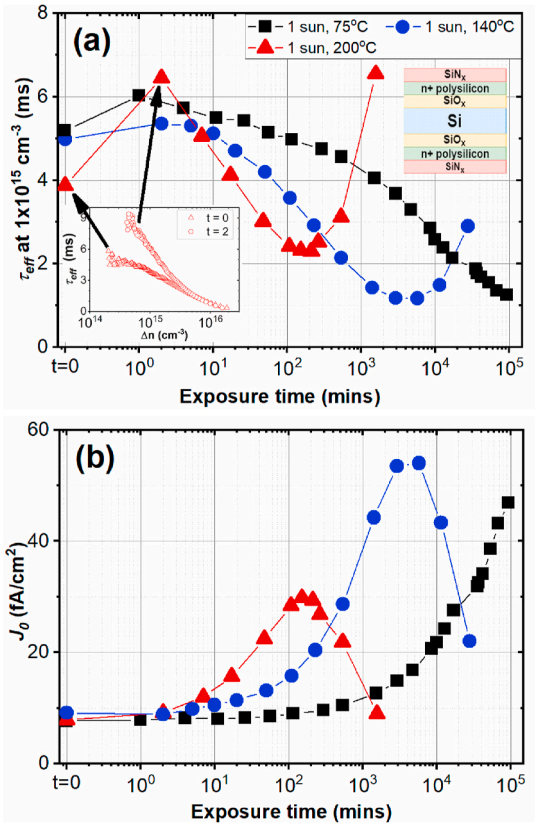

Fig. 4. Comparison of degradation behavior for different degradation temperatures with 1-sun light soaking - (a) τ_{eff} measured at an injection level of 1 × 10^{15} cm^{-3}, (b) single-side J_0 values. The lines are guides to the eye. Also shown in Fig. 4 (a) are injection-level dependent effective lifetimes for the first two measurements of the sample illuminated at 200 °C.

3.3. Correlation between degradation behaviors and illumination intensities

The dependence of the degradation behavior on illumination intensity and wavelength is demonstrated in Fig. 5. Comparing the degradation behaviors of samples exposed to different light intensities (0.1, 0.5 and 1 sun), the degradation magnitude and rate increase slightly as the light intensity rises. In addition to a white LED light source (correlated color temperature of around 4000 K), we also applied an infrared light source (850 nm) with similar photon flux (estimated by the output current from a reference solar cell) to further investigate the influence of the illumination spectrum. The two samples exposed to infrared and white LED illumination show almost identical degradation rate and magnitude. On the other hand, samples annealed in the dark at 200 °C also show some degradation, but with a considerably slower degradation rate and a lower maximum degradation magnitude, when compared to the sister samples degraded under 1 sun at 200 °C. The almost identical degradation kinetics upon light soaking with different illumination sources, together with the degradation behavior upon dark annealing, imply that ultraviolet (UV) damage [32,33] is unlikely to be the root cause of the observed degradation phenomenon.

Winter et al. [21] also observed degradations in surface passivation quality of phosphorus doped poly-Si passivation layers when samples subjected to dark annealing at 200 °C or illumination at 185 °C. For samples annealed at 200 °C in dark, Winter et al. reported a J_0 change from ~16 fA/cm^2 to ~75 fA/cm^2 after 20 h. The degradation is more severe, in terms of both the rate and the magnitude, when compared with our results where J_0 increased from ~10 fA/cm^2 to ~20 fA/cm^2 after 6000 min (or 100 h) of dark annealing. For the illuminated samples, the literature presented that, under 1 sun illumination at 185 °C, J_0 increased from ~16 fA/cm^2 to ~70 fA/cm^2 to reach its maximum value

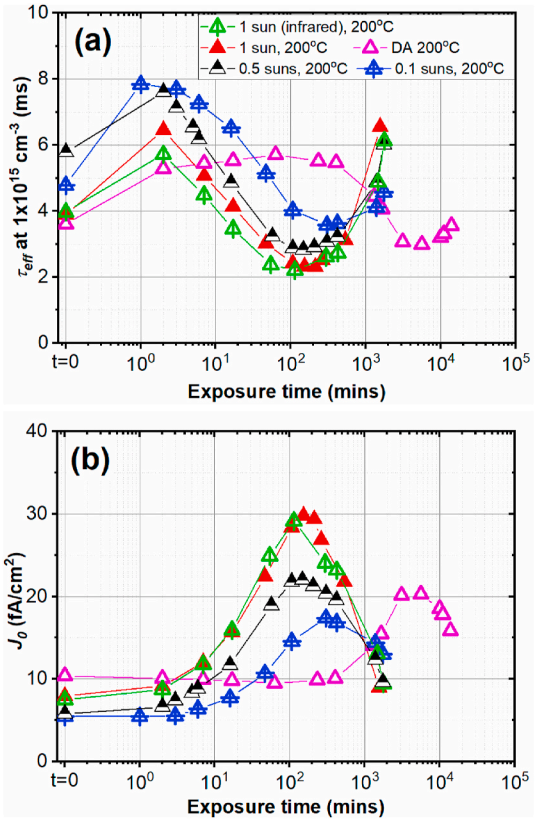

Fig. 5. Comparison of degradation behavior tested at 200 °C for various light intensities and different illumination spectrums - (a) τ_{eff} measured at injection level of 1 × 10^{15} cm^{-3}, (b) J_0 upon light soaking and dark annealing. The lines are guides to the eye.

in 30 h, which appears a lower degradation speed but higher magnitude compared to the change of J_0 from ~8 fA/cm^2 to ~30 fA/cm^2 observed in our sample after 2 h illumination under 1 sun at 200 °C. The variation in the degradation kinetics could be due to the slight difference in the testing conditions, and also be potentially related the poly-Si or the dielectric films on the samples. The following section explores the influence of the processing conditions and properties of the poly-Si films on the degradation behaviors.

3.4. Correlation between degradation behaviors and poly-Si fabrication process

To investigate whether the degradation is only applicable to a particular poly-Si fabrication process, we compare the lifetime stability in the industrially processed LPCVD poly-Si films with PECVD poly-Si films processed in our lab at ANU. The results are demonstrated in Fig. 6. These samples feature a similar phosphorus doped poly-Si passivation layer structure, but were fabricated with different tools and processing conditions, coated with different SiN_x capping layers, and annealed with different firing profiles either with a belt furnace or an RTA furnace (with processing conditions outlined in Fig. 1 and Table 1). Lab processed wafers have thinner poly-Si layers (~50 nm) compared to the industrial samples (~100 nm), enabling us to examine if the degradation is limited to thick poly-Si films. It is noted that the LPCVD poly-Si films were deposited on Cz-Si substrates, whereas FZ-Si substrates were used for the PECVD poly-Si process. Since the changes in τ_{eff} and J_0 are mainly attributed to the surface passivation quality as illustrated in Section 3.1 above, we expect negligible influence of the wafer type (n-Cz and n-FZ) on the overall conclusion.

Both PECVD and LPCVD poly-Si films show significant lifetime reduction upon light soaking under 1-sun illumination at 140 °C. The measured J_0 values increased significantly, from ~9 fA/cm^2 to ~54 fA/cm^2, and 5 fA/cm^2 to 30 fA/cm^2 for the LPCVD and PECVD poly-Si films respectively. This observation, in combination with the results recently presented by Winter et al. [21], suggests that the unstable surface passivation could be a feature of poly-Si structures in general. This degradation phenomenon leads to a substantial reduction in the iV_{oc} of the samples (shown in Fig. 6 (b)), dropping from 720 mV to 695 mV for the PECVD poly-Si films, and 720 mV–680 mV for the LPCVD films. The results highlight the importance of considering this potential degradation effect when adopting solar cells with poly-Si passivating contacts in mass production.

Moreover, the two types of poly-Si films exhibit different degrees of degradation when exposed to the same testing conditions, implying that the degradation behaviors might be partly related to the sample preparation processes, and are possibly affected by the properties of the poly-Si layers, such as thickness, doping level and crystallinity, or the SiN_x films, as well as the firing profiles. These factors are investigated below in Sections 3.5 and 3.6.

3.5. Correlation between degradation behaviors and firing profile

Fig. 7 illustrates the influence of the firing profile on the degradation behavior of the industrial poly-Si samples (coated with same SiN_x films) under 1-sun illumination at 140 °C. The samples were heated to a peak firing temperature of 600 °C, 700 °C and 750 °C for 5 s respectively with a 20 °C/s ramp-up rate, and then cooled down to room temperature with a rate of 70 °C/s. A sample fired in a belt furnace, employing a conventional firing profile (actual peak firing temperature of 770 ± 30 °C) used for solar cell fabrication, is also included. We have observed similar degradation behaviors on samples fired at 700 °C and 750 °C in an RTP

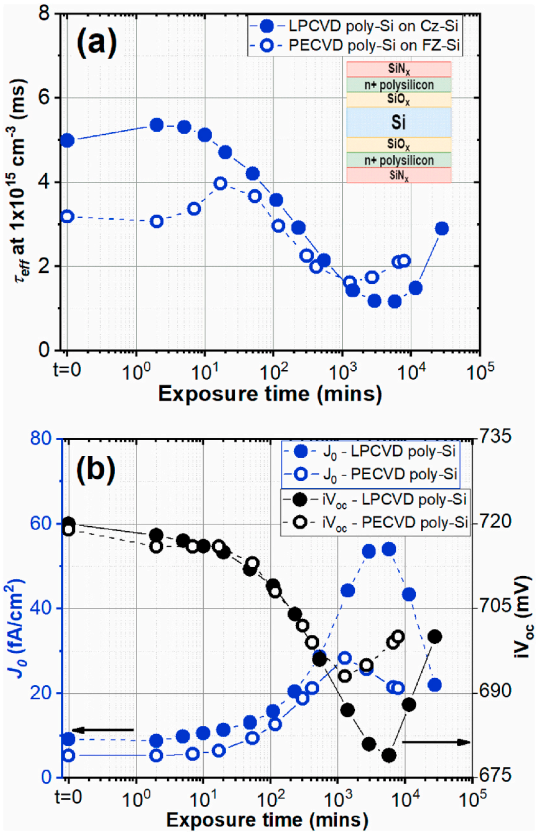

Fig. 6. Changes in (a) τ_{eff}, (b) J_0 and iV_{oc} of LPCVD and PECVD poly-Si films under 1-sun illumination at 140°C. The lifetimes were measured at injection level of 1 × 10^{15} cm^{-3}. The lines are guides to the eye.

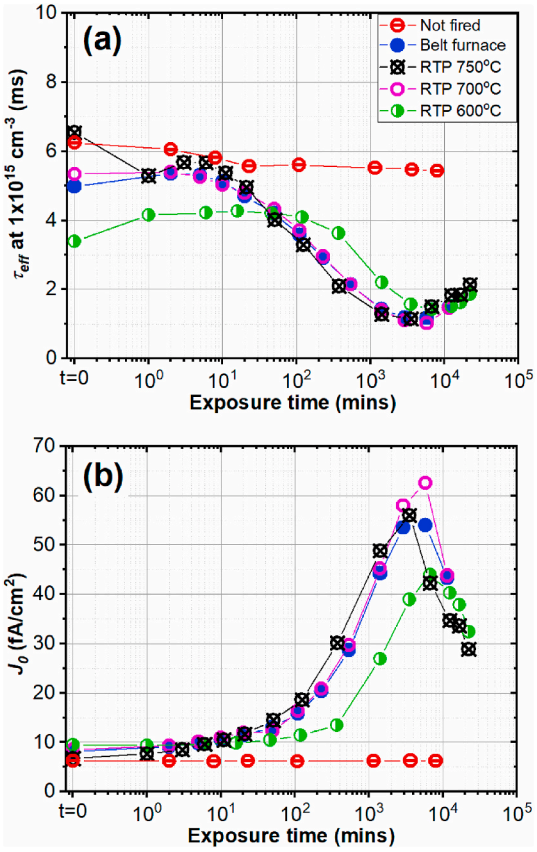

Fig. 7. Relationship between degradation behaviors under 1-sun illumination at 140°C and the firing profile applied. Changes of (a) τ_{eff} at 1 × 10^{15} cm^{-3}, and (b) J_0 during light soaking. The lines are guides to the eyes.

furnace and the sample fired with an industrial belt furnace. On the other hand, the sample fired at 600 °C shows slightly less degradation. Interestingly, samples not subjected to the firing treatment appear to be stable during light soaking, suggesting that the degradation behaviors are firing triggered. Our result echoes some previous works on other passivation films, such as SiN_x and AlO_x [34,35], where a similar dependence between firing and the long-term instability of the films are reported.

In Fig. 7 (a), it is found that the non-fired sample has a relatively higher τ_{eff} compared to the fired wafers (except the sample fired at 750 °C with RTP). The different starting τ_{eff} values could possibly be related to inhomogeneity induced by the processing as stated in the previous section, or the firing instability of the TOPCon/SiN_x structure, as reported by Feldmann et al. [36].

3.6. Correlation between degradation behavior and SiN_x film properties

The degradation and recovery phenomena in poly-Si observed in this study share some similarity with LeTID effects commonly observed on p-type boron-doped mc-Si [16,37–42], particularly in terms of the role of firing [43,44]. It has been demonstrated that LeTID behavior is strongly sensitive to the SiN_x film properties [42,45]. Here, we compare the degradation behavior in our poly-Si samples capped with SiN_x films deposited by three different PECVD tools, where these SiN_x films were found to lead to distinct LeTID behaviors in our previous study [46]. The difference in their degradation behavior is depicted in Fig. 8. It can be observed that the three studied SiN_x films all yield obvious degradation, but with slightly different kinetics. The film deposited with a Roth and Rau AK400 (SiN_x - II) leads to the highest increase of J_0 values, and perhaps surprisingly, this particular SiN_x film was found not to cause apparent bulk degradation activities in our previous LeTID study [46]. Film densities of the three SiN_x layers have been found in an order of SiN_x - I > SiN_x - III > SiN_x - II, which are inversely correlated with the degradation in J_0 (shown in Fig. 8 (b)) The correlation could suggest the involvement of hydrogen in the degradation mechanism.

In addition to samples coated with various SiN_x, samples without SiN_x capping layers (removed after firing through HF dip) were also studied. It can be observed from Fig. 9 that the samples with and without the SiN_x capping layers (SiN_x - II as shown in Fig. 8) show distinct behaviors. Samples capped with SiN_x during degradation showed a strong degradation and also a full recovery during the test period, whereas the samples without the SiN_x capping layer exhibited a continuous reduction of lifetime without any sign of recovery. This might suggest that the presence of the SiN_x layer during the light soaking could play a role in the recovery process, where the SiN_x films are speculated to perform either as a barrier to avoid hydrogen further effusing from the poly-Si, or as a hydrogen source to inject hydrogen to the poly-Si. This is also supported by the distinct response of various SiN_x films discussed above in Fig. 8, where denser films act as a more stable hydrogen source or are more effective in preventing the out-diffusion of hydrogen, leading to smaller degradation during light soaking. Note that the non-fired control sample without SiN_x did not show any lifetime and J_0 changes, in agreement with results discussed above that the degradation is triggered by firing.

As evident in the XRD result discussed above, the observed degradation phenomenon is unlikely to be caused by a change in the crystal properties of the poly-Si structure during the degradation. It is speculated that the degradations or the regenerations afterwards are related to hydrogen, given the fact that a recovery of J_0 is only observable on samples with SiN_x capping layers, which are known to act as a source of

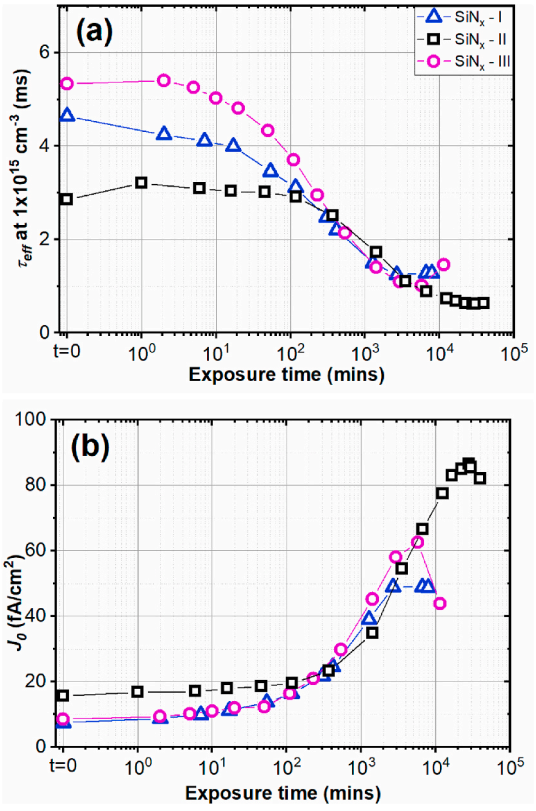

Fig. 8. Influence of SiN_x films on degradation activities under 1 sun illumination at 140 °C. Changes of (a) τ_{eff} at 1 × 10^{15} cm^{-3}, and (b) J_0 during light soaking. The three SiN_x films were of similar thickness, but deposited with different equipment. The lines are guides to the eyes. SiN_x I, II and III were respectively deposited using an Oxford PlasmaLab 100, a Roth and Rau AK400 or a Centrotherm batch-type PECVD tool.

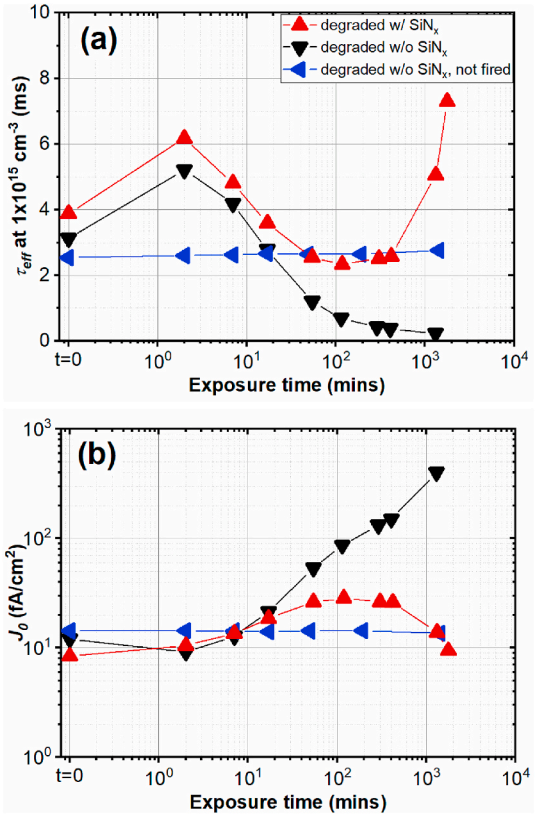

Fig. 9. Dependence of SiN_x film on degradation activities under 1 sun at 200 °C. Changes of (a) τ_{eff} at 1 × 10^{15} cm^{-3}, and (b) J_0 in logarithmic scale during light soaking. The samples are coated with SiN_x - II shown in Fig. 8. The lines are guides to the eyes.

hydrogen [47,48], and also the different degradation kinetics obtained with various SiN_x films. Moreover, the degradation observed in this work shares some key similarities to LeTID [43,44,49] and other surface related degradation reported in the literature [35,50], in which the degradation is only detected after firing. This suggests that the defects leading to these degradations could involve the same precursor or could be activated by a similar mechanism, such as the migration of hydrogen [42,51] or a reconfiguration of hydrogen bonding states [52,53]. Interestingly, a recent study by Yang et al. [22] reported a different response on phosphorus doped and boron doped poly-Si structures upon light soaking and dark annealing. Further studies on the difference between p^+ and n^+ poly-Si could provide valuable insight to identify the role of hydrogen in the different passivation structures, and at the same time, to clarify the underlying mechanism for the observed surface degradation.

4. Conclusion

We observed a degradation and recovery of lifetimes in samples with phosphorus doped poly-Si passivating structures upon light soaking at elevated temperature. The τ_{eff} trend correlates well with the change of J_0, and bulk lifetimes in the samples are found to be stable during the test measured by room-temperature super-acid passivation technique, indicating that the lifetime change is due to the instability in the surface passivation quality. Various factors affecting degradation behaviors were investigated, including the degradation conditions, the fabrication equipment (PECVD poly or LPCVD poly), the firing profile and the SiN_x capping layers. It was found that the degradation magnitude and rate increase with light intensity and temperature. The degradation is unlikely to be caused by UV damage, as it is also observed upon dark annealing at 200 °C and when the samples are subjected to infrared illumination. Although the degradation is only detected on samples after firing, we did not observe a strong dependence on the firing profile. Samples coated with different SiN_x films show only slightly different degradation responses. However, samples without the SiN_x capping layer show very severe degradation without any sign of recovery during the test period, suggesting that the presence of SiN_x films could play an important role in the regeneration process. Samples before and after degradation were characterized by GIXRD, showing minimal changes in the crystalline properties of the poly-Si films during the degradation. It is suggested that hydrogen is involved in the observed degradation or regeneration phenomena.

Declaration of competing interest

The authors declare that they have no known competing financial interests or personal relationships that could have appeared to influence the work reported in this paper.

CRediT authorship contribution statement

Di Kang: Writing - original draft, Methodology, Conceptualization. **Hang Cheong Sio:** Supervision, Writing - review & editing. **Di Yan:** Formal analysis, Writing - review & editing. **Wenhao Chen:** Data curation. **Jie Yang:** Investigation, Resources. **Jingsheng Jin:** Investigation. **Xinyu Zhang:** Resources, Funding acquisition. **Daniel Macdonald:** Project administration, Writing - review & editing.

Acknowledgements

This work has been supported by the Australian Renewable Energy Agency (ARENA) through projects RND017 and 1-A060. Access to the Australian National Fabrication Facility (ANFF) ACT node is gratefully acknowledged.

References

[1] A. Cuevas, P.A. Basore, G. Giroult-Matlakowski, C. Dubois, Surface recombination velocity of highly doped n-type silicon, J. Appl. Phys. 80 (6) (1996) 3370–3375.
[2] M.A. Green, The passivated emitter and rear cell (PERC): from conception to mass production, Sol. Energy Mater. Sol. Cell. 143 (2015) 190–197.
[3] A. Criado, E. Calleja, J. Martinez, J. Piqueras, E. Muñoz, Pn Junction applications and transport properties in polysilicon rods, Solid State Electron. 22 (8) (1979) 693–700.
[4] F. Feldmann, M. Simon, M. Bivour, C. Reichel, M. Hermle, S.W. Glunz, Carrier-selective contacts for Si solar cells, Appl. Phys. Lett. 104 (18) (2014), 181105.
[5] F. Haase, C. Hollemann, S. Schäfer, A. Merkle, M. Rienäcker, J. Krügener, R. Brendel, R. Peibst, Laser contact openings for local poly-Si-metal contacts enabling 26.1%-efficient POLO-IBC solar cells, Sol. Energy Mater. Sol. Cell. 186 (2018) 184–193.
[6] F. Feldmann, M. Bivour, C. Reichel, M. Hermle, S.W. Glunz, Passivated rear contacts for high-efficiency n-type Si solar cells providing high interface passivation quality and excellent transport characteristics, Sol. Energy Mater. Sol. Cell. 120 (2014) 270–274.
[7] A. Rohatgi, B. Rounsaville, Y. Ok, A.M. Tam, F. Zimbardi, A.D. Upadhyaya, Y. Tao, K. Madani, A. Richter, J. Benick, M. Hermle, Fabrication and modeling of high-efficiency front junction N-type silicon solar cells with tunnel oxide passivating back contact, IEEE J. Photovoltaics 7 (5) (2017) 1236–1243.
[8] P. Stradins, A. Dameron, S. Essig, V. Lasalvia, B. Lee, Y. Liu, J.-W. Luo, W. Nemeth, A. Norman, M. Page, Passivated Tunneling Contacts to N-Type Wafer Silicon and Their Implementation into High Performance Solar Cells, 2014.
[9] A. Richter, J. Benick, F. Feldmann, A. Fell, M. Hermle, S.W. Glunz, n-Type Si solar cells with passivating electron contact: identifying sources for efficiency limitations by wafer thickness and resistivity variation, Sol. Energy Mater. Sol. Cell. 173 (2017) 96–105.
[10] Y. Chen, D. Chen, C. Liu, Z. Wang, Y. Zou, Y. He, Y. Wang, L. Yuan, J. Gong, W. Lin, X. Zhang, Y. Yang, H. Shen, Z. Feng, P.P. Altermatt, P.J. Verlinden, Mass production of industrial tunnel oxide passivated contacts (i-TOPCon) silicon solar cells with average efficiency over 23% and modules over 345 W, Prog. Photovoltaics Res. Appl. 27 (10) (2019) 827–834.
[11] B. Nemeth, S.P. Harvey, J.V. Li, D.L. Young, A. Upadhyaya, V. LaSalvia, B.G. Lee, M.R. Page, P. Stradins, Effect of the SiO2 interlayer properties with solid-source hydrogenation on passivated contact performance and surface passivation, Energy Procedia 124 (2017) 295–301.
[12] D.L. Young, H.M. Branz, F. Liu, R. Reedy, B. To, Q. Wang, Electron transport and band structure in phosphorus-doped polycrystalline silicon films, J. Appl. Phys. 105 (3) (2009), 033715.
[13] P. Sana, J. Salami, A. Rohatgi, Fabrication and analysis of high-efficiency polycrystalline silicon solar cells, IEEE Trans. Electron. Dev. 40 (8) (1993) 1461–1468.
[14] F. Feldmann, M. Bivour, C. Reichel, H. Steinkemper, M. Hermle, S.W. Glunz, Tunnel oxide passivated contacts as an alternative to partial rear contacts, Sol. Energy Mater. Sol. Cell. 131 (2014) 46–50.
[15] D. Yan, A. Cuevas, J. Bullock, Y. Wan, C. Samundsett, Phosphorus-diffused polysilicon contacts for solar cells, Sol. Energy Mater. Sol. Cell. 142 (2015) 75–82.
[16] K. Ramspeck, S. Zimmermann, H. Nagel, A. Metz, Y. Gassenbauer, B. Birkmann, Light Induced Degradation of Rear Passivated Mc-Si Solar Cells, 27th European Photovoltaic Solar Energy Conference and Exhibition, 2012, pp. 861–865.
[17] F. Kersten, P. Engelhart, H.-C. Ploigt, A. Stekolnikov, T. Lindner, F. Stenzel, M. Bartzsch, A. Szpeth, K. Petter, J. Heitmann, J.W. Müller, Degradation of multicrystalline silicon solar cells and modules after illumination at elevated temperature, Sol. Energy Mater. Sol. Cell. 142 (2015) 83–86.
[18] D. Bredemeier, D. Walter, J. Schmidt, Light-induced lifetime degradation in high-performance multicrystalline silicon: detailed kinetics of the defect activation, Sol. Energy Mater. Sol. Cell. 173 (2017) 2–5.
[19] C. Modanese, M. Wagner, F. Wolny, A. Oehlke, H.S. Laine, A. Inglese, H. Vahlman, M. Yli-Koski, H. Savin, Impact of copper on light-induced degradation in Czochralski silicon PERC solar cells, Sol. Energy Mater. Sol. Cell. 186 (2018) 373–377.
[20] K. Nakayashiki, J. Hofstetter, A.E. Morishige, T.A. Li, D.B. Needleman, M. A. Jensen, T. Buonassisi, Engineering solutions and root-cause analysis for light-induced degradation in p-type multicrystalline silicon PERC modules, IEEE J. Photovoltaics 6 (4) (2016) 860–868.
[21] M. Winter, S. Bordihn, R. Peibst, R. Brendel, J. Schmidt, Degradation and regeneration of n+ doped poly-Si surface passivation on p-type and n-type Cz-Si under illumination and dark annealing, IEEE J. Photovoltaics 10 (2020) 1–8.
[22] Y. Yang, P.P. Altermatt, Y. Cui, Y. Hu, D. Chen, L. Chen, G. Xu, X. Zhang, Y. Chen, P. Hamer, R.S. Bonilla, Z. Feng, P.J. Verlinden, Effect of carrier-induced hydrogenation on the passivation of the poly-Si/SiOx/c-Si interface, AIP Conf. Proc. 2018 (1) (1999), 040026.
[23] J. Bullock, D. Kiriya, N. Grant, A. Azcatl, M. Hettick, T. Kho, P. Phang, H.C. Sio, D. Yan, D. Macdonald, M.A. Quevedo-Lopez, R.M. Wallace, A. Cuevas, A. Javey, Superacid passivation of crystalline silicon surfaces, ACS Appl. Mater. Interfaces 8 (36) (2016) 24205–24211.
[24] J.-I. Polzin, F. Feldmann, B. Steinhauser, M. Hermle, S. Glunz, Realization of TOPCon Using Industrial Scale PECVD Equipment, 2018.
[25] R. Basnet, S.P. Phang, C. Samundsett, D. Yan, W. Liang, C. Sun, S. Armand, R. Einhaus, J. Degoulange, D. Macdonald, 22.6% efficient solar cells with polysilicon passivating contacts on n-type solar-grade wafers, Solar RRL 3 (11) (2019), 1900297.

[26] R.A. Sinton, A. Cuevas, M. Stuckings, Quasi-steady-state photoconductance, a new method for solar cell material and device characterization, in: Conference Record of the Twenty Fifth IEEE Photovoltaic Specialists Conference - 1996, 1996, pp. 457–460.
[27] D.E. Kane, R.M. Swanson, Measurement of the emitter saturation current by a contactless photoconductivity decay method, in: Proceedings of the IEEE 18th Photovoltaic Specialist Conference, 1985, p. 578.
[28] A.I. Pointon, N.E. Grant, E.C. Wheeler-Jones, P.P. Altermatt, J.D. Murphy, Superacid-derived surface passivation for measurement of ultra-long lifetimes in silicon photovoltaic materials, Sol. Energy Mater. Sol. Cell. 183 (2018) 164–172.
[29] C. Sen, C. Chan, P. Hamer, M. Wright, U. Varshney, S. Liu, D. Chen, A. Samadi, A. Ciesla, C. Chong, B. Hallam, M. Abbott, Annealing prior to contact firing: a potential new approach to suppress LeTID, Sol. Energy Mater. Sol. Cell. 200 (2019) 109938.
[30] F. Fertig, K. Krauß, S. Rein, Light-induced degradation of PECVD aluminium oxide passivated silicon solar cells, Phys. Status Solidi Rapid Res. Lett. 9 (1) (2015) 41–46.
[31] A. Cuevas, D. Macdonald, Measuring and interpreting the lifetime of silicon wafers, Sol. Energy 76 (1) (2004) 255–262.
[32] M. Tayyib, J.O. Odden, T.O. Saetre, UV-induced degradation study of multicrystalline silicon solar cells made from different silicon materials, Energy Procedia 38 (2013) 626–635.
[33] C.R. Osterwald, J. Pruett, T. Moriarty, Crystalline silicon short-circuit current degradation study: initial results, in: Conference Record of the Thirty-First IEEE Photovoltaic Specialists Conference, 2005, 2005, pp. 1335–1338.
[34] D. Sperber, A. Heilemann, A. Herguth, G. Hahn, Temperature and light-induced changes in bulk and passivation quality of boron-doped float-zone silicon coated with SiNx:H, IEEE J. Photovoltaics 7 (2) (2017) 463–470.
[35] K. Kim, R. Chen, D. Chen, P. Hamer, A.C.n. Wenham, S. Wenham, Z. Hameiri, Degradation of surface passivation and bulk in p-type monocrystalline silicon wafers at elevated temperature, IEEE J. Photovoltaics 9 (1) (2019) 97–105.
[36] F. Feldmann, T. Fellmeth, B. Steinhauser, H. Nagel, D. Ourinson, S. Mack, E. Lohmüller, J.-I. Polzin, J. Benick, J. Rentsch, M. Hermle, S. Glunz, Large Area TOPCon Cells Realized by a PECVD Tube Process, 2019.
[37] D. Bredemeier, D. Walter, S. Herlufsen, J. Schmidt, Lifetime degradation and regeneration in multicrystalline silicon under illumination at elevated temperature, AIP Adv. 6 (3) (2016), 035119.
[38] P.E.F. Kersten, H.-C. Ploigt, F. Stenzel, K. Petter, T. Lindner, A. Szpeth, M. Bartzsch, A. Stekolnikov, M. Scherff, J. Heitmann, J.W. Müller, in: A New Light Induced Volume Degradation Effect of Mc-Si Solar Cells and Modules, 31st European Photovoltaic Solar Energy Conference and Exhibition, 2016, pp. 1830–1834.
[39] J. Lindroos, K. Petter, K. Sporleder, M. Turek, P. Pacho, M. Rinio, Light beam induced current of light-induced degradation in high-performance multicrystalline Al-BSF cells, Energy Procedia 124 (2017) 99–106.
[40] H. Vahlman, A. Haarahiltunen, W. Kwapil, J. Schön, M. Yli-Koski, A. Inglese, C. Modanese, H. Savin, Effect of low-temperature annealing on defect causing copper-related light-induced degradation in p-type silicon, Energy Procedia 124 (2017) 188–196.
[41] D. Chen, P.G. Hamer, M. Kim, T.H. Fung, G. Bourret-Sicotte, S. Liu, C.E. Chan, A. Ciesla, R. Chen, M.D. Abbott, B.J. Hallam, S.R. Wenham, Hydrogen induced degradation: a possible mechanism for light- and elevated temperature-induced degradation in n-type silicon, Sol. Energy Mater. Sol. Cell. 185 (2018) 174–182.
[42] C. Vargas, K. Kim, G. Coletti, D. Payne, C. Chan, S. Wenham, Z. Hameiri, Carrier-induced degradation in multicrystalline silicon: dependence on the silicon nitride passivation layer and hydrogen released during firing, IEEE J. Photovoltaics 8 (2) (2018) 413–420.
[43] R. Eberle, W. Kwapil, F. Schindler, M.C. Schubert, S.W. Glunz, Impact of the firing temperature profile on light induced degradation of multicrystalline silicon, Phys. Status Solidi Rapid Res. Lett. 10 (12) (2016) 861–865.
[44] R. Eberle, W. Kwapil, F. Schindler, S.W. Glunz, M.C. Schubert, Firing temperature profile impact on light induced degradation in multicrystalline silicon, Energy Procedia 124 (2017) 712–717.
[45] D. Bredemeier, D.C. Walter, R. Heller, J. Schmidt, Impact of hydrogen-rich silicon nitride material properties on light-induced lifetime degradation in multicrystalline silicon, Phys. Status Solidi Rapid Res. Lett. 13 (8) (2019), 1900201.
[46] D. Kang, H.C. Sio, X. Zhang, Q. Wang, H. Jin, D. Macdonald, LeTID in p-type and n-type mono-like and float-zone silicon, and their dependence on SiNx film properties, in: 36th European Photovoltaic Solar Energy Conference and Exhibition, Marseille, 2019.
[47] T.N. Truong, D. Yan, C. Samundsett, R. Basnet, M. Tebyetekerwa, L. Li, F. Kremer, A. Cuevas, D. Macdonald, H.T. Nguyen, Hydrogenation of phosphorus-doped polycrystalline silicon films for passivating contact solar cells, ACS Appl. Mater. Interfaces 11 (5) (2019) 5554–5560.
[48] M. Schnabel, B. Van de Loo, W. Nemeth, B. Macco, P. Stradins, W.M.M. Kessels, D. Young, Hydrogen passivation of poly-Si/SiOx contacts for Si solar cells using Al 2O3 studied with deuterium, Appl. Phys. Lett. 112 (2018), 203901.
[49] D. Chen, M. Kim, B.V. Stefani, B.J. Hallam, M.D. Abbott, C.E. Chan, R. Chen, D.N. R. Payne, N. Nampalli, A. Ciesla, T.H. Fung, K. Kim, S.R. Wenham, Evidence of an identical firing-activated carrier-induced defect in monocrystalline and multicrystalline silicon, Sol. Energy Mater. Sol. Cell. 172 (2017) 293–300.
[50] D. Sperber, A. Graf, D. Skorka, A. Herguth, G. Hahn, Degradation of surface passivation on crystalline silicon and its impact on light-induced degradation experiments, IEEE J. Photovoltaics 7 (6) (2017) 1627–1634.
[51] T.C. Kho, K.R. McIntosh, J.T. Tan, A.F. Thomson, F.W. Chen, Removal of hydrogen and deposition of surface charge during rapid thermal annealing, in: 2008 33rd IEEE Photovoltaic Specialists Conference, 2008, pp. 1–5.
[52] S.A. McQuaid, M.J. Binns, R.C. Newman, E.C. Lightowlers, J.B. Clegg, Solubility of hydrogen in silicon at 1300 °C, Appl. Phys. Lett. 62 (14) (1993) 1612–1614.
[53] R. Jones, B.J. Coomer, J. Goss, B. Hourahine, A. Resende, The interaction of hydrogen with deep level defects in silicon, Solid State Phenom. 71 (2000).